

Performance assessment of typical buildings in Singapore to long-distance earthquakes

Goh, Key Seng

2014

Goh, K. S. (2014). Performance assessment of typical buildings in Singapore to long-distance earthquakes. Doctoral thesis, Nanyang Technological University, Singapore.

<https://hdl.handle.net/10356/61717>

<https://doi.org/10.32657/10356/61717>



**NANYANG
TECHNOLOGICAL
UNIVERSITY**

**PERFORMANCE ASSESSMENT OF TYPICAL
BUILDINGS IN SINGAPORE TO LONG-
DISTANCE EARTHQUAKES**

GOH KEY SENG

SCHOOL OF CIVIL AND ENVIRONMENTAL ENGINEERING

2014

**PERFORMANCE ASSESSMENT OF TYPICAL
BUILDINGS IN SINGAPORE TO LONG-
DISTANCE EARTHQUAKES**

GOH KEY SENG

School of Civil and Environmental Engineering

A thesis submitted to the Nanyang Technological University
in partial fulfillment of the requirement for the degree of
Doctor of Philosophy

2014

ACKNOWLEDGEMENT

The author would like to express his sincere appreciation to his supervisor, Professor Pan Tso-Chien for his patience, encouragement, kindness and guidance along the way. This work would be impossible without guidance from Prof Pan. The guidance from Dr. Kusnowidjaja Megawati in the early stage of this work is also much appreciated.

The author would like to acknowledge Professor Harianto Rahardjo for his valuable suggestions and criticisms. The author would like to thank Associate Professor Li Bing for his suggestion and fruitful discussions on the modeling of beam-column joint. The author would also like to thank Dr. Tony Yang from University of British Columbia for his assistant in the *OpenSEEs* modeling.

The author would also like to thank Dr. Huang Liping, Dr. Zheng Haitao, Dr. Meya Walling, Dr. Avik Samantha and Dr. Yang Guichang for the extensive discussions and valuable suggestions. Besides, helps from Stephani Alvin, Ho Qiying, Debbie Low Chuan Min, Fiona Low Xin Yi, and Carolin Ruan Weiting on the administration matters are much appreciated. The author would also like to thank Marie Hamidah, Zhu Cheng, Han Xiaohan and others who have also formed an important part in his research.

The author would like to express his love and gratitude to his parents for their encouragement and understanding throughout his life.

Finally, the author wishes to acknowledge the financial support provided by Nanyang Technological University, Singapore.

TABLE OF CONTENTS

ACKNOWLEDGEMENT	i
ABSTRACT	vi
LIST OF TABLES	viii
LIST OF FIGURES	x
LIST OF SYMBOLS	xix
CHAPTER 1	
INTRODUCTION	1
1.1 Background	1
1.2 Research Aim and Scope	5
1.3 Originality and Contributions	12
1.4 Organization of Thesis	13
CHAPTER 2	
EMPIRICAL RELATIONSHIPS BETWEEN NATURAL VIBRATION PERIOD AND HEIGHT OF BUILDINGS IN SINGAPORE	15
2.1 Literature Review	15
2.2 Singapore Geology	19
2.3 Methodology	20
2.3.1 Instrumentation	22
2.3.2 Data Processing	24
2.4 Results	25
2.5 Effect of Soil-Structure Interaction	36
2.6 Comparison with Recorded Data during Earthquake Events	42
2.7 Comparison with Existing Period-Height Relationships	45
2.8 Chapter Summary	47

CHAPTER 3	
GENERIC STRUCTURAL MODELS	49
3.1 Overview of Structural Model	50
3.1.1 Configurations and Elements	50
3.1.2 Material Properties	56
3.1.3 Beam-Column Joint Model	58
3.1.4 Calibration of Joint Model	62
3.2 Natural Vibration Period of Generic Models	69
3.3 Chapter Summary	70
CHAPTER 4	
METHODOLOGY FOR ESTIMATING HUMAN PERCEPTION TO TREMORS IN HIGH-RISE BUILDINGS	72
4.1 Methodology	73
4.2 Characterization of Ground Motion	76
4.2.1 Recorded Ground Motion	76
4.2.2 Scaling of Ground Motions	76
4.3 Guideline for Threshold of Human Perception to Vibration	78
4.4 Relationships between Level of Perception to Tremors and Ground Motion Intensity	80
4.5 Validations	83
4.6 Chapter Summary	90
CHAPTER 5	
SEISMIC PERFORMANCE OF TYPICAL BUILDINGS IN SINGAPORE TO MAXIMUM CREDIBLE EARTHQUAKE GROUND MOTIONS	91
5.1 Potential Failure Modes	91
5.2 Static Pushover Analysis	92

5.2.1	Static Lateral Load	93
5.2.2	Results	95
5.3	Maximum Credible Ground Motions	98
5.3.1	Target Spectra	98
5.3.2	Recorded Ground Motions	101
5.3.3	Scaling of Ground Motions	102
5.4	Effect of Soft-Soil Amplification	109
5.4.1	Structural Analysis Results	115
5.5	Chapter Summary	119
CHAPTER 6		
TORSIONAL RESPONSE OF NONDUCTILE STRUCTURES WITH SOFT- FIRST-STOREY		
		120
6.1	Literature Review	120
6.1.1	Torsional Response	121
6.1.2	Soft-Storey Effect	123
6.2	Mathematical Model	124
6.2.1	Stiffness and Strength Ratios	125
6.2.2	Overstrength Ratio	127
6.2.3	Stiffness and Strength Eccentricity	128
6.2.4	Resisting Elements	131
6.2.5	Uncoupled Torsional to Lateral Frequency Ratio	132
6.3	Ground Motions	135
6.4	Hysteretic Model	136
6.5	Results and Discussions	138
6.5.1	General Observations	139
6.5.2	Effect of Deterioration Coefficient, γ	145
6.6	Ductility Demand-Capacity Curves	147

6.7 Chapter Summary	151
CHAPTER 7	
CONCLUSIONS AND RECOMMENDATIONS	154
7.1 Conclusions	154
7.2 Recommendations	156
CHAPTER 8	
REFERENCES	158
APPENDIX A: LOCATION OF BUILDINGS FOR AMBIENT VIBRATION MEASUREMENTS	169
APPENDIX B: VALIDATION OF USING A SIMPLIFIED TWO-STOREY MODEL TO REPRESENT A MULTI-STOREY MODEL	176

ABSTRACT

Although Singapore is located in a low seismicity area, the country is exposed to long-distance earthquakes originated from Sumatra. As part of the effort to assess the seismic performance of buildings in Singapore, relationships between the natural vibration period and the height of high-rise residential buildings in Singapore are derived empirically by conducting regression analysis on ambient vibration test (AVT) results of 116 buildings. It is found that the vibration periods estimated from the proposed period-height relationship for buildings located at soft-soil site are about 40% longer than the vibration periods estimated for buildings located at firm-soil site. Measurements are also conducted to study the influence of buildings on the measured frequency of the surrounding soil. The results show that the distance of building influence on the measured frequency of the surrounding soil may reach up to one building height for a firm-soil site and two building heights for a soft-soil site.

Two generic building models of 15 and 30 stories representing typical high-rise residential buildings in Singapore are constructed using *OpenSEEs*. A methodology is proposed for estimating the level of perception to tremors of occupants living in high-rise residential buildings, which is based on statistical analysis of analytical results of seismic response of generic building models to recorded ground motions. The results estimated using the proposed methodology are found to match well with the reports from the local newspapers and the authorities.

Pushover analyses are conducted to determine the seismic capacity of the generic building models. The overstrength ratios of the 15-storey and 30-storey

generic models are found to be 5.47 and 6.90, respectively. The ground motions at rock site due to the maximum credible earthquakes (MCE) in Sumatran strike-slip fault and subduction zone are generated using spectrum-matching method in frequency domain. The MCE ground motions at a typical soft-soil site in Singapore are subsequently generated using equivalent linear model of the horizontally-layered soil deposit, which is implemented in the widely-used computer program *SHAKE91*. Time history analyses are conducted for the generic building models subjected to the simulated ground motions. It is found that shear failure is unlikely to occur at the beam-column joints of the generic building models due to the MCE ground motions. However, torsional effects, which may amplify the displacement responses of the generic models, are not considered in these analyses.

Torsional response of nonductile structures with soft-first-storey subjected to bidirectional ground motions is subsequently studied using a simplified two-storey model with two-way eccentricities. The stiffness and strength ratios, stiffness and strength eccentricities, ductility capacity, and overstrength ratio are varied to examine the effects of these parameters on the torsional responses. Ductility demand-capacity curves are then constructed, which can be used to approximately assess the seismic performance of existing structures, and as guidelines for designing new structures in Singapore to withstand the MCE ground motions considering the coupling of torsional and soft-first-storey effects. It is concluded that nonductile structure with overstrength ratio above 5.0 is less likely to fail during the MCE event. As the overstrength ratios of the two generic building models are larger than 5.0, the generic building models are thus unlikely to fail when subjected to the MCE ground motions at the soft-soil site considering torsional effects.

LIST OF TABLES

Table 1-1	List of tremor events reportedly felt in Singapore
Table 2-1	Building period coefficient, C_t , and exponent, x , for different structural systems according to IBC 2012 (ICC, 2012) (H in meters)
Table 2-2	Summary of AVT measurements
Table 2-3	Comparison between the measured natural vibration periods of 19 instrumented residential buildings during September 30, 2009 event with the estimated natural vibration periods using the proposed period-height relationships
Table 3-1	Material properties for reinforced concrete frame elements
Table 3-2	Summary of masonry wall properties
Table 3-3	Summary of natural vibration period of the generic models computed from <i>OpenSEEs</i> and Eq. 2-10 to Eq.2-13
Table 4-1	Ten significant Sumatran subduction earthquakes that caused perceivable tremors in Singapore during the last 10 years
Table 4-2	The ARSA values of the recorded ground motions during the three earthquake events at firm-soil site and soft-soil site
Table 4-3	Estimated percentage of occupants to perceive tremors during December 26, 2004, March 28, 2005 and September 30, 2009 Sumatran earthquake events in (a) 15-storey; (b) 30-storey buildings
Table 5-1	Summary of the 6 recorded Sumatran fault earthquakes

Table 5-2	Soil profiles of the soft-soil site, which is overlain by marine clay deposit
Table 6-1	Masses at each storey for models <i>F-S</i> , <i>F-F</i> and <i>S-S</i>
Table 6-2	The first three periods for symmetric and asymmetric models, <i>F-S</i> , <i>F-F</i> , <i>S-S</i>
Table A-1	Details of measured buildings at Kallang Formation
Table A-2	Details of measured buildings at Bukit Timah Granite
Table A-3	Details of measured buildings at Jurong Formation
Table A-4	Details of measured buildings at Old Alluvium
Table B-1	The degree of freedoms and the 1st natural vibration periods of multi-storey models

LIST OF FIGURES

- Figure 1-1 The Sunda Trench and Sumatran Fault (Pan et al., 2004)
- Figure 1-2 Epicenters of earthquakes in the Sumatran region since January 1960 to February 2013. Source: National Earthquake Information Center Database. USGS.
- Figure 1-3 Number of tremor events reportedly felt per decade (1830-2010) and percentage of population living in public residential buildings in Singapore (1960-2012)
- Figure 1-4 Epicenters of earthquakes which caused perceivable tremors in Singapore (year 1833 to 2012)
- Figure 2-1 Geological map of Singapore (DSTA, 2009) overlaid with the location of the measured buildings
- Figure 2-2 Photos of (a) 25-storey point block; (b) 16-storey slab block
- Figure 2-3 A set of tri-axial velocity seismometer
- Figure 2-4 The HVSR plots of the AVT data at: (a) top of 16-storey slab block in channel 1; (b) top of 16-storey slab block in channel 2; (c) top of 25-storey point block in channel 1; (d) top of 25-storey point block in channel 2
- Figure 2-5 Spectrogram of natural frequency observed at top of a 25-storey point block in (a) Channel 1; (b) Channel 2

- Figure 2-6 Spectrogram of natural frequency observed at top of a 16-storey slab block in (a) Channel 1; (b) Channel 2
- Figure 2-7 Comparison between the HVSR of the ambient vibrations recorded on top of a 20-storey point block and a 20-storey slab block located at soft-soil site in: (a) Transverse direction (Channel 1); (b) Longitudinal direction (Channel 2)
- Figure 2-8 Summary of AVT measurements with height and number of storey as x-axis, natural period as y-axis and regression analysis is done for (a) Kallang Formation (KF); (b) Jurong Formation (JF); (c) Old Alluvium (OA); (d) Bukit Timah Granite (BT)
- Figure 2-9 Plot of mean and standard deviation for buildings at (a) soft-soil site; (b) firm-soil site
- Figure 2-10 Location of the measuring point at distance R away from the building with height H .
- Figure 2-11 The HVSR of the microtremors measured on top of a 25-storey point block located at firm-soil site, ground floor, $0.5H$ away from the building, $1H$ away from the building, $1.5H$ away from the building and $2H$ away from the building
- Figure 2-12 The HVSR of the microtremors measured on top of a 30-storey point block located at soft-soil site, ground floor, $0.5H$ away from the building, $1H$ away from the building, $2H$ away from the building, and $3H$ away from the building

- Figure 2-13 Transfer function of the data recorded in a 29-storey high-rise residential building during 30 September 2009 Sumatran earthquake event
- Figure 2-14 Comparison with other published period-height relationships
- Figure 3-1 Graphical illustration of the: (a) 15-storey generic model; (b) 30-storey generic model
- Figure 3-2 Typical floor plan of (a) point block; (b) slab block
- Figure 3-3 Summary of concrete frames elements
- Figure 3-4 Stress-strain relationship for unconfined and confined concrete model according to Mander et al. (1988)
- Figure 3-5 Schematic diagram of *Joint2D* element (Altoontash, 2004)
- Figure 3-6 Compression strut model for calibration of joint-element shear panel component (Mitra and Lowes, 2007)
- Figure 3-7 Calibrated shear panel backbone curve and multilinear idealization by Altoontash (2004)
- Figure 3-8 Calibrated shear panel backbone curve and bilinear idealization (present study)
- Figure 3-9 Reinforcing detailing of specimens: (a) A1; (b) M1; (c) A2; and (d) M2 (Li et al., 2002)
- Figure 3-10 Cyclic lateral loading and displacement history (Li et al., 2002)

- Figure 3-11 Graphical illustration of the numerical simulation of beam-column joint model
- Figure 3-12 Comparison between experiment and simulation results for specimen: (a) A1; (b) M1; (c) A1; and (d) M2.
- Figure 3-13 Comparison of stiffness in each cycles obtained from experiment and simulation
- Figure 3-14 Comparison of column shear forces in each cycles obtained from experiment and simulation
- Figure 3-15 Comparison of maximum joint shear stress for each specimen obtained from experiment and simulation
- Figure 3-16 Comparison of strength loss at last cycle for each specimen obtained from experiment and simulation
- Figure 3-17 Mode shape of the 1st vibration mode of the: (a) 15-storey generic model, T=0.67 sec; (b) 30-storey generic model, T=1.31 sec
- Figure 4-1 Framework for evaluating human perception to tremors
- Figure 4-2 Mean and standard deviation of the 10 sets of recorded ground motions scaled to ARSA value of 1.5 gal in period band 0.1 sec to 2.0 sec
- Figure 4-3 Summary of human perception threshold to vibration specified by AIJ-GEH-2004
- Figure 4-4 Regression relationships between perception level and ARSA for the 15-storey generic model at (a) 15th storey; and (b) 7th storey

- Figure 4-5 Regression relationships between perception level and ARSA for the 30-storey generic model at (a) 30th storey; and (b) 15th storey
- Figure 4-6 Epicenters of the (a) December 26, 2004; (b) March 28, 2005; and (c) September 30, 2009 Sumatran earthquake events
- Figure 4-7 The surface geology of Singapore (DSTA, 2009) overlaid with the location of tremors reportedly felt in Singapore during December 26th, 2004, March 28th, 2005 and September 30th, 2009 Sumatran earthquake events
- Figure 5-1 Overstrength ratio and displacement ductility factor (reprinted from work by Balendra et al., 1999)
- Figure 5-2 Base shear versus roof displacement for: (a) 15-storey generic model; (b) 30-storey generic model
- Figure 5-3 Pseudo-acceleration response spectrum (5% damping ratio) at rock site in Singapore resulting from: (a) the maximum credible Sumatran fault earthquake ($M_w=7.5$, $R= 425$ km); (b) the maximum credible Sumatran subduction earthquake ($M_w=9.0$, $R= 700$ km)
- Figure 5-4 Procedure of ground motion scaling in frequency domain
- Figure 5-5 Comparison between the target spectrum and the spectrum of scaled ground motion with number of iterations equal to (a) 1; (b) 2; (c) 5; (d) 10
- Figure 5-6 Predicted $\mu+\sigma$ response spectrum (5% damping ratio) for the maximum credible fault earthquake ($M_w=7.5$, $R= 425$ km) and the acceleration response spectra of the 6 sets of scaled ground motions

- Figure 5-7 Predicted $\mu+\sigma$ response spectrum (5% damping ratio) for the maximum credible fault earthquake ($M_w=7.5$, $R= 425$ km), and the mean and mean plus one standard deviation of the acceleration response spectra of the 6 sets of scaled ground motions
- Figure 5-8 Predicted $\mu+\sigma$ response spectrum (5% damping ratio) for the maximum credible subduction earthquake ($M_w=9.0$, $R= 700$ km), and the acceleration response spectra of the 10 sets of scaled ground motions
- Figure 5-9 Predicted $\mu+\sigma$ response spectrum (5% damping ratio) for the maximum credible subduction earthquake ($M_w=9.0$, $R= 700$ km), and the mean and mean plus one standard deviation of the acceleration response spectra of the 10 sets of scaled ground motions
- Figure 5-10 Recorded and scaled ground motions in Singapore during 22nd Apr 1997 Sumatran fault earthquake in E-W and N-S direction
- Figure 5-11 Recorded and scaled ground motions during 30 Sept 2009 Sumatran subduction earthquake event in E-W and N-S direction
- Figure 5-12 Pseudo-acceleration response spectra (5% damping ratio) of the maximum credible Sumatran fault earthquake ground motions at soft-soil site and the corresponding mean and mean plus one standard deviation
- Figure 5-13 Spectral amplification factors of ground motions at soft-soil site due to maximum credible Sumatran fault earthquake with respect to rock site

- Figure 5-14 Pseudo-acceleration response spectra (5% damping ratio) of the maximum credible Sumatran subduction earthquake ground motions at soft-soil site and the corresponding mean and mean plus one standard deviation
- Figure 5-15 Spectral amplification factors of ground motions at soft-soil site due to maximum credible Sumatran subduction earthquake with respect to rock site
- Figure 5-16 Simulated ground acceleration at the soft-soil site from the scaled 22 Apr 1997 Sumatran fault earthquake event in E-W and N-S direction
- Figure 5-17 Simulated ground acceleration at the soft-soil site from the scaled 30 Sept 2009 Sumatran subduction earthquake event in E-W and N-S direction
- Figure 5-18 Maximum interstorey drift profile in the 15-storey generic model due to maximum credible Sumatran fault and subduction earthquakes
- Figure 5-19 Maximum interstorey drift profile in the 30-storey generic model due to maximum credible Sumatran fault and subduction earthquakes
- Figure 5-20 Maximum induced joint shear stress in the: (a) 15-storey generic model and (b) 30-storey generic model subjected to maximum credible Sumatran earthquake ground motions at rock and soft-soil site. Error bars represent standard deviations of the results
- Figure 6-1 3-Dimensional illustration of a simplified two-storey model with two-way eccentricities subjected to bidirectional ground motions
- Figure 6-2 Plan view of the mathematical model in 1st and 2nd storey

- Figure 6-3 Backbone curve for hysteretic model (Ibarra et al., 2005)
- Figure 6-4 Effect of variation in stiffness ratio and stiffness eccentricity on the displacement amplification of irregular elastic models with respect to regular elastic models
- Figure 6-5 Effect of variation in stiffness ratio and stiffness eccentricity on the displacement amplification of irregular models with respect to regular models with overstrength ratio of 2.5
- Figure 6-6 Effect of variation in stiffness ratio and stiffness eccentricity on the displacement amplification of irregular models with respect to regular models with overstrength ratio of 1.5
- Figure 6-7 Effect of deterioration coefficient, γ on the: (a) normalized displacement $u/u_{\gamma=\infty}$, and (b) coefficient of variation, σ/\bar{u} (%)
- Figure 6-8 Ductility demand-capacity curves
- Figure B-1 Ground motion time history of the maximum credible Sumatran subduction earthquake and the corresponding response spectral displacement
- Figure B-2 Comparison between the top displacement responses of multi-storey models and the equivalent simplified two-storey models
- Figure B-3 Percentage differences between the maximum top displacement responses of multi-storey models and the equivalent two-storey models
- Figure B-4 Normalized 1st mode shape of: (a) ten-storey model, (b) twenty-storey model, (c) thirty-storey model with different stiffness ratio

Figure B-5 1st mode participation ratio of the two-storey and multi-storey models with different stiffness ratio

LIST OF SYMBOLS

Chapter 2

C_t and x	Building period coefficient based on the building types
T	Building fundamental natural vibration period in second
H	Building height in meter
N	Number of stories
$Z(f)$	Building response at frequency f
$H(f)$	Horizontal spectrum at frequency f
$V(f)$	Vertical spectrum at frequency f

Chapter 3

f_c	Unconfined concrete compressive strength (MPa)
ε_{sc}	Unconfined concrete strain at f_c
f_{cu}	Unconfined concrete crushing strength (MPa)
ε_{su}	Unconfined concrete strain at f_{cu}
f_t	Unconfined concrete tensile strength (MPa)
E_{ts}	Unconfined concrete tension softening slope (MPa)
F_y	Steel yield stress (MPa)
E	Steel modulus of elasticity (GPa)
b	Steel hardening ratio
f_{cm}	Masonry wall compressive strength
ε_{scm}	Masonry wall strain at f_{cm}
f_{cum}	Masonry wall crushing strain
ε_{sum}	Masonry wall strain at f_{cum}

τ_{strut}	Shear stress in the shear-panel component
f_{c_strut}	Strut stress
w_{strut}	In-plane width of the strut
α_{strut}	Angle of inclination of the strut with the horizontal
w	In-plane width of the joint
h	In-plane height of the joint

Chapter 4

$P_{\%,I}$	Estimated percentage of occupants to perceive tremors at i th storey of the building
y_{ARSA}	ARSA value of the ground motion

Chapter 5

V_s	Shear contributions assigned to steel
V_c	Shear contributions assigned to concrete
μ_δ	Displacement ductility
k	A parameter equal to 1 for $\mu_\delta \leq 2$, equal to 0.7 for $\mu_\delta \geq 6$, and varies linearly for intermediate μ_δ values
A_{st}	Area of shear reinforcement parallel to the horizontal shear force within spacing s
f_{yt}	Yield strength of transverse reinforcement
h	Section depth parallel shear force
d	Effective depth = $0.8h$
P	Axial compression force
f'_c	Concrete compressive strength, MPa
A_g	Gross section

a/d	Shear span/ effective depth
V_e	Elastic base shear
Ω	Overstrength ratio
μ	Ductility factor
V_y	Base shear at significant yield point
V_d	Design base shear
Δ_u	Ultimate displacement
Δ_y	Significant yield displacement
C_{vx}	Vertical distribution factor
V	Total horizontal earthquake base shear force
w_i	Portion of the total building weight W located on or assigned to floor level i
h_i	Height from the base to floor level i
M_w	Moment magnitude
R	Epicentral distance
Y, Y_H	Horizontal PGA, PGV or RSA values (5% damping ratio) in units of cm/s^2 , cm/s and cm/s^2 , respectively
ϕ	S source-to-station azimuth measured from the strike of the fault plane clockwise
a_3	Geometrical attenuation rate
a_4	Anelastic attenuation
ε_H	Variations in the PGA, PGV and RSA
$V_{S,30}$	Average shear-wave velocity values of the upper 30 m
G_{\max}	Maximum shear modulus
G	shear modulus

Chapter 6

K_1	Total stiffness in the first-storey
K_2	Total stiffness in the second-storey
α_k	Stiffness ratio
α_R	Strength ratio
V_y	Base shear force at yield of the model
V_d	Design base shear force of the model
Ω	Overstrength ratio
e_S	Stiffness eccentricity
e_R	Resistance eccentricity
D	Length of the edge parallel to the direction of stiffness eccentricity
Ω_θ	Uncoupled torsional to lateral frequency ratio of a system
ω_θ	Uncoupled torsional frequency of the system
ω_l	Uncoupled lateral frequency of the system
K_{nx} and K_{ny}	Total lateral stiffness of the models in n th storey in x-direction and y-direction respectively
$K_{n\theta}$	Total torsional stiffness in the n th storey of the model
k_{nxi} and k_{nyi}	Initial stiffness of the of the i th resisting element in n th storey in the x and y directions, respectively
x_i, y_i	Distances from the origin to the i th resisting element
ω_x and ω_y	Uncoupled lateral frequencies in x-direction and y-direction, respectively
ω_θ	Uncoupled torsional frequency
m_{1x}, m_{2x}	Masses in the x-direction in 1 st and 2 nd storey, respectively
m_{1y}, m_{2y}	Masses in the y-direction in 1 st and 2 nd storey, respectively
$m_{1\theta}, m_{2\theta}$	Mass moment of inertia in 1 st and 2 nd storey, respectively

T_x, T_y and T_θ	Uncoupled period in x-direction, the uncoupled period in y-direction, and the uncoupled torsional period, respectively
K_e	Elastic (initial) stiffness
μ_{cap}	Ductility capacity
δ_y	Yield deformation
F_y	Yield strength
δ_c	Cap deformation
F_c	Peak strength
F_r	Residual strength
K_s	Strain hardening stiffness
K_c	Post-capping stiffness
γ	Deterioration coefficient
c	An exponent that controls the rate of deterioration
u	Displacement response
u_R	Displacement response of regular model
$u_{\gamma=\infty}$	Displacement response of model with no deterioration
σ	Standard deviation
μ_d	Ductility demand
δ_{max}	Maximum displacement response

CHAPTER 1

INTRODUCTION

1.1 BACKGROUND

Singapore, a modern city with a population of more than 5 million living in an area of about 600 km² and gross domestic product (GDP) per capita of US\$50,000 (Singapore Department of Statistics, 2012), is a classic case of a modern metropolis of low-hazard but high-exposure to the seismicity in Sumatra. The island nation is located about 400 km away from the high seismicity Sumatra fault, which lies about 250 km northeast of Sunda trench (Figure 1-1). The 1650 km long fault runs along the western side of the Sumatra Island, coinciding with the Bukit Barisan mountain chain. The overall shape of the fault is sinusoidal, with the northern half of the fault concave to the southwest and the southern half of the fault concave to the northeast. The Sumatran fault is highly segmented, comprising of nineteen major segments with cross-strike width of step-overs between adjacent segments of about 5 to 12 km. The lengths of the segments range from 20 km to 220 km (Pan et al., 2004). Although Singapore is located in a low seismicity area, the country is exposed to long-distance earthquake originated from Sumatra. A good example of the potential risk posted by the long-distance earthquakes is the Mexico earthquake in 1985, which caused severe damages at an epicentral distance of about 350 km. Figure 1-2 shows the epicenters of earthquakes in the Sumatran region since January 1960 to February 2013. Megawati and Pan (2002) have identified that the maximum credible earthquake (MCE) ground motions in Singapore are likely to be caused by two large earthquakes with different source mechanism. One is a Sumatran fault earthquake with an epicentral distance of around 425 km and a moment magnitude of 7.5 ($M_w=7.5$, $R=425$ km). The other one is a Sumatran

subduction earthquake with an epicentral distance of 700 km and a moment magnitude of 9.0 ($M_w=9.0$, $R=700$ km). The MCE in the Sumatran fault and subduction zone may generate ground motions that pose threat to the high-rise buildings in Singapore, especially for the buildings located at soft-soil site.

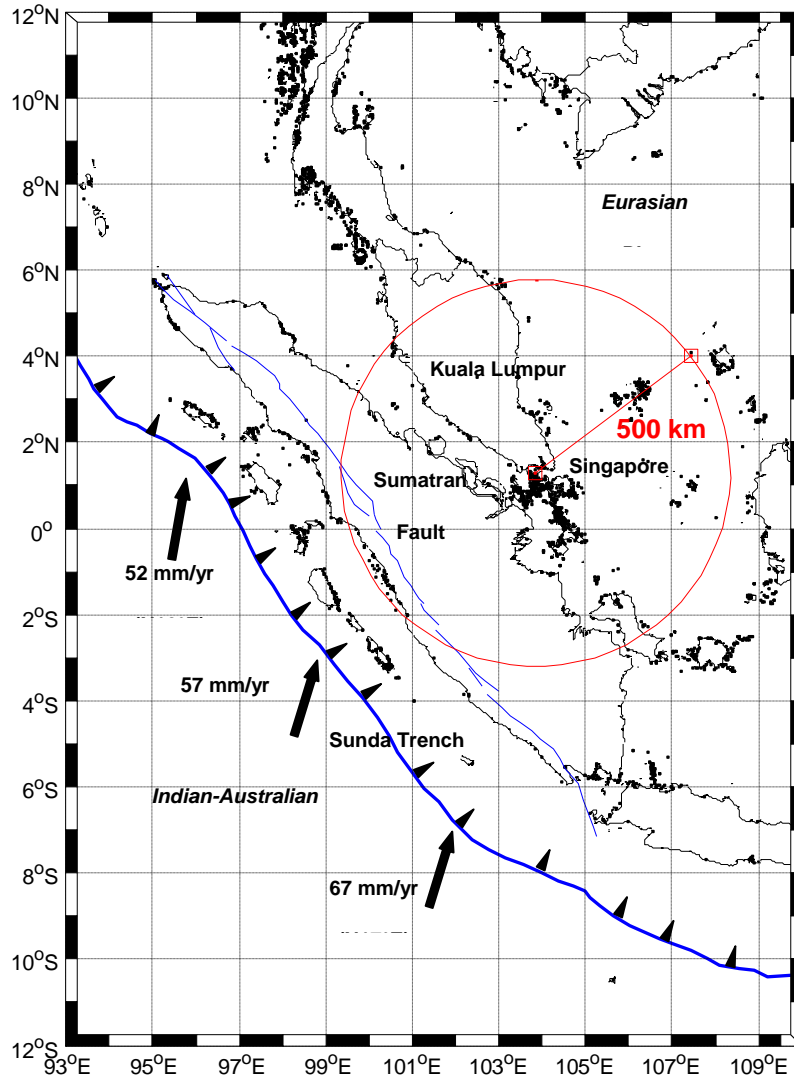


Figure 1-1 The Sunda Trench and Sumatran Fault (Pan et al., 2004)

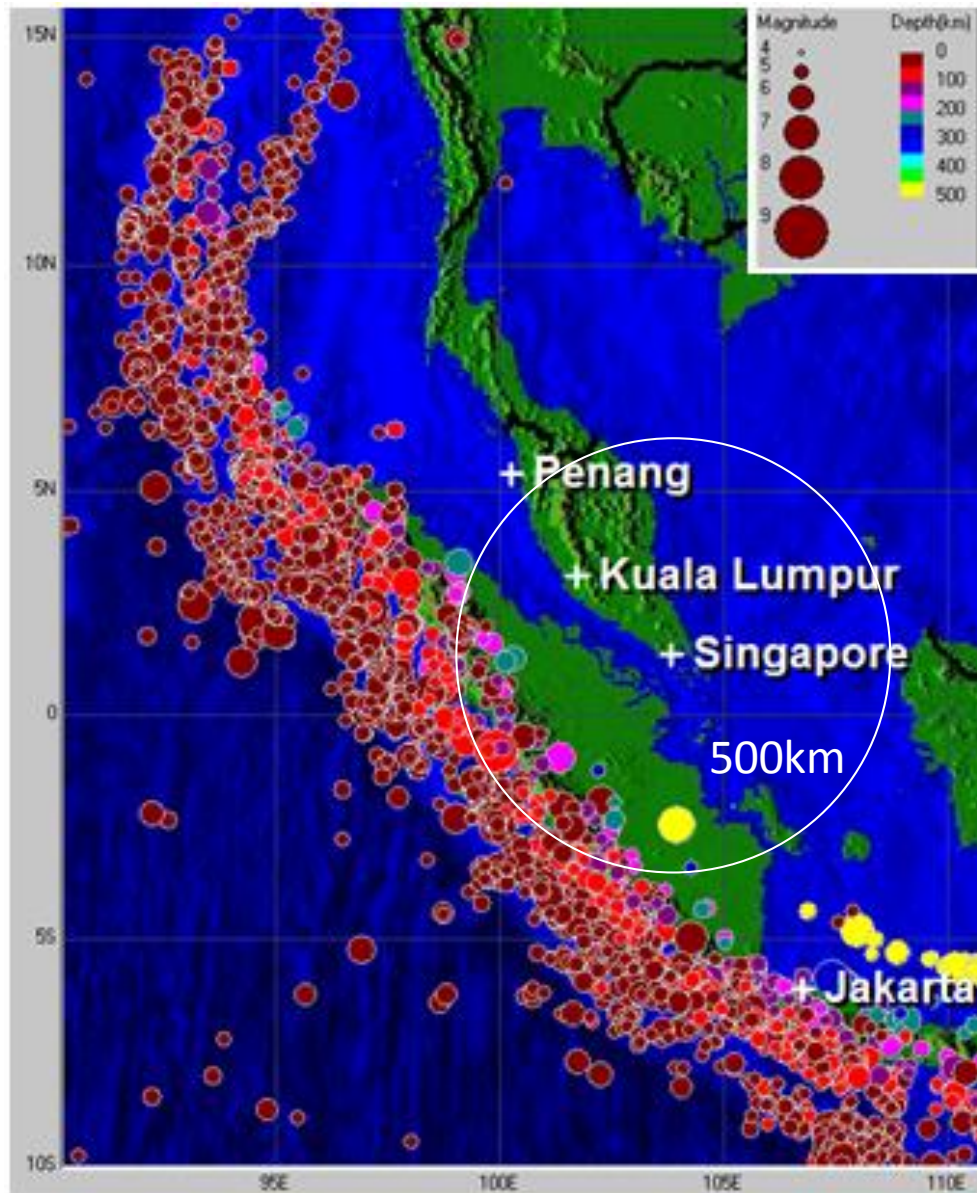


Figure 1-2 Epicenters of earthquakes in the Sumatran region since January 1960 to February 2013. Source: National Earthquake Information Center Database. USGS.

Due to land shortage, more than 80% (HDB, 2012) of the population lives in high-rise public residential buildings, which are reinforced concrete (RC) frame tall buildings. The design of buildings in Singapore is mainly based on the British Standards, BS8110 (BSI, 1997), which is primarily for buildings subjected to gravity load and only recommends a nominal lateral resistance, in terms of a notional horizontal load, equal to 1.5% of the total characteristic dead weight of a building. As seismic-resistant design is not required for most buildings, natural vibration period of buildings is usually not of main concern to the engineers. However, as part of the effort to assess the seismic performance of buildings in Singapore subjected to long-distance Sumatran earthquakes, the natural vibration period of residential buildings in Singapore is needed to estimate the response of buildings when subjected to the long-distance earthquakes from Sumatra (Pan et al., 2014).

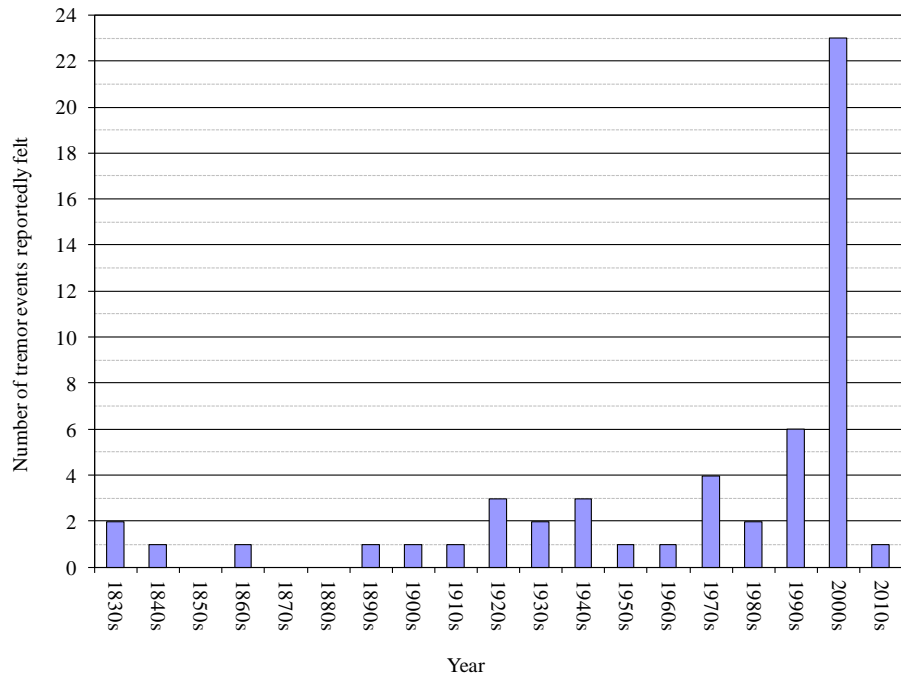
In order to meet the mass housing demands and to reduce the time taken for design and construction, the high-rise public residential buildings are usually designed in a similar way. Thus, most of the high-rise public residential buildings can be represented by some sample buildings with typical geometrical shapes. Based on the geometrical shape and height of buildings, the high-rise public residential buildings can be classified into seven categories. They are: 1) Buildings with rectangular plan (slab blocks), 2) Buildings with square plan (point blocks), 3) Buildings with L-shape plan, 4) Buildings with U-shape plan, 5) Low-rise building, 6) Car Park, and 7) Others. The irregular plan of the high-rise residential buildings may create torsional effects when subjected to lateral load. For some other social function reasons, some unique structural systems, such as open first-storey, appear in the public residential buildings, which may create soft-first-storey effects. It is concerned that the coupling of the torsional and soft-first-storey effects may significantly amplify the responses of the buildings when subjected to MCE ground motions.

Comparing with those expected during MCE events, the weak tremors may not cause casualties to the occupants or damages to the structures. However, the weak but perceivable tremors may have psychological impacts on the occupants, where the occupants may feel discomfort and panic although the tremors are weak and unlikely to cause structural damages. The tremor events reportedly felt in Singapore due to the long-distance Sumatran earthquakes have been increasing dramatically in recent decades. Figure 1-3a shows the number of tremor events reportedly felt in chronological order. Table 1-1 shows the list of tremor events reportedly felt in Singapore in chronological order. Figure 1-3b shows the percentage of population living in high-rise public residential buildings in recent decades (HDB, 2012). The epicenters of earthquakes which caused perceivable tremors in Singapore are shown in Figure 1-4. From Figure 1-3a, it can be seen that the number of tremor events reportedly felt in Singapore due to the long-distance earthquakes increases dramatically from 1970s to 2000s, coinciding with the dramatic increase in the population living in public residential buildings from 1960 to 2010. This may due to the nature of tremors in Singapore which are dominated by long-distance earthquakes originated from Sumatra. The long-distance earthquakes have long-period ground motions, and the predominant period may coincide with the natural vibration period of the high-rise public residential buildings in Singapore. Thus, the high-rise buildings have larger response than low-rise buildings due to resonance effect.

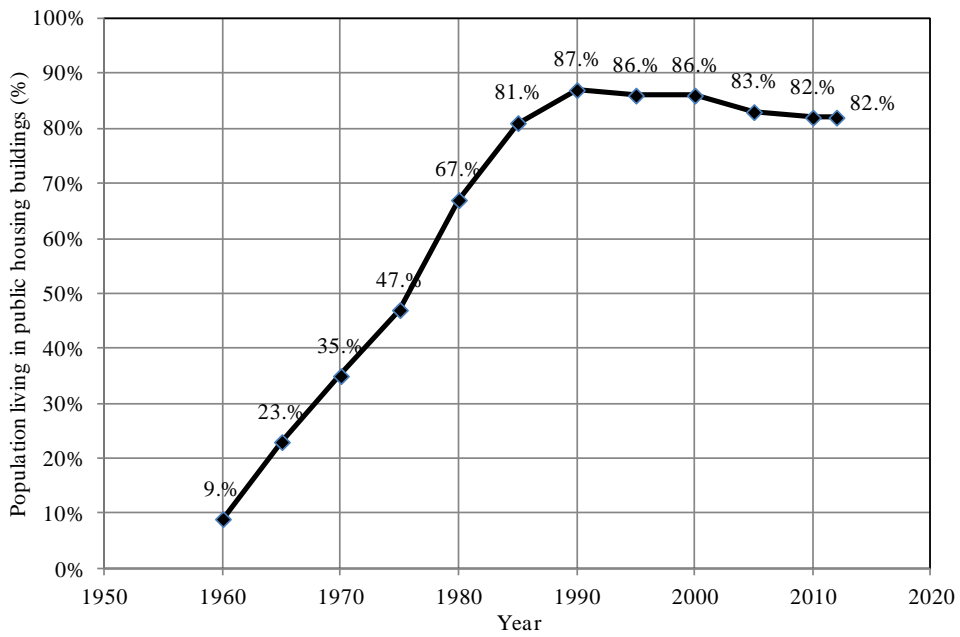
1.2 RESEARCH AIM AND SCOPE

This research aims to assess the seismic performances of typical buildings in Singapore subjected to long-distance Sumatran earthquake ground motions, which include perceivable weak tremors and MCE ground motions. The objectives of this research are listed as follows:

- (a) To propose relationships between natural vibration period and height of buildings in Singapore.
- (b) To propose a methodology for estimating human perception of tremors in high-rise buildings.
- (c) To assess the seismic performance of typical structures in Singapore subjected to ground motions due to the MCE in the Sumatran fault and subduction zone without considering torsional effects.
- (d) To study the torsional response of nonductile structures with soft-first-storey when subjected to the MCE ground motions.



(a)



(b)

Figure 1-3 Number of tremor events reportedly felt per decade (1830-2010) and percentage of population living in public residential buildings in Singapore (1960-2012)

Table 1-1 List of tremor events reportedly felt in Singapore

No.	Event Date and Time (UTC unless specified)		Epicenter		Depth (km)	Distance (km)	Magnitude	Magnitude Type	MMI
	Latitude	Longitude	Latitude	Longitude					
1	1833, Nov. 24, 20:35 (LT)		-3.5	101.5		600	8.75	Mw	II-III
2	1837			-		-		-	I-II
3	1843, Jan. 6, 00:30: (LT)		0	99		630		-	I
4	1861, Feb. 16, 19:25: (LT)		2	98		630	8.4	Mw	IV
5	1892, May 17, 20:10: (LT)			-		-		-	IV-V
6	1909, Jun. 3, 18:40:48.0		-2	101		470	7.2	Ms	IV-V
7	1914, Jun. 25, 19:07:18.0		-4.5	102.5		650	7.5	Ms	IV-V
8	1922, Jan. 31, 09:50: (LT)			-		-		-	II
9	1926, Jun. 28, 03:23:25.0		-1.5	99.5		570	6.75		III-IV
10	1926, Jun. 28, 06:15:41.0		-1	99.5		540	6.5		III
11	1935, Dec. 28, 02:35:22.0		0	98.25		630	7.5	Ms	II
12	1936, Sep. 19, 01:01:47.0		3.75	97.5		750	7	Ms	III
13	1948, Jan. 13, 10:50: (LT)			-		-		-	II-III
14	1948, Dec. 28, 22:30: (LT)			-		-		-	IV
15	1949, Mar. 10, 12:00: (LT)			-		-		-	II
16	1952, Mar. 15, 11:15:47.0		-3.1	102.4		500		-	III
17	1962, Dec. 31, 11:01:04.4		0.5	99.9		440		-	II
18	1971, Feb. 4, 15:33:28.6		0.64	98.83		550	7.1	Ms	IV
19	1972, Dec. 18, 13:57:03.8		-1.83	99.65		570	5.6	mb	I-II
20	1975, Jan. 8, 01:58:55.1		-3	101.78		520	6	mb	III
21	1977, Mar. 8, 23:17:34		0.5	100.04	19.5	440	6.1	Mw	III
22	1984, Nov. 17, 06:49:38.6		-0.23	97.84	24.7	650	7.1	Mw	II-III
23	1986, Aug. 12, 05:09:07		0.17	100.28	15	410	5.4	Mw	II-III
24	1991, Jul. 2, 05:14:35.1		-1.31	99.5	40	510	6.3	Mw	II-III
							5.5	ML	
25	1994, Feb. 16, 17:07:51.7		-5.15	104.27	16.2	720	6.9	Mw	II
26	1994, May 11, 08:18:23.3		-2.16	99.6	15	570	6.4	Mw	III
27	1995, Oct. 6, 18:09:51.2		-1.93	101.31	16.7	455	6.8	Mw	III-IV
28	1996, Oct. 10, 15:21:08.7		3.43	97.78	22.8	697	6.3	Mw	
							5.8	mb	
29	1998, Apr. 1, 17:56:31.8		-0.78	98.84	41.9	548	7	Mw	
							5.7	mb	
30	2000, Jun. 4, 16:28:46.5		-4.73	101.94	7	703	7.9	Mw	
							6.2	mb	

Table 1-1 Con't

31	2000, Jun. 4, 16:39:45.6	-4.672	102.14		690	6.8	mb	
						6.6	Ms	
32	2000, Jun. 7, 23:45:34.9	-4.63	101.82	16.6	692	6.7	Mw	
						6.7	Ms	
						6.2	mb	
33	2001, Feb, 13, 19:28:45.1	-5.4	102.36	21.2	662	7.4	Mw	
34	2004, Feb, 22, 06:46:32.1	-1.68	100.31	50	461	6	Mw	
35	2004 May 11, 08:28:48.28	0.41	97.82	21	600	6.2	Mw	
36	2004 Jul 25, 14:35:19.06	-2.43	103.98	582	405	7.3	Mw	III
37	2004 Dec 26, 00:58:45	3.3	95.98	30	915	9	Mw	II-III
38	2005 Mar 28, 16:09:36.53	2.09	97.11	30	757	9.1	Mw	II
39	2005 Apr 10, 10:29:11.28	-1.68	99.54	12	587	6.7	Mw	II-III
40	2005 Apr 10, 11:14:19.62	1.92	96.48	24	822	6.1	Mw	II
41	2005 Apr 17, 21:23:52.4	-1.66	99.54	23	580	5.4	Mw	III
42	2005 May 14. 05:05:24.60	0.42	98.24	39	631	6.8	Mw	III
43	2006 Jul 27, 11:16:40.37	1.707	97.146	23	747	6	Mw	
44	2006, Aug 11, 20:54:17.3	2.1	96.18	20.6	857	6.2	Mw	
45	2006 Dec 17, 21:39:17.90	0.57	99.83	18.2	454	5.8	Mw	III
46	2007 Mar 6, 03:49:38.9	-0.49	100.5	19	421	6.4	Mw	
47	2007 Mar 6, 05:49:26.92	-0.48	100.55	20	416	6.3	Mw	III
48	2007 Sep 12, 11:10:26.83	-4.44	101.37	34	693	8.5	Mw	III
49	2007 Sep 12, 23:49:03.72	-2.62	100.84	35	548	8.1	Mw	III
50	2007 Sep 13, 03:35:28.72	-2.13	99.63	22	603	7.2	Mw	II
51	2009 Sep 30, 10:16:09	-0.725	99.856	81	460	7.6	Mw	III
52	2009 Oct 1, 01:52:28	-2.508	101.484	15	470	6.6	Mw	II
53	2012 Apr 11, 08:38:37	-2.3	93.1	22	1240	8.6	Mw	I

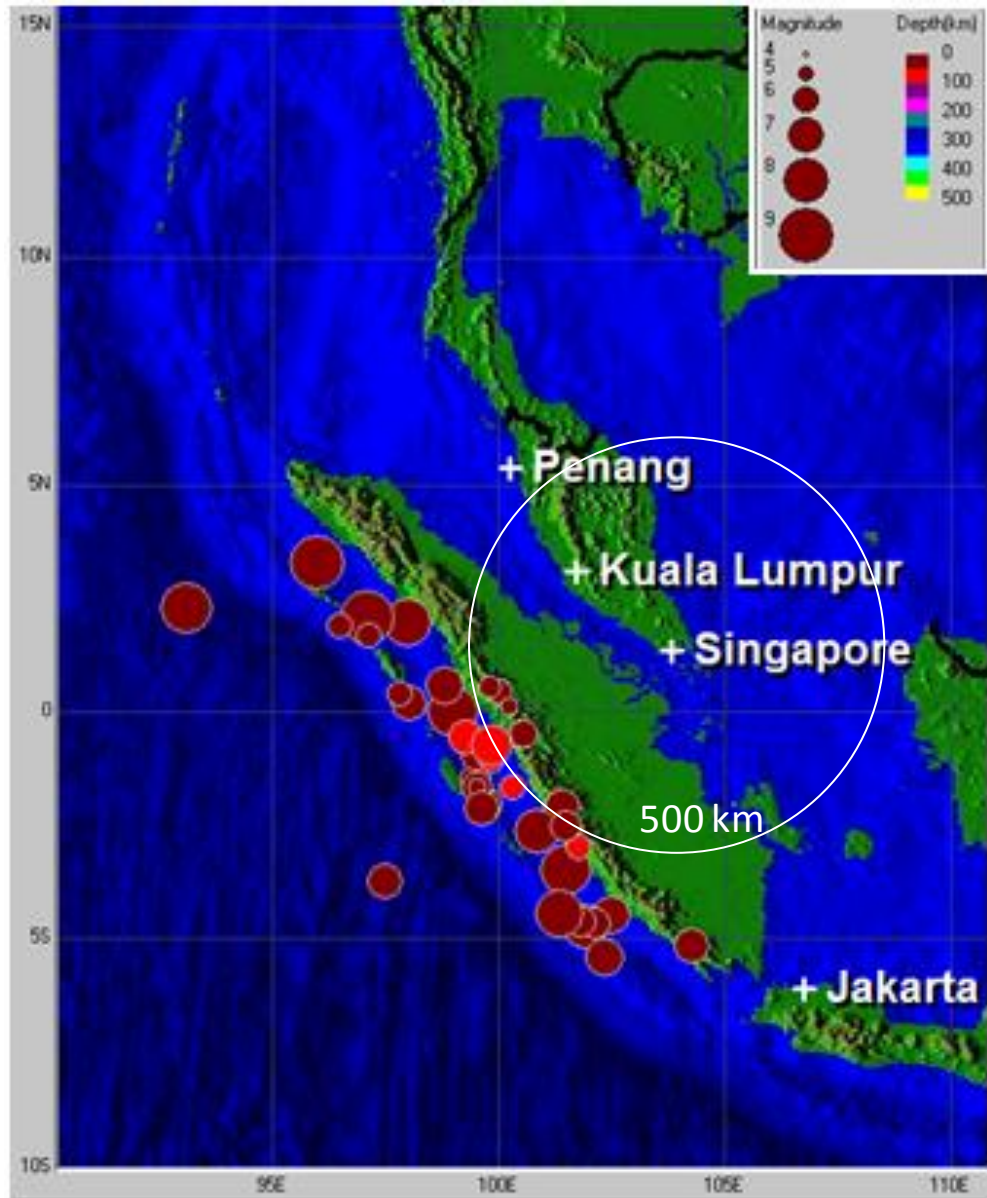


Figure 1-4 Epicenters of earthquakes which caused perceivable tremors in Singapore (year 1833 to 2012)

In view of the research objectives stated above, the scopes of this research are as follows:

- (a) *Empirical relationships between natural vibration period and height of residential buildings in Singapore* are developed by conducting ambient vibration tests (AVT) on high-rise residential buildings. Additional data of natural vibration periods of the instrumented residential buildings obtained from the building response recorded during the September 30, 2009 Sumatran earthquake event are used to validate the proposed period-height relationships. Measurements are conducted to study the influence of buildings on the measured frequency of the surrounding soil.
- (b) *Generic models which represent typical buildings in Singapore* are constructed using *OpenSEEs*. The generic models are made as closely as possible to the existing residential buildings in Singapore. Special attentions are given on the modeling of the beam-column joints.
- (c) *A methodology to estimate the human perception to tremors in high-rise buildings* is proposed. The methodology is based on statistical analysis of analytical results of seismic response of generic models to recorded ground motions. Reports from the local newspaper and the authorities are used to validate the proposed methodology.
- (d) *Seismic performances of the generic models subjected to the MCE ground motions* at rock site and soft-soil site in Singapore are assessed. Pushover analysis is conducted to obtain the seismic capacity of the models.

- (e) *Torsional response of nonductile structures with soft-first-storey* is studied using simplified two-storey model with two-way eccentricities subjected to bi-directional ground motions. Hysteretic model which includes strength deterioration and stiffness degradation properties is used to capture the deterioration of element stiffness and strength.

1.3 ORIGINALITY AND CONTRIBUTIONS

The originality and contributions of the current research are as follows:

- (a) *Empirical relationships between natural vibration period and height of residential buildings in Singapore.* To the best knowledge of the author, there is no published relationship between natural vibration period and height for residential buildings in Singapore. This study will help the engineers and researchers to understand the dynamic characteristic of residential buildings in Singapore. The period-height relationships can help to approximate the response of residential buildings in Singapore subjected to long-distance earthquakes.
- (b) *Methodology to estimate the human perception to tremors in high-rise buildings.* This methodology will play an important role in the development of emergency response plan in the event of tremors due to long-distance earthquakes originated from Sumatra. The methodology will also form a basis for the development of seismic intensity for modern cities where majority of the population lives in high-rise residential buildings.

- (c) *Seismic performances of the generic models subjected to the MCE ground motions.* The behavior of the nonseismically detailed beam-column joints, which can be typically found in residential buildings in Singapore, are included in the generic models. The shear failure of the beam-column joints can be captured from the analysis.

- (d) *Torsional response of nonductile structures with soft-first-storey.* Ductility demand-capacity curves are constructed for nonductile buildings considering coupling of torsional response and soft-first-storey. That can be used to approximately assess the seismic performance of existing structures, and as guidelines for designing new structures in Singapore to withstand the MCE ground motions.

1.4 ORGANIZATION OF THESIS

In *chapter 2*, empirical relationships between natural vibration period and height of residential buildings in Singapore are developed by conducting ambient vibration tests (AVT) on high-rise residential buildings. Measurements are also conducted to study the influence of buildings on the measured frequency of the surrounding soil.

Chapter 3 describes the structural modeling of the generic models which represent typical high-rise residential buildings in Singapore. Special attention is given on the modeling of beam-wide column joint.

Chapter 4 proposes a methodology to estimate human perception to tremors in high-rise buildings. Three tremor events reportedly felt in Singapore are used to validate the proposed methodology.

CHAPTER 1: INTRODUCTION

Chapter 5 presents the seismic performance assessment of the generic models subjected to MCE ground motions at rock site and soft-soil site.

Chapter 6 presents the torsional response of nonductile structures with soft-first-storey subjected to MCE ground motions at soft-soil site.

Chapter 7 presents the summary of this thesis and recommendation for future study.

CHAPTER 2

EMPIRICAL RELATIONSHIPS BETWEEN NATURAL VIBRATION PERIOD AND HEIGHT OF BUILDINGS IN SINGAPORE

In this study, relationships between natural vibration period and height of high-rise residential buildings in Singapore are derived empirically based on a large set of ambient vibration measurement data of 116 buildings and the earthquake response measurement data of 19 additional buildings (Pan et al., 2013). Measurements are also conducted to study the influence of buildings on the measured frequency of the surrounding soil. This study will help the engineers and researchers to understand the dynamic characteristic of residential buildings in Singapore. The relationships will play important roles in seismic assessment of buildings in Singapore to long-distance earthquakes. The period-height relationships can help to approximate the response of residential buildings in Singapore subjected to long-distance earthquakes.

2.1 LITERATURE REVIEW

The natural vibration period of buildings is an essential parameter in earthquake resistant design and performance assessment. The equivalent seismic lateral force in static design method is determined from a design spectrum, which is a function of the fundamental vibration period of a building. For structures with

CHAPTER 2: EMPIRICAL RELATIONSHIPS BETWEEN NATURAL VIBRATION PERIOD AND HEIGHT OF BUILDINGS IN SINGAPORE

moment-resisting frames, the 2012 edition of International Building Code (ICC, 2012) provides the approximate formula as

$$T = C_t H^x \quad \text{Eq. 2-1}$$

where C_t and x represent building period coefficient based on the building types (Table 2-1), T is building fundamental natural vibration period in second, and H is building height in meter. The same units will be used throughout this chapter.

Table 2-1 Building period coefficient, C_t , and exponent, x , for different structural systems according to IBC 2012 (ICC, 2012) (H in meters)

Structural type	C_t	x
Steel moment-resisting frames	0.072	0.8
Concrete moment-resisting frames	0.047	0.9
Eccentrically braced steel frames	0.073	0.75
All other structural systems	0.049	0.75

Hong and Hwang (2000) examined 21 reinforced concrete (RC) moment resisting frame buildings in Taiwan under seismic excitation. The height (number of stories) of the buildings ranged from 8.45 to 77.1 m. The fundamental vibration period in either longitudinal or transverse direction of the buildings in Taiwan was predicted by

$$T = 0.0294H^{0.804} \quad \text{Eq. 2-2}$$

Crowley and Pinho (2006) used SeismoStruct, a fibre-modeling finite element program for seismic analysis of framed structures, to model RC frames

CHAPTER 2: EMPIRICAL RELATIONSHIPS BETWEEN NATURAL VIBRATION PERIOD AND HEIGHT OF BUILDINGS IN SINGAPORE

corresponding to actual buildings (3 to 8 stories) from five different European countries exposed to earthquake action (Greece, Italy, Portugal, Romania, ex-Yugoslavia). The 2D RC frames were modeled as bare frames, fully infilled frames and infilled frames with openings and a weighted average of the period of vibration of these types of frames was then calculated by taking into account their frequency of occurrence within the building stock. The equations for calculating the period of uncracked infilled buildings using a weighted mean period of vibration for each frame, was represented as

$$T = 0.038H \quad \text{Eq. 2-3}$$

The same models with reduced member stiffness were used to create the fully infilled frames and the infilled frames with openings. The study led to a simplified period-height equation for use in the assessment of existing RC buildings, taking due account of the presence of infill panels.

$$T = 0.055H \quad \text{Eq. 2-4}$$

Navarro et al. (2007) performed microtremor measurements at the top of 39 RC buildings ranging from 2 to 9 stories using a three-component seismometer. The empirical relationship obtained for Adra town (Spain) was

$$T = (0.049 \pm 0.001)N \quad \text{Eq. 2-5}$$

where N is the number of stories.

Guler et al. (2008) examined the relationship between the height and fundamental period of vibration of Turkish RC moment resisting frames ranging

CHAPTER 2: EMPIRICAL RELATIONSHIPS BETWEEN NATURAL VIBRATION PERIOD AND HEIGHT OF BUILDINGS IN SINGAPORE

from 4 to 12 stories from ambient vibrations and compared the results with code-specified period formula. A relationship between height and fundamental vibration period of buildings was obtained using low-amplitude vibration according to the following formula:

$$T = 0.026H^{0.90} \quad \text{Eq. 2-6}$$

Gallipoli et al. (2009) performed microtremor measurements on 80 buildings located at Potenza and Senigallia, Italy, belonging to the most representative and common typologies. They were selected to cover a wide span of characteristics such as design, construction age and height. The results obtained using microtremor measurements were compared with those of earthquakes using four different techniques: horizontal-to-vertical spectral ratio (HVSR), standard spectral ratio (SSR), non-parametric damping analysis (NonPaDAn) and half bandwidth method (HBW). It was reported that the estimates from SSR, HVSR, NonPaDAn and HBW were in agreement with each other. The results also showed that the theoretical period-height relationships overestimated the experimental data obtained in this study.

Gallipoli et al. (2010) presented the results of ambient noise measurements inside buildings in four European countries performed by the participants of NATO Science for Peace project. The analyzed database comprised 65 buildings from Italy, 47 from Slovenia, 62 from Croatia and 70 from Republic of Macedonia. The height of the buildings ranged from 1 to 20 stories. The result was strikingly similar to that obtained by Navarro et al. (2007) for Spanish RC buildings. The best statistical result was provided in the form

$$T = 0.016H \quad \text{Eq. 2-7}$$

CHAPTER 2: EMPIRICAL RELATIONSHIPS BETWEEN NATURAL VIBRATION PERIOD AND HEIGHT OF BUILDINGS IN SINGAPORE

Michel et al. (2010) recorded ambient vibrations at about 60 buildings of various types (RC and masonry) in Grenoble City (France). The data were used together with 26 RC buildings of Grenoble and 28 RC buildings in Nice (France). A simple formula was derived from simple regression on the data

$$T = 0.013H = 0.039N \quad \text{Eq. 2-8}$$

2.2 SINGAPORE GEOLOGY

The geological formation will be used to group the measured buildings in the derivation of relationships between natural vibration period and height of buildings in Singapore. In Singapore, there are ten geological formations recognized. They are: Kallang Formation, Tekong Formation, Huat Choe Formation, Old Alluvium, Dyke Rocks, Jurong Formation, Bukit Timah Granite, Palaeozoic Volcanics, Gombak Granite and Sajahat Formation (DSTA, 2009). Among the ten geological formations, four of them cover most of the Singapore main island. They are the Bukit Timah Granite, Jurong Formation, Old Alluvium and Kallang Formation. The surface geological map of Singapore is shown in Figure 2-1.

The Bukit Timah Granite occupies the central and the central north of Singapore. They are covered by residual soil, with depth ranging from 10 to 60 meters. The Jurong Formation consists of sedimentary rocks of Upper Triassic and lower to middle Jurassic age. The eastern part of the Island is covered by the Old Alluvium and the Kallang Formation, the two major Quaternary units, underlain by the extension of the Bukit Timah Granite. The Old Alluvium consists of loose sand and fine gravel with silt and clay lenses. The Kallang Formation consists of Holocene sediments of marine, alluvial, littoral and estuarine origin. The thickness

of these Quaternary deposits varies, at some sites more than 185 meters. (DSTA, 2009)

2.3 METHODOLOGY

There are two different approaches to conduct dynamic tests on structures: forced vibration test (FVT) and ambient vibration test (AVT) (Hudson, 1997; Brownjohn, 2003). Because of the difficulties associated with the logistics and machinery needed for FVT, AVT has become a major approach in recent researches on determining the dynamic characteristics of large buildings. Ambient vibrations of buildings could also be caused by wind and internal sources (machines, pedestrians, etc). The observed vibration properties of structures integrate all the complexity of these structures including the load bearing system, heavy and stiff non-structural elements, weather (Clinton et al., 2006) and also soil-structure interaction (Trifunac et al., 1999; Gallipoli et al., 2004; Giulio et al., 2005). In this study, AVT is used to determine the natural vibration period of high-rise residential buildings in Singapore. Figure 2-2 shows the photos of a 25-storey point block and a 16-storey slab block.

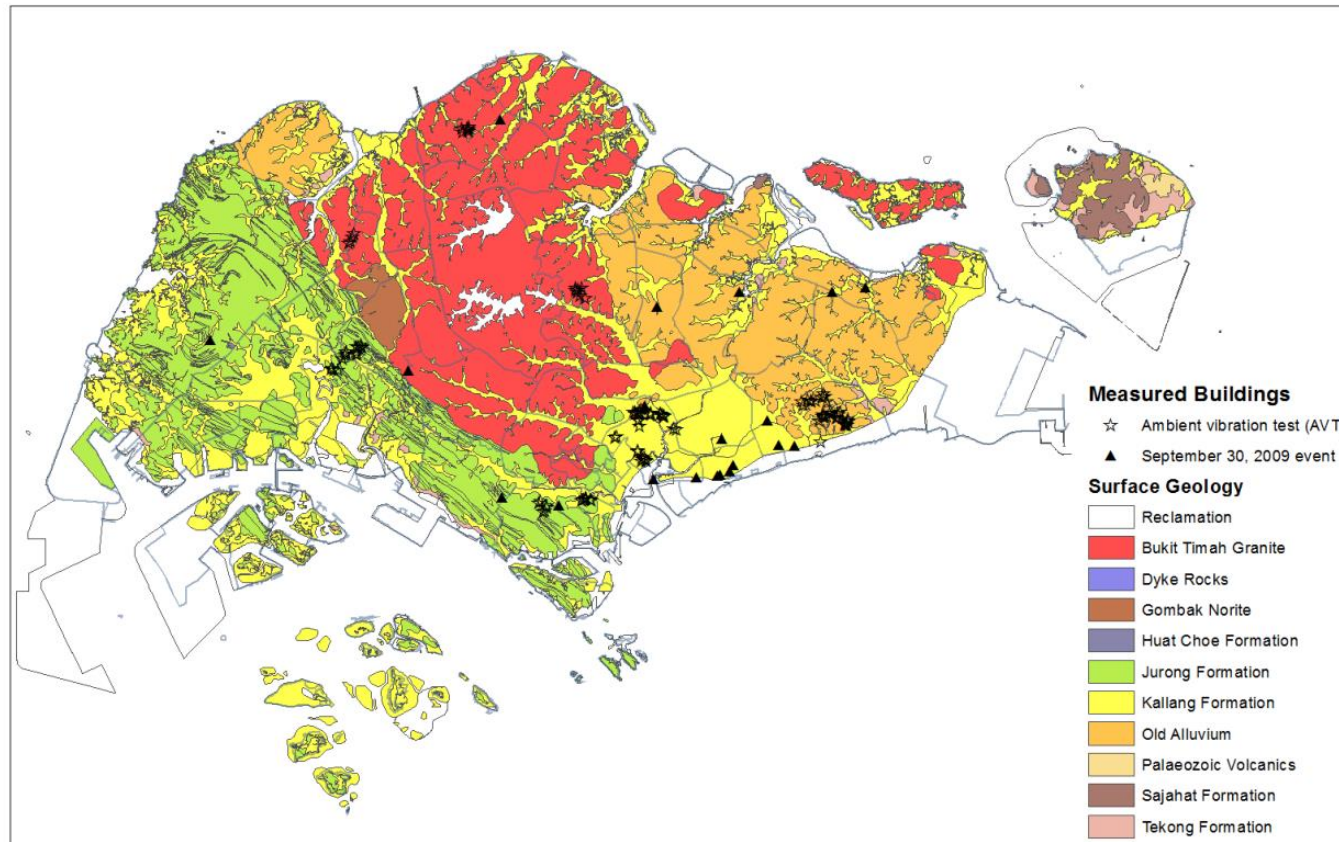


Figure 2-1 Geological map of Singapore (DSTA, 2009) overlaid with the location of the measured buildings



(a) (b)
Figure 2-2 Photos of (a) 25-storey point block; (b) 16-storey slab block

2.3.1 INSTRUMENTATION

To conduct AVT in high-rise residential buildings, a tri-axial velocity seismometer is used to measure the vibration in buildings. The models of the recorder and the velocity seismometer are HKS-9550 and VSE-15D6, respectively. The tri-axial seismometer consists of 2 horizontal sensors which are perpendicular to each other (Channel 1 and Channel 2) and a vertical sensor. The velocity seismometer is able to measure vibration with frequency range from 0.2 to 70 Hz and with magnitude range from 1×10^{-7} to 0.1 m/s. Figure 2-3 shows a set of the tri-axial velocity seismometer. The measuring points are chosen at the highest floor of

CHAPTER 2: EMPIRICAL RELATIONSHIPS BETWEEN NATURAL VIBRATION PERIOD AND HEIGHT OF BUILDINGS IN SINGAPORE

the buildings as there appears to have the largest amplitude of vibration. The sensor is located near the lift core, which is the main contributor to the stiffness of a building. Occasionally, due to logistics problem and space available, the measuring points are moved to staircase, which is usually next to the lift core. For buildings with rectangular plan (slab blocks), Channel 1 of the sensor is aligned parallel to the transverse direction (shorter edge) of the buildings, while Channel 2 is aligned parallel to the longitudinal direction (longer edge). For buildings with square plan (point blocks), the Channel 1 is aligned pointing to the direction of the lift entrance while Channel 2 is aligned perpendicular to Channel 1. For buildings other than slab blocks and point blocks, the sensor is aligned to the direction convenient to identify. The sensor is leveled each time before being put into operation in order to capture the signals in the horizontal and vertical directions accurately. Every measurement contains 10 minutes of recoded data.



Figure 2-3 A set of tri-axial velocity seismometer

2.3.2 DATA PROCESSING

There are several methods which are commonly used in determining the natural vibration period of buildings from ambient vibration data (Gallipoli et al. 2009). In this study, the Horizontal-to-Vertical Spectra Ratio (HVSr) is used to identify the natural vibration period of high-rise residential buildings in Singapore.

The HVSr method is a common method used in microtremors analysis and ambient vibration analysis. The HVSr method is based on the assumption that the spectral amplitude of the vertical component of motion are relatively insensitive to site effects and that contain mainly the effect of the source and attenuation along the source-station path. Thus, the results of the ratio between the horizontal and vertical spectral will eventually have the effects of attenuation and source eliminated. In the current study, HVSr method is used to estimate the natural vibration period of buildings. The excitation sources are mainly wind excitation and human activities. The horizontal spectrum contains mainly the vibration characteristics of the building measured, while the vertical spectrum contains mainly the effect of excitation sources. By dividing the horizontal to the vertical spectra, the effect of excitation source will eventually be eliminated. The H/V ratio can be calculated as follows:

$$Z(f) = \frac{H(f)}{V(f)} \quad \text{Eq. 2-9}$$

where $Z(f)$ represents the building response at frequency f ; $H(f)$ and $V(f)$ are the spectral amplitudes of the horizontal and vertical component at frequency f , respectively.

Nakamura (1989) used HVSR to evaluate sediment-induced amplifications using microtremors. Castro et al. (1998) used the method to estimate the characteristic frequency of vibration of two dams located in southern Italy, using spectral amplitude of 13 local earthquakes recorded by three-component digital stations installed on top of the dams and on the free field. Gallipoli et al. (2004) made a series of microtremors measurements in the buildings and civil structures using HVSR to investigate the effect of soil-structure interaction of tall buildings. It was confirmed that HVSR is able to detect building fundamental modes and once known the building natural frequency. Di Giulio et al. (2005) performed measurements on the top, at the base, and half building height away from the buildings at the southern Tyrrhenian sea, 40 km off the coast of Palermo. The analysis showed that the natural vibration frequency of the building cannot be found from the HVSR of the free-field microtremor measurement.

2.4 RESULTS

The HVSR are obtained by splitting the ambient vibrations recorded at the top of buildings (Channel 1, Channel 2 and Vertical) into slices. The length of each slice is 20 seconds and Fast Fourier Transformation (FFT) is then performed on these slices. Ratio between the averaged FFT in the horizontal to vertical direction (HVSR) is then calculated for each slice. The HVSR of all the slices are averaged over the whole response history. Figure 2-4 shows the HVSR of the recorded ambient vibration at the top of the 16-storey slab block and 25-storey point block (Figure 2-2). The natural frequency (period) can be obtained by simple peak-picking method. From Figure 2-4(a) and 2-4(b), the natural frequency (period) of the 16-storey slab block in Channel 1 is 1.03 Hz (0.97 sec) while in Channel 2 is 1.13 Hz (0.89 sec). From Figure 2-4(c) and 2-4(d), the natural frequency (period) of the 25-storey point block in Channel 1 is 0.78 Hz (1.28 sec) while in Channel 2 is 0.73 Hz (1.37 sec). Thus the natural period of the 1st mode of vibrations of the 16-

CHAPTER 2: EMPIRICAL RELATIONSHIPS BETWEEN NATURAL VIBRATION PERIOD AND HEIGHT OF BUILDINGS IN SINGAPORE

storey slab block and the 25-storey point block are 0.97 sec and 1.37 sec respectively.

Figures 2-5 and 2-6 are spectrogram plots of the entire response history of data recorded on top of a 25-storey point block and a 16-storey slab block respectively. Each spectrogram is made by dividing the velocity time series into length of time and taking Fast Fourier Transform (FFT) of this time window. The magnitude of the FFT is then represented by a color contour along the y axis at the time on the x axis to which the FFT corresponds. The length of each slice of time is 20 s with 2.5 s overlap between slices. From Figure 2-5, it is shown that the first vibration frequency (period) in both Channel 1 and Channel 2 is around 0.8 Hz (1.2 sec). From Figure 2-6, it is shown that the first vibration frequency (period) in both Channel 1 and Channel 2 is around 1.0 Hz (1.0 sec). It is shown that the frequency content of the recorded data is consistent over the whole time length, which means that the natural vibration period (or frequency) obtained from the measurement are reliable.

CHAPTER 2: EMPIRICAL RELATIONSHIPS BETWEEN NATURAL VIBRATION PERIOD AND HEIGHT OF BUILDINGS IN SINGAPORE

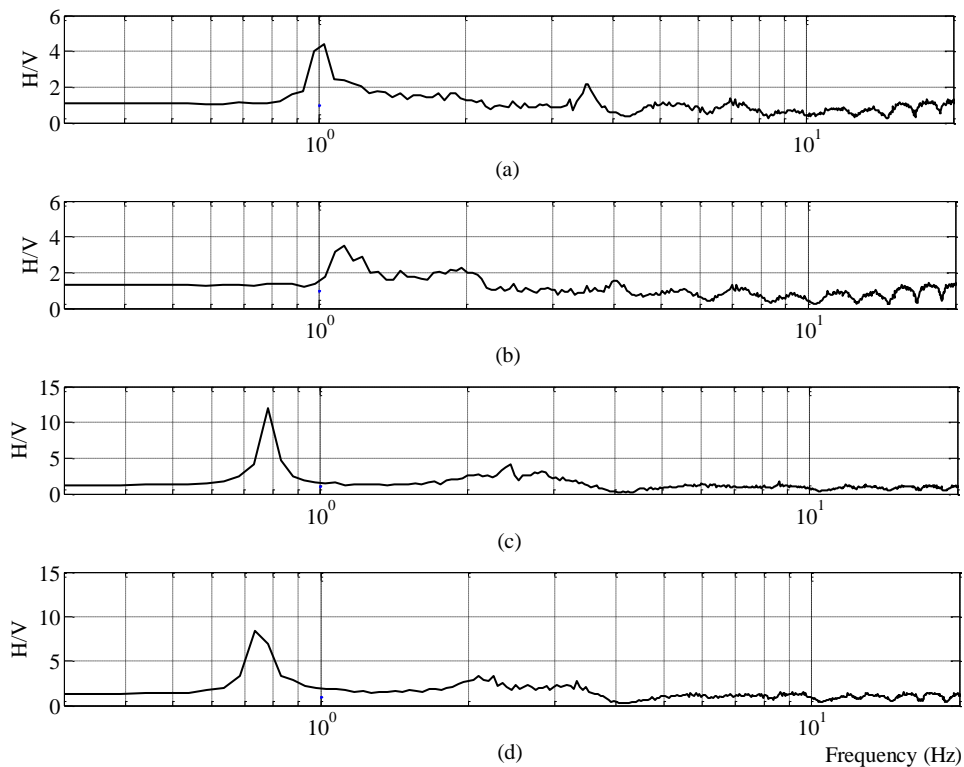


Figure 2-4 The HVSR plots of the AVT data at: (a) top of 16-storey slab block in channel 1; (b) top of 16-storey slab block in channel 2; (c) top of 25-storey point block in channel 1; (d) top of 25-storey point block in channel 2

There are in total 116 high-rise residential buildings investigated. The buildings are chosen based on site properties, buildings geometry and number of stories. Table 2-2 summarizes the results of the AVT measurements of the 116 high-rise residential buildings. In the geometry column, L= Buildings with L-shape plan, S= Buildings with square plan (point block), R= Buildings with rectangular plan (slab block), and O= other types of geometry. In the soil conditions column, JF= Jurong Formation, KF= Kallang Formation, OA= Old Alluvium, BT= Bukit Timah Granite. The height of buildings is estimated based on typical storey height of 3.6 m for the first story and 2.8 m for the second story and above. The locations of the measured buildings are shown in Figure 2-1. The block number, street name of the measured buildings are shown in Appendix A

CHAPTER 2: EMPIRICAL RELATIONSHIPS BETWEEN NATURAL VIBRATION PERIOD AND HEIGHT OF BUILDINGS IN SINGAPORE

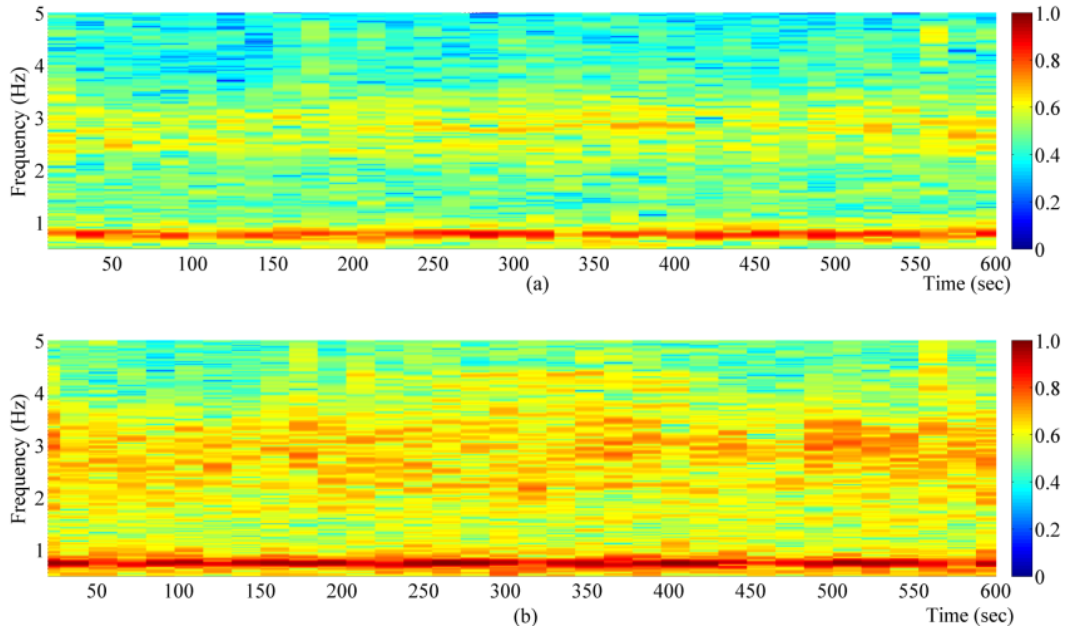


Figure 2-5 Spectrogram of natural frequency observed at top of a 25-storey point block in (a) Channel 1; (b) Channel 2

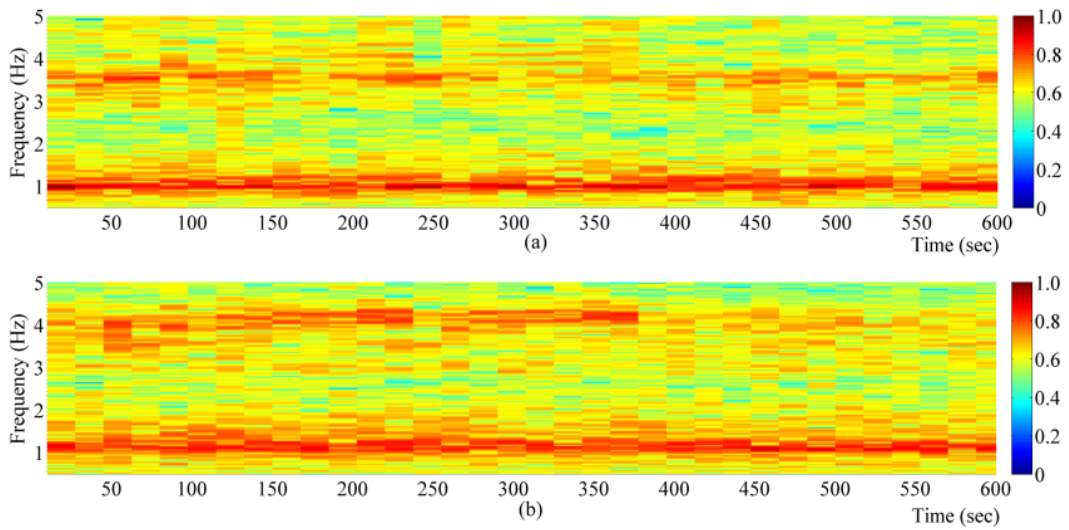


Figure 2-6 Spectrogram of natural frequency observed at top of a 16-storey slab block in (a) Channel 1; (b) Channel 2

*CHAPTER 2: EMPIRICAL RELATIONSHIPS BETWEEN NATURAL VIBRATION PERIOD AND
HEIGHT OF BUILDINGS IN SINGAPORE*

Table 2-2 Summary of AVT measurements

No.	Soil Conditions	Geometry	Number of Storey, N	Height, H (m)	Natural Period, T (s)
1	JF	L	8	23.2	0.36
2	JF	S	25	70.8	1.02
3	JF	S	25	70.8	1.01
4	JF	S	30	84.8	1.37
5	JF	S	30	84.8	1.32
6	JF	R	11	31.6	0.49
7	JF	R	12	34.4	0.44
8	JF	O	17	48.4	0.78
9	KF	O	25	70.8	1.37
10	KF	O	25	70.8	1.37
11	JF	R	8	23.2	0.43
12	JF	L	10	28.8	0.51
13	JF	R	13	37.2	0.61
14	JF	S	25	70.8	1.08
15	JF	S	25	70.8	1.05
16	JF	R	12	34.4	0.57
17	JF	R	4	12.0	0.22
18	OA	R	4	12.0	0.24
19	OA	L	12	34.4	0.53
20	OA	R	13	37.2	0.65
21	OA	R	4	12.0	0.24
22	OA	R	13	37.2	0.63
23	OA	L	13	37.2	0.56
24	OA	R	13	37.2	0.63
25	OA	L	12	34.4	0.54
26	OA	L	12	34.4	0.58
27	OA	R	16	45.6	0.72
28	OA	R	16	45.6	0.72
29	OA	R	15	42.8	0.65
30	OA	R	16	45.6	0.67
31	OA	R	16	45.6	0.68
32	OA	R	16	45.6	0.66
33	OA	R	15	42.8	0.72
34	OA	R	16	45.6	0.70
35	OA	L	20	56.8	0.73
36	OA	L	23	65.2	0.97
37	OA	L	21	59.6	0.87
38	OA	L	24	68.0	0.93
39	OA	R	12	34.4	0.54
40	OA	S	25	70.8	1.14
41	OA	R	11	31.6	0.56
42	OA	R	12	34.4	0.54
43	OA	R	9	26.0	0.44

*CHAPTER 2: EMPIRICAL RELATIONSHIPS BETWEEN NATURAL VIBRATION PERIOD AND
HEIGHT OF BUILDINGS IN SINGAPORE*

Table 2-2 Con't

No.	Soil Conditions	Geometry	Number of Storey, N	Height, H (m)	Natural Period, T (s)
44	OA	O	12	34.4	0.58
45	OA	R	12	34.4	0.54
46	OA	R	13	37.2	0.58
47	OA	O	13	37.2	0.62
48	OA	R	19	54.0	0.85
49	OA	O	12	34.4	0.55
50	OA	R	14	40.0	0.67
51	JF	R	16	45.6	0.75
52	KF	R	20	56.8	1.14
53	JF	S	25	70.8	1.08
54	JF	L	18	51.2	0.69
55	JF	R	9	26.0	0.36
56	JF	R	16	45.6	0.66
57	KF	R	14	40.0	0.87
58	KF	L	13	37.2	0.80
59	KF	R	14	40.0	0.85
60	KF	R	16	45.6	0.87
61	KF	O	12	34.4	0.60
62	JF	R	12	34.4	0.54
63	JF	R	12	34.4	0.57
64	JF	R	12	34.4	0.55
65	JF	R	16	45.6	0.76
66	JF	R	17	48.4	0.85
67	JF	R	20	56.8	0.95
68	JF	S	26	73.6	1.23
69	KF	L	12	34.4	0.49
70	KF	O	10	28.8	0.65
71	KF	L	11	31.6	0.69
72	KF	R	12	34.4	0.70
73	KF	R	14	40.0	0.79
74	KF	R	12	34.4	0.78
75	KF	L	12	34.4	0.72
76	KF	O	15	42.8	1.02
77	KF	L	12	34.4	0.68
78	KF	S	25	70.8	1.32
79	KF	L	13	37.2	0.85
80	KF	R	13	37.2	0.85
81	KF	R	13	37.2	0.75
82	KF	O	18	51.2	0.89
83	KF	R	13	37.2	0.76
84	KF	O	21	59.6	1.02
85	KF	S	21	59.6	1.02

*CHAPTER 2: EMPIRICAL RELATIONSHIPS BETWEEN NATURAL VIBRATION PERIOD AND
HEIGHT OF BUILDINGS IN SINGAPORE*

Table 2-2 Con't

No.	Soil Conditions	Geometry	Number of Storey, N	Height, H (m)	Natural Period, T (s)
86	KF	S	25	70.8	1.20
87	KF	R	12	34.4	0.55
88	KF	O	21	59.6	0.97
89	KF	O	19	54.0	0.89
90	KF	R	16	45.6	0.78
91	KF	S	20	56.8	1.08
92	KF	S	25	70.8	1.32
93	KF	R	16	45.6	1.14
94	KF	R	16	45.6	0.97
95	KF	R	20	56.8	1.28
96	KF	R	12	34.4	0.73
97	KF	R	14	40.0	0.91
98	KF	R	14	40.0	0.87
99	BT	O	13	37.2	0.56
100	BT	L	12	34.4	0.51
101	BT	L	12	34.4	0.51
102	BT	R	9	26.0	0.37
103	BT	O	11	31.6	0.47
104	BT	O	10	28.8	0.51
105	BT	R	12	34.4	0.58
106	BT	R	10	28.8	0.50
107	BT	R	12	34.4	0.48
108	BT	O	11	31.6	0.50
109	BT	R	12	34.4	0.51
110	BT	R	11	31.6	0.55
111	BT	R	12	34.4	0.58
112	BT	R	12	34.4	0.58
113	BT	R	12	34.4	0.61
114	BT	O	10	28.8	0.54
115	BT	O	16	45.6	0.73
116	BT	O	11	31.6	0.60

The question is posed on whether or not plan aspect ratio should be included as a parameter in the derivation of the relationships. Hong and Hwang (2000) included the horizontal dimension of a building in the regression analysis. They concluded that height of a building played an important role in predicting the fundamental vibration period, compared with the length and width of the building. In this study, a 20-storey slab block and a 20-storey point block, which has rectangular plan and square plan respectively, are chosen for comparison. Figure 2-7 shows the HVSR of the recorded ambient vibration on top of the 20-storey point block and the 20-storey slab block located at soft-soil site. The upper-panel of Figure 2-7 shows the HVSR of the recorded ambient vibration in Channel 1 (parallel to the transverse direction, i.e. shorter edge) and the lower-panel shows the HVSR of the recorded ambient vibration in Channel 2 (parallel to the longitudinal direction, i.e. longer edge). For point block, since the building is square in plan, the channel 1 and channel 2 are parallel to the two edges respectively. From Figure 2-7(a), it can be seen that the natural vibration period (frequency) of the point block and the slab block recorded in Channel 1 are 1.08 sec (0.93 Hz) and 1.14 sec (0.88 Hz) respectively. From Figure 2-7(b), the natural vibration period (frequency) of the point block and the slab block in Channel 2 are 0.97 sec (1.03 Hz) and 0.79 sec (1.27 Hz) respectively. The natural vibration period of the point block and the slab block in transverse direction is very close, whilst the natural vibration period of the point block in longitudinal direction are around 20% longer than the natural vibration period of the slab block in the same direction. This is most probably caused by the longer dimension of the slab block in the longitudinal direction, which has contributed extra stiffness to the building in the longitudinal direction. In contrast, point block has relatively symmetrical dimension, which resulted in the natural vibration period of the point block in both directions very close. However, the natural vibration period of 1st mode of vibrations of the two buildings is still very close (1.08 sec and 1.14 sec). Thus it is concluded that the effect of the plan

aspect ratio of the buildings can be omitted from the derivation for the 1st mode of vibration period.

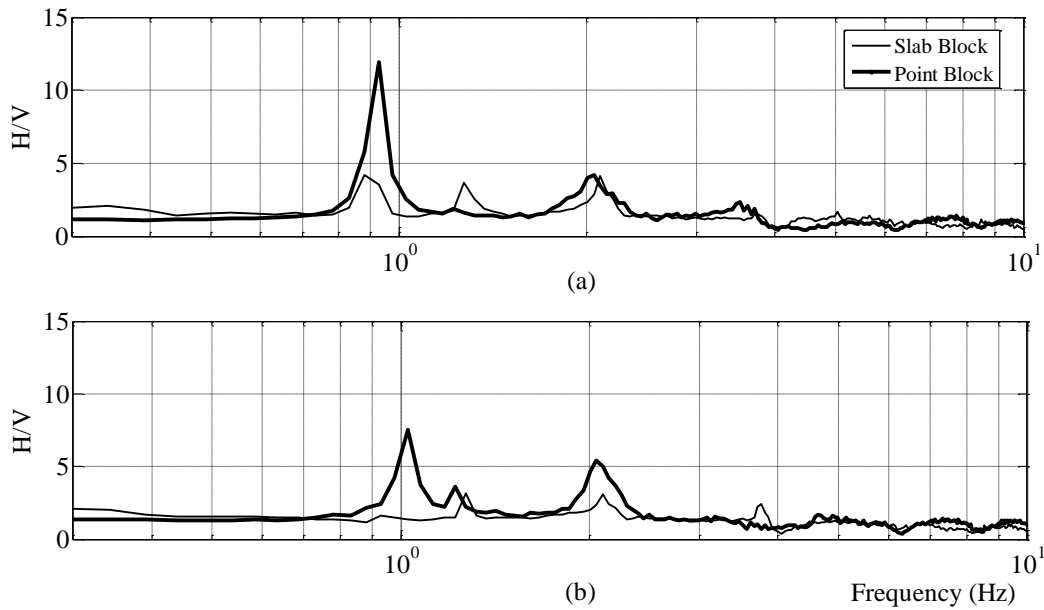


Figure 2-7 Comparison between the HVSR of the ambient vibrations recorded on top of a 20-storey point block and a 20-storey slab block located at soft-soil site in: (a) Transverse direction (Channel 1); (b) Longitudinal direction (Channel 2)

The typical method for deriving the empirical relationships relating period and height of buildings is by performing regression analysis on the data. The typical formula for tackling this problem is:

$$T = \alpha N^{\beta} \quad \text{Eq. 2-10}$$

where N is the number of stories or the height of buildings in meter, T is the natural vibration period of buildings in second, α and β are the regression coefficients. Regression analysis is carried out for buildings with different site properties, which are Bukit Timah Granite (BT), Jurong Formation (JF), Kallang Formation (KF) and

CHAPTER 2: EMPIRICAL RELATIONSHIPS BETWEEN NATURAL VIBRATION PERIOD AND HEIGHT OF BUILDINGS IN SINGAPORE

Old alluvium (OA) (Figure 2-8). Figure 2-8 depicts the results of AVT measurements, with heights and number of stories in the x-axis and natural vibration period of buildings in the y-axis. It can be seen that the regressions for natural vibration period of buildings located at Jurong Formation, Old Alluvium and Bukit Timah Granite are very close to one another (Figure 2-8). However, for buildings located at Kallang Formation, the natural vibration period is generally longer than the buildings located at Jurong Formation, Old Alluvium and Bukit Timah Granite. Thus the data measured at Kallang Formation can be treated as a group (soft-soil) while data measured at Jurong Formation, Old Alluvium and Bukit Timah Granite as another group (firm-soil) (Figure 2-9). Thus the final formulas are presented in the following form as:

For soft-soil site

$$T = 0.0927N^{0.8183} \quad \text{Eq. 2-11}$$

$$T = 0.0372H^{0.8325} \quad \text{Eq. 2-12}$$

For firm-soil site

$$T = 0.0657N^{0.8607} \quad \text{Eq. 2-13}$$

$$T = 0.0244H^{0.8840} \quad \text{Eq. 2-14}$$

where T is natural vibration period of buildings in seconds; H is height of the buildings in meter; and N is number of stories of buildings. Comparing the regression relationships for buildings located at soft-soil site with firm-soil site, it is noticeable that the natural vibration period estimated from period-height

CHAPTER 2: EMPIRICAL RELATIONSHIPS BETWEEN NATURAL VIBRATION PERIOD AND HEIGHT OF BUILDINGS IN SINGAPORE

relationship for buildings located at soft-soil site is about 40% longer than that estimated using relationship for buildings located at firm-soil site. Figure 2-9 shows the plot of mean and standard deviation of the buildings measured. It should be noted that the relationships derived are only applicable to buildings with number of stories ranges from 4 to 30 stories.

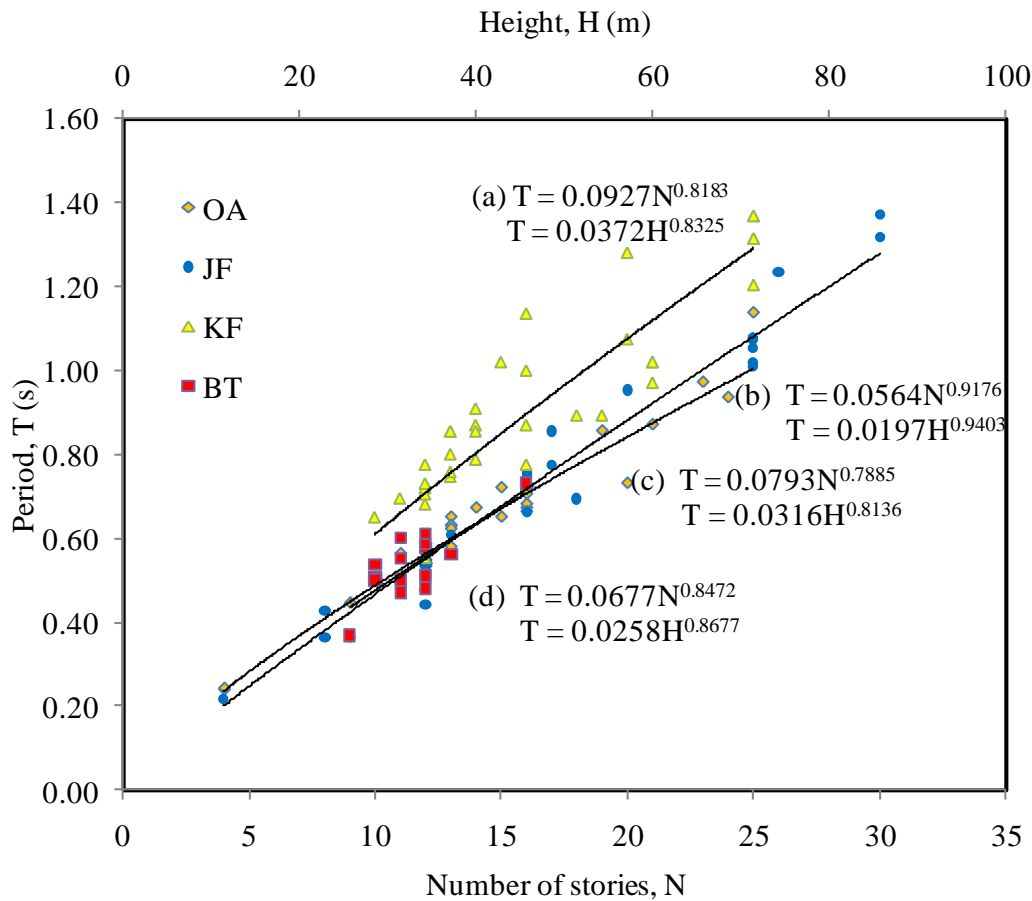


Figure 2-8 Summary of AVT measurements with height and number of storey as x-axis, natural period as y-axis and regression analysis is done for (a) Kallang Formation (KF); (b) Jurong Formation (JF); (c) Old Alluvium (OA); (d) Bukit Timah Granite (BT)

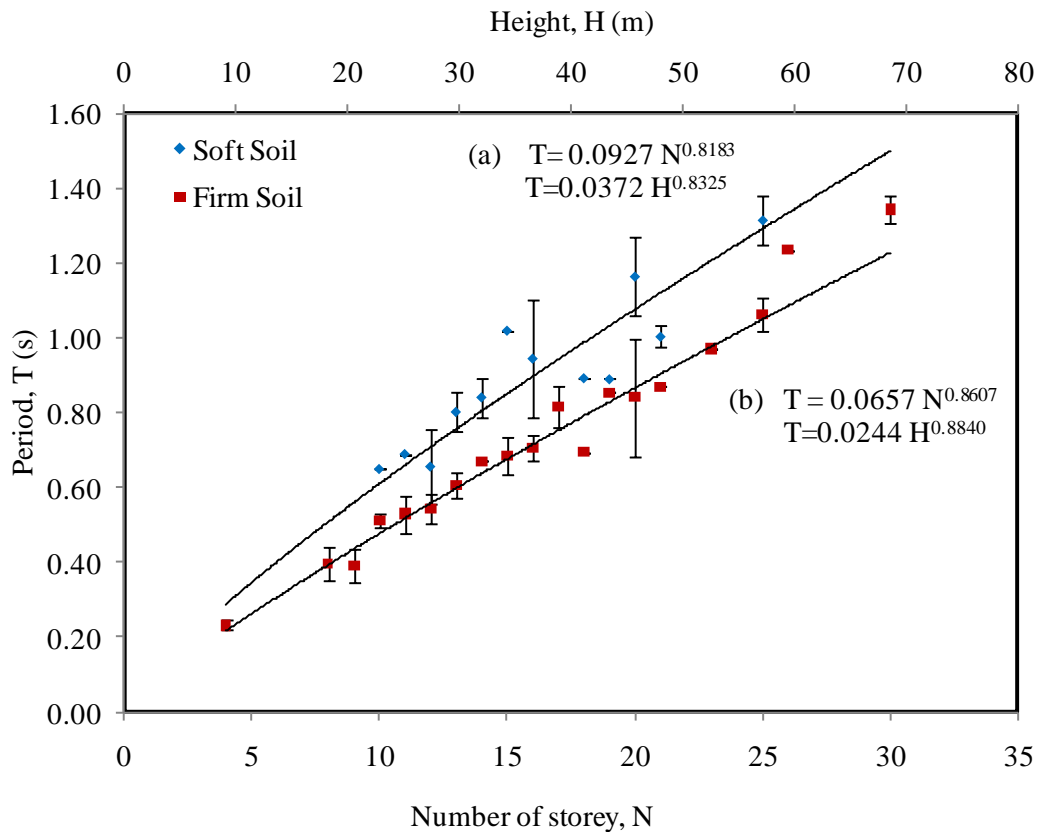


Figure 2-9 Plot of mean and standard deviation for buildings at (a) soft-soil site; (b) firm-soil site

2.5 EFFECT OF SOIL-STRUCTURE INTERACTION

In previous section, regression analyses have been performed on the data collected and empirical period-height relationships are derived for buildings located at soft-soil site and firm-soil site separately. It can be seen that for buildings with the same height, the one located at soft-soil site will have a natural vibration period 40% longer than buildings located at firm-soil. This is most probably caused by the soil-structure interaction of the buildings located at soft-soil site, where the bases of the buildings are not “fixed” at the ground surface and they may move together with the soft-soil beneath them. In the present study, the soil-structure interaction has

been shown to have played an important role in affecting the measured natural vibration period of the buildings (Figure 2-9). Gallipoli et al. (2004) studied the dynamic interaction between soil and structure by performing measurements in a water tower structure in Macerate, Italy. They conducted HVSR measurements on the top and at the base, and at 12, 30 and 100 m away from the base of water tower structure. They found that the influence of the tower remained even at a distance of twice the heights of the structure. Mucciarelli et al. (1996) conducted HVSR measurements at the Hera Lacinia Column site, in the Calabria region of Italy. It was found that a peak representing the frequency of the column was present in free field measurements taken near the column. This peak became insignificant at a distance approximately equal to the height of the column.

In this study, microtremor measurements are also carried out to study the influence of buildings in affecting the measured frequency of soil surrounding the buildings. For this purpose, two point blocks with 25-stories and 30-stories located at firm-soil site (Old Alluvium) and soft-soil site (Kallang Formation) respectively are chosen. The buildings are selected as there is a large open space around the buildings, and there is thus no obvious influence from other buildings nearby. For the 25-story point block at firm-soil site, the measurements are performed at: (a) top floor; (b) ground floor; (c) 0.5 building height away from the building (0.5H); (d) 1 building height away from the building (1H); (e) 1.5 building heights away from the building (1.5H); and (f) 2 building heights away from the building (2H). For the 30-story point block at soft-soil site, the measurements are performed at: (a) top floor; (b) ground floor; (c) 0.5 building height away from the building (0.5H); (d) 1 building height away from the building (1H); (e) 2 building heights away from the building (2H); and (f) 3 building heights away from the building (3H). The height of the buildings is estimated using typical storey height of 3.6 m for 1st story and 2.8 m for 2nd story and above. Thus the height of the 25-story and 30-story point block can be estimated as 70.8 m and 84.8 m, respectively. Figure 2-10 shows the location

CHAPTER 2: EMPIRICAL RELATIONSHIPS BETWEEN NATURAL VIBRATION PERIOD AND HEIGHT OF BUILDINGS IN SINGAPORE

of the measuring point at a distance R away from a building with height H . For consistency, the sensor is aligned to be parallel to the two edges of the building for all the measuring points, as shown in Figure 2-10. HVSR method is used to identify the natural frequency of the buildings and the sites. Figures 2-11 and 2-12 show the HVSR plots of the ambient vibrations measured at firm-soil site and soft-soil site, respectively.

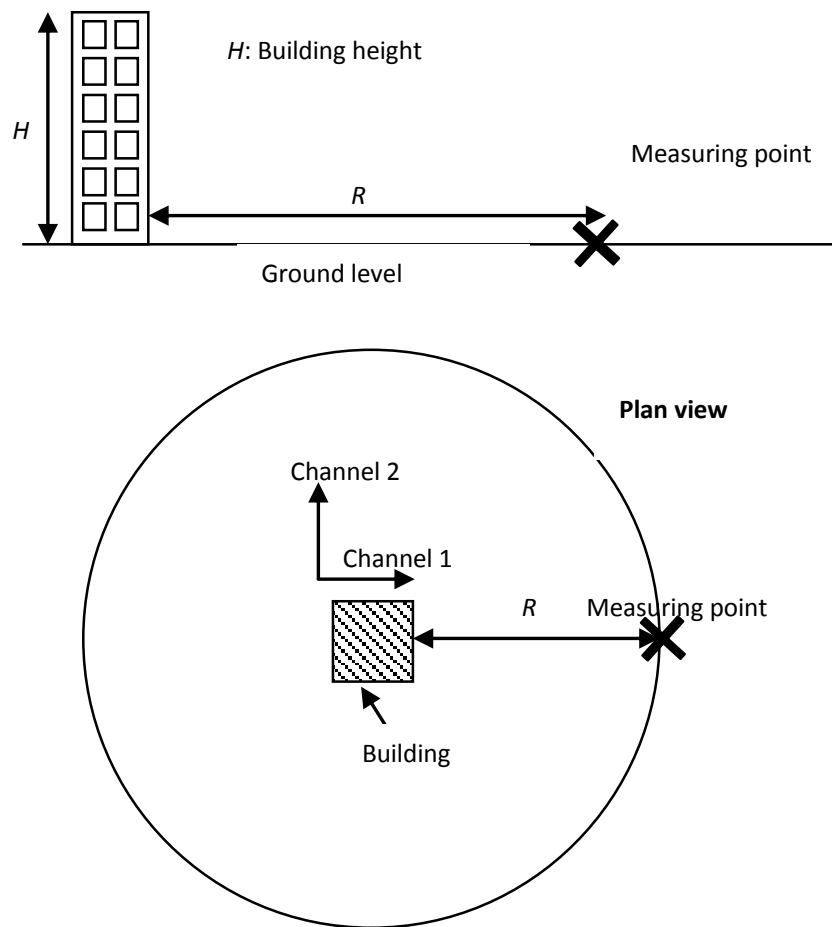


Figure 2-10 Location of the measuring point at distance R away from the building with height H .

For the measurements conducted at firm-soil site (Figure 2-11), the natural frequencies of 1st and 2nd modes of vibrations of the 25-story point block in Channel

CHAPTER 2: EMPIRICAL RELATIONSHIPS BETWEEN NATURAL VIBRATION PERIOD AND HEIGHT OF BUILDINGS IN SINGAPORE

1 are found to be 1.00 Hz and 3.50 Hz, respectively; for Channel 2, the natural frequencies of 1st and 2nd modes of vibrations are 0.92 Hz and 3.11 Hz, respectively. At ground floor, the HVSR plot in Channel 1 shows peak at 3.50 Hz, which is very close to the 2nd mode of vibrations of the building in Channel 1; for the HVSR plot in Channel 2, peaks are found at around 0.95 Hz and 3.11 Hz, which are very close to the 1st and 2nd modes of vibrations of the building in Channel 2. At 0.5H, peaks are found at around 3.42 Hz and 3.10 Hz in Channels 1 and 2, respectively, which are very close to the 2nd mode of vibration of the building. The HVSR plots at 1H, 1.5H and 2H are similar, showing peaks at around 5.3 Hz. The HVSR plot of the measurement conducted on top floor of the building does not show peak at 5.3 Hz. It is thus suggested that the soil at distance larger than 1H away from the building is free from the influence of the building. The soil frequency is thus around 5.3 Hz.

For the measurements conducted at soft-soil site (Figure 2-12), the natural frequencies of 1st, 2nd and 3rd modes of vibrations of the 30-story point block in Channel 1 appear to be 0.77 Hz, 1.02 Hz and 2.52 Hz, respectively; for Channel 2, the natural frequencies of 1st, 2nd and 3rd modes of vibrations are 0.80 Hz, 1.22 Hz and 2.83 Hz, respectively. At ground floor, the HVSR plot in Channel 1 shows peak at around 0.76 Hz, which is very close to the 1st mode of vibrations of the building in Channel 1; the HVSR plot in Channel 2 shows peaks at around 0.77 Hz and 1.27 Hz, which are very close to the 1st and 2nd mode of vibrations of the building in Channel 2. At 0.5 H and 1H, the HVSR plots show peaks at around 1.2 Hz and 1.80 Hz. The 1st peak is close to the 2nd mode of vibrations of the building. However, the frequency of 2nd peak is not shown in the HVSR plots of measurement conducted on top of building. These suggest that peaks representing the building frequency as well as soil frequency can be seen from the HVSR plots of measurements conducted within 1H away from the building. At 2H and 3H, the HVSR plots show pronounced peaks at around 1.90 Hz, suggesting that the soil at distance greater than 2H away from the building is free from influence of the building. In other

CHAPTER 2: EMPIRICAL RELATIONSHIPS BETWEEN NATURAL VIBRATION PERIOD AND HEIGHT OF BUILDINGS IN SINGAPORE

words, the HVSR plots of measurements conducted at distance larger than 2H away from the building show only the frequency of the soil. Thus the peaks found in the HVSR plots of measurements at 2H and 3H represent the site frequency (i.e. 1.90 Hz).

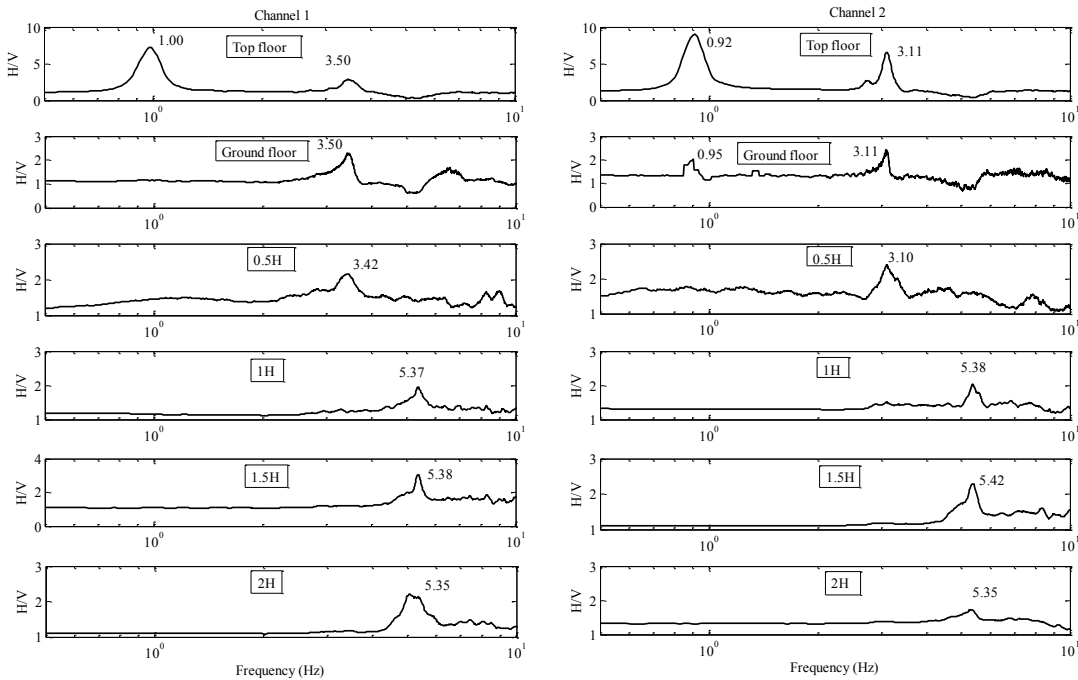


Figure 2-11 The HVSR of the microtremors measured on top of a 25-storey point block located at firm-soil site, ground floor, 0.5H away from the building, 1H away from the building, 1.5H away from the building and 2H away from the building

Based on the measurements described above, it is found that the distance of building influence on the surrounding soil at soft-soil site is greater than firm-soil site. At firm-soil site, the influence of the building on the surrounding soil may reach up to one building height measured from the base of the building. Peaks representing vibration frequency of building could be seen from the HVSR plots of the measurements conducted at distance less than one building height, and thus the soil frequency cannot be clearly identified. The soil frequency can only clearly be

CHAPTER 2: EMPIRICAL RELATIONSHIPS BETWEEN NATURAL VIBRATION PERIOD AND HEIGHT OF BUILDINGS IN SINGAPORE

identified at points which are more than 1H distance away from the building. This is similar to the finding of Mucciarelli et al. (1996).

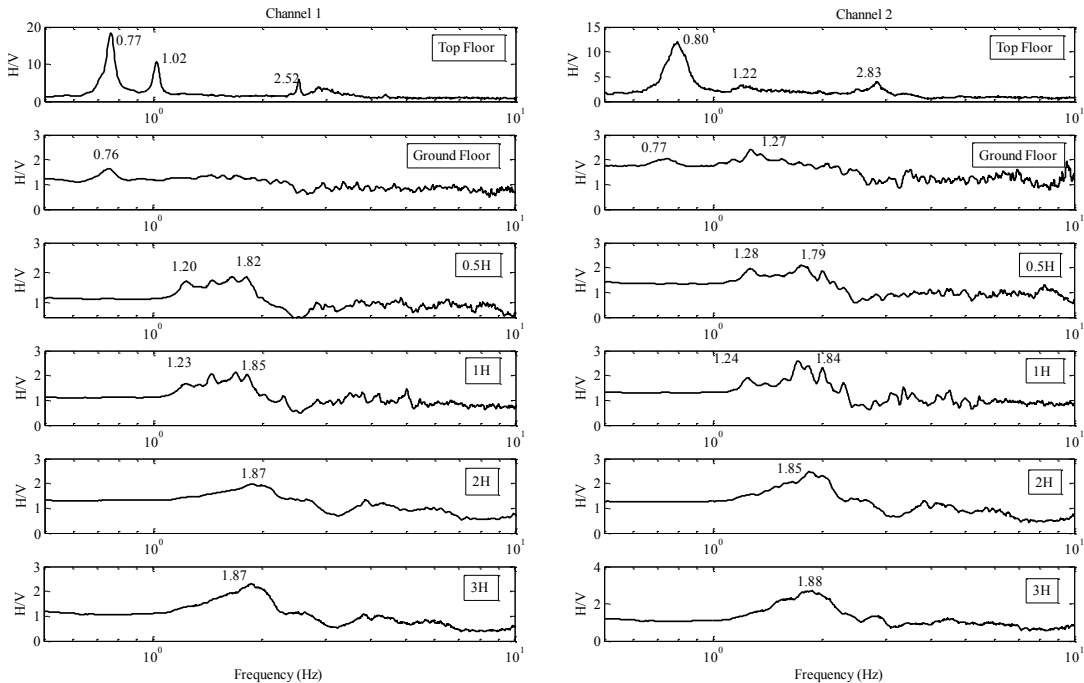


Figure 2-12 The HVSR of the microtremors measured on top of a 30-storey point block located at soft-soil site, ground floor, 0.5H away from the building, 1H away from the building, 2H away from the building, and 3H away from the building

Different conclusion is made on the influence of building on the surrounding soil at soft-soil site. From the measurements at soft-soil site, it is suggested that the influence from the building can reach up to two building heights from the base of the building, which is two times larger radius of influence than the firm-soil site. Peaks representing vibration frequency of building could be seen from the HVSR plots of the measurements conducted at distance less than two building heights. The soil frequency thus could not be clearly identified from the measurements conducted at distance less than two building heights away from the building at soft-soil site. This is similar to the finding by Gallipoli et al. (2004).

CHAPTER 2: EMPIRICAL RELATIONSHIPS BETWEEN NATURAL VIBRATION PERIOD AND HEIGHT OF BUILDINGS IN SINGAPORE

Caution thus has to be taken when conducting free-field microtremors measurement at soft-soil site as well as firm-soil-site in order to prevent any influence from nearby buildings on the measured HVSR. It is shown in this study that, for measuring points located within the building influence, the soil frequency could not be clearly identified from HVSR plots. Peaks representing the natural frequency of the nearby building may appear in the plots. It is thus advised that free-field microtremors measurement at firm-soil site to be conducted at a distance more than one building height away from the nearest building. While for soft-soil site, measurement should be conducted at distance more than two building heights away from the nearest building.

2.6 COMPARISON WITH RECORDED DATA DURING EARTHQUAKE EVENTS

The empirical period-height relationships derived in the previous section are based on microtremor measurements of 116 buildings. However, it is necessary for us to study the differences between the natural vibration periods of buildings obtained from microtremors and those obtained during earthquake events.

As part of the effort to monitor the seismic performance of buildings in Singapore, 19 residential buildings have been instrumented with seismic sensors to capture the responses of buildings subjected to tremors. The sensors have been installed at the ground floor and top story of the buildings. The 1st to 3rd columns from the left side of Table 2-3 shows the relevant information of the buildings instrumented.

CHAPTER 2: EMPIRICAL RELATIONSHIPS BETWEEN NATURAL VIBRATION PERIOD AND HEIGHT OF BUILDINGS IN SINGAPORE

Table 2-3 Comparison between the measured natural vibration periods of 19 instrumented residential buildings during September 30, 2009 event with the estimated natural vibration periods using the proposed period-height relationships

No.	Site properties	Number of storey	Natural vibration period measured (sec)	Natural vibration period estimated from Eq. 11-14 (sec)	Percentage difference (%)
1	BT	9	0.46	0.44	-5.4
2	JF	10	0.43	0.48	10.9
3	OA	13	0.59	0.60	1.3
4	KF	13	0.71	0.76	6.5
5	BT	15	0.66	0.68	2.4
6	OA	17	0.72	0.75	4.5
7	OA	18	0.82	0.79	-3.6
8	KF	18	1.06	0.99	-6.9
9	KF	18	0.95	0.99	4.2
10	KF	21	1.23	1.12	-8.9
11	KF	21	1.22	1.12	-8.2
12	KF	23	1.16	1.21	4.3
13	KF	23	1.28	1.21	-5.8
14	KF	29	1.65	1.46	-11.5
15	KF	30	1.50	1.50	0
16	KF	10	0.57	0.61	7.0
17	OA	15	0.67	0.68	0.9
18	JF	16	0.71	0.71	0.6
19	JF	24	1.09	1.01	-7.1

On September 30, 2009, an $M_w= 7.6$ earthquake occurred just off the southern coast of Sumatra, Indonesia. The major shock hit at 18:16:10 local time (10:16:10 UTC). The epicenter is 45 kilometers west-northwest of Padang Sumatra (Latitude=-2.508°, Longitude=101.484°), and it is about 460 km away from Singapore. The peak ground accelerations (PGA) recorded at rock site, Jurong Formation and Kallang Formation in Singapore due to the earthquake event are 0.44 gal, 1.2 gal and 3.0 gal, respectively. The ground motions in Singapore due to this earthquake event are weak, and thus nonlinear response is not expected to occur in the buildings. Transfer function of the data recorded in the buildings during 30 September 2009 Sumatran earthquake event has been calculated. The natural vibration period of the buildings is determined using peak picking method. For

CHAPTER 2: EMPIRICAL RELATIONSHIPS BETWEEN NATURAL VIBRATION PERIOD AND HEIGHT OF BUILDINGS IN SINGAPORE

illustration purpose, Figure 2-13 shows the transfer function of the data recorded in a 29-storey high-rise residential building during the earthquake event. By simple peak picking method, the vibration period of 1st mode of the building can be determined as 1.65 sec. The 4th columns from the left side of Table 2-3 shows the natural vibration period of the buildings obtained from the recorded responses of the buildings during this event. The natural vibration periods of the buildings are also estimated using the proposed relationships of Eqs. 2-10 to 2-13, and the results are compared with the natural vibration period obtained from the recorded data during the earthquake event. As can be seen from 6th column from the left side of Table 2-3, the absolute differences between the estimated and the measured natural vibration period during earthquake event is less than 12%.

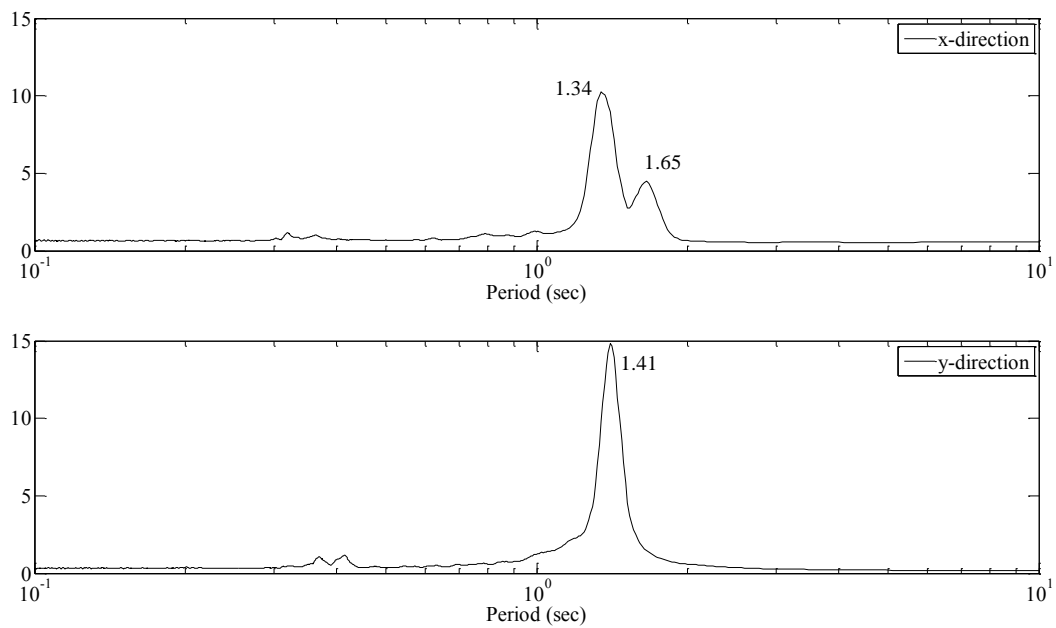


Figure 2-13 Transfer function of the data recorded in a 29-storey high-rise residential building during 30 September 2009 Sumatran earthquake event

2.7 COMPARISON WITH EXISTING PERIOD-HEIGHT RELATIONSHIPS

The proposed empirical period-height relationships are compared with other existing relationships, as shown in Figure 2-14. The proposed period-height relationship for buildings located at soft-soil is depicted by thick-dashed line, while the proposed period-height relationship for buildings located at firm-soil is depicted by thick-solid line. The other published period-height relationships used for comparison include relationships of Guler et al. (2008), Hong and Hwang (2000), Michel et al. (2010) and Gallipoli et al. (2009) for buildings in Turkey, Taiwan, France and European countries, respectively.

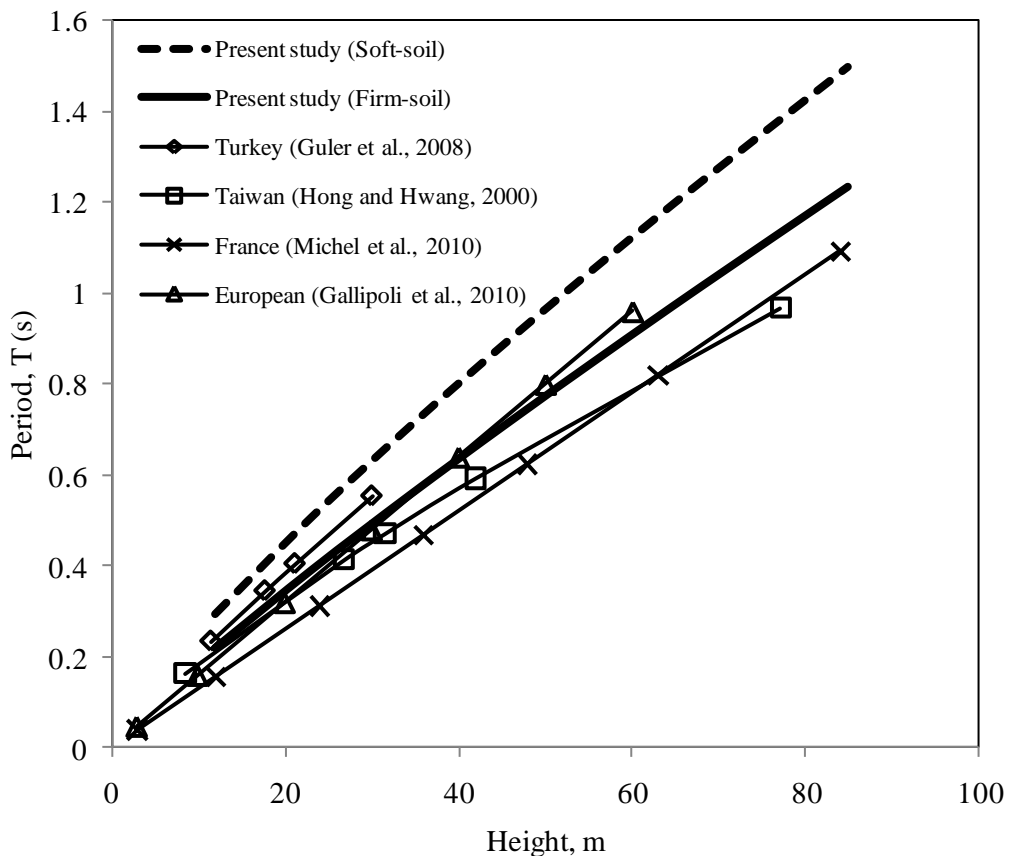


Figure 2-14 Comparison with other published period-height relationships

CHAPTER 2: EMPIRICAL RELATIONSHIPS BETWEEN NATURAL VIBRATION PERIOD AND HEIGHT OF BUILDINGS IN SINGAPORE

As can be seen from Figure 2-14, the natural vibration periods estimated by the proposed period-height relationship of buildings located at soft-soil site is generally longer than that estimated by the other period-height relationships. Using the proposed period-height relationship for buildings located at firm-soil, the estimated vibration period is slightly longer than the vibration period estimated by formulas of Michel et al. (2010) and Hong and Hwang (2000). For buildings lower than 15 stories, the estimated vibration period of the proposed relationship for firm-soil site agrees quite well with the vibration period estimated by Gallipoli et al. (2009) for European buildings.

The International Building Code (ICC, 2012) provide a quick estimate on the natural vibration period of concrete and steel moment-resisting frame not exceeding 12 stories in height using the following approximate formula:

$$T = \frac{N}{10} \quad \text{Eq. 2-15}$$

where T is natural vibration period of buildings in second, and N is number of stories. However, it is obvious that Eq. 2-15 is not suitable to be used to estimate the natural vibration periods of buildings in Singapore, as it generally estimates much longer natural vibration period of buildings. For example, a 10-stories building in Singapore has a mean measured natural vibration period of 0.51 s, but Eq. 2-15 gives an estimation of 1.0 s, which is twice longer than the measured natural vibration period. Thus, it is suggested that the proposed period-height relationships should be used for estimating the natural vibration periods of buildings in Singapore.

2.8 CHAPTER SUMMARY

In this chapter, relationships between natural vibration period and height of buildings have been derived empirically based on AVT measurements conducted on 116 high-rise residential buildings. Regression analyses have been carried out on the measured natural vibration periods of the buildings considering the site properties. Measurements have also been conducted to examine the influence of buildings on the measured frequency of surrounding soil. The following conclusions can be drawn from this study:

1. The plan aspect ratio of the measured buildings has been found to be insignificant in affecting the natural vibration period of 1st mode of the buildings. The natural vibration periods estimated using the proposed period-height relationship for buildings located at soft-soil site is found to be about 40% longer than those estimated using the relationship for buildings located at firm-soil site.
2. The radius of building influence on the measured frequency of the surrounding soil reaches up to one building height for firm-soil site and two building heights for soft-soil site. Peaks representing natural frequency of nearby building may appear in the HVSR plots of measurements conducted within the radius of building influence. It is thus advised that free-field microtremor measurements to be conducted at distance more than one building height and two building heights away from the nearest building for firm-soil site and soft-soil site, respectively.

CHAPTER 2: EMPIRICAL RELATIONSHIPS BETWEEN NATURAL VIBRATION PERIOD AND HEIGHT OF BUILDINGS IN SINGAPORE

3. Additional data of natural vibration periods of 19 instrumented residential buildings, which have a height ranging from 9 stories to 30 stories, were obtained from the building response recorded during the September 30, 2009 Sumatran earthquake event. The natural vibration periods of these buildings are compared with the natural vibration periods estimated using the proposed period-height relationships, and the absolute differences are found to be below 12%.

4. The natural vibration periods estimated using the proposed period-height relationship for buildings located at soft-soil is generally longer than the vibration periods estimated using period-height relationships derived by previous researches. However, the vibration periods estimated using the proposed period-height relationship for buildings located at firm-soil site agrees well with those estimated using period-height relationships derived by previous researches.

CHAPTER 3

GENERIC STRUCTURAL MODELS

In order to conduct seismic assessment of buildings in Singapore, accurate structural modeling is needed to simulate the response of structures subjected to ground motion excitations. In this chapter, the structural modeling of generic models which represent typical high-rise public residential buildings in Singapore is presented. There are two generic models constructed, namely 15-storey and 30-storey generic models. The 15-storey generic model represents typical 15-storey rectangular plan building (slab block), while the 30-storey generic model represents typical 30-storey square plan building (point block) in Singapore. The structural analyses are run using the Open Source for Earthquake Engineering Simulation (OpenSEEs, 2009), a software developed by the Pacific Earthquake Engineering Research (PEER) centre. There are several notable aspects of the structural modeling presented in this section:

- (a) Fiber element models are used.
- (b) A joint panel model is used to simulate beam-column joint behavior, and it is calibrated with experimental results. The modeling of the beam-column joint element will be discussed in section 3.1.3.
- (c) The generic models are reinforced concrete infilled frame buildings with shear wall systems and soft-first-storey.

- (d) The infilled wall is modeled using equivalent diagonal struts. The first-storey is not modeled with diagonal struts to simulate soft-first-storey effect.
- (e) The bases of the models are fixed to the ground.

The generic models are intentionally made as closely as possible to the existing high-rise public residential buildings in Singapore. This helps to ensure accurate prediction of the structural response of high-rise residential buildings in Singapore subjected to ground motion excitations. The behavior of the nonseismically detailed beam-column joints, which can be typically found in residential buildings in Singapore, are included in the generic models. The beam-column joint shear failure can be captured. This chapter summarizes the development of the generic models, which includes the calibration of the beam-column joint model and the natural vibration period of the generic models. The structural response of the generic models subjected to potential giant Sumatran earthquake ground motions has been studied by Pan et al. (2011) and Goh et al. (2012).

3.1 OVERVIEW OF STRUCTURAL MODEL

3.1.1 CONFIGURATIONS AND ELEMENTS

Figures 3-1 shows the graphical illustrations of the generic models. The height for 1st storey is 3.6 m, while the heights for 2nd storey and above are 2.8 m. For the 15-storey generic model, the bay width is 3 m, and there are 31 bays in total. For the 30-storey generic model, the bay width is 3.5m, and there are 9 bays in total.

Figure 3-2 shows the typical floor plan of a point block and a slab block in Singapore.

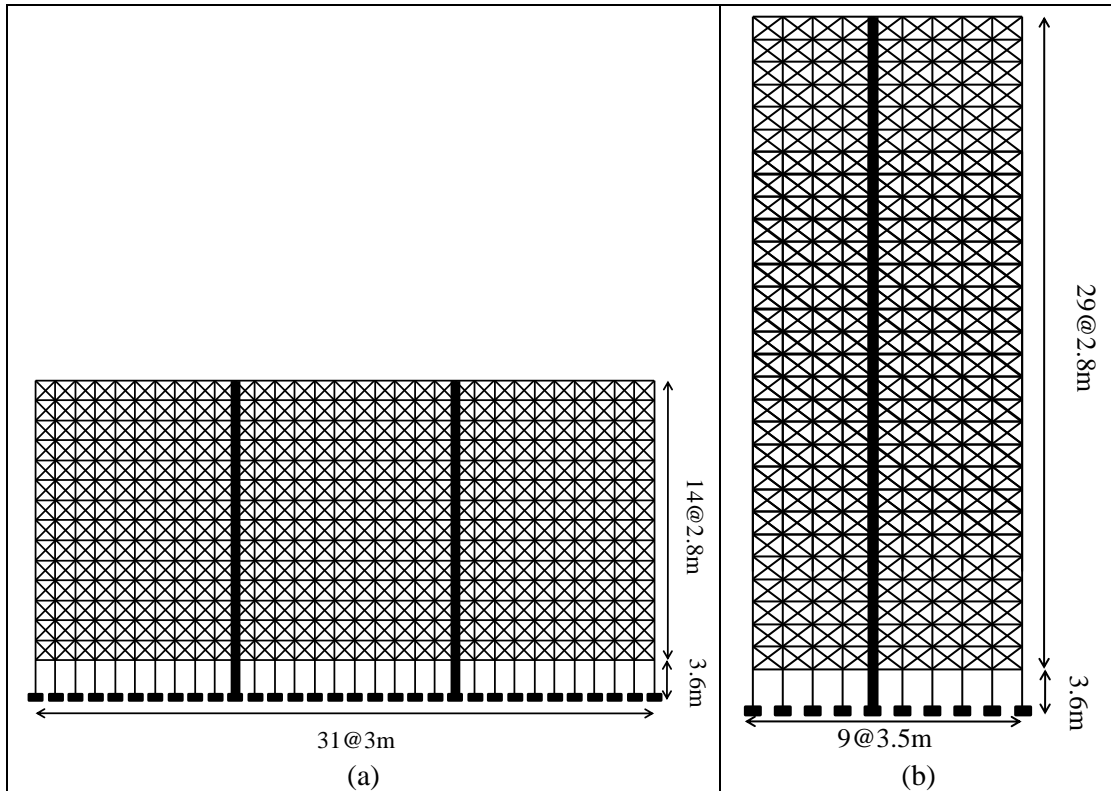


Figure 3-1 Graphical illustration of the: (a) 15-storey generic model; (b) 30-storey generic model.

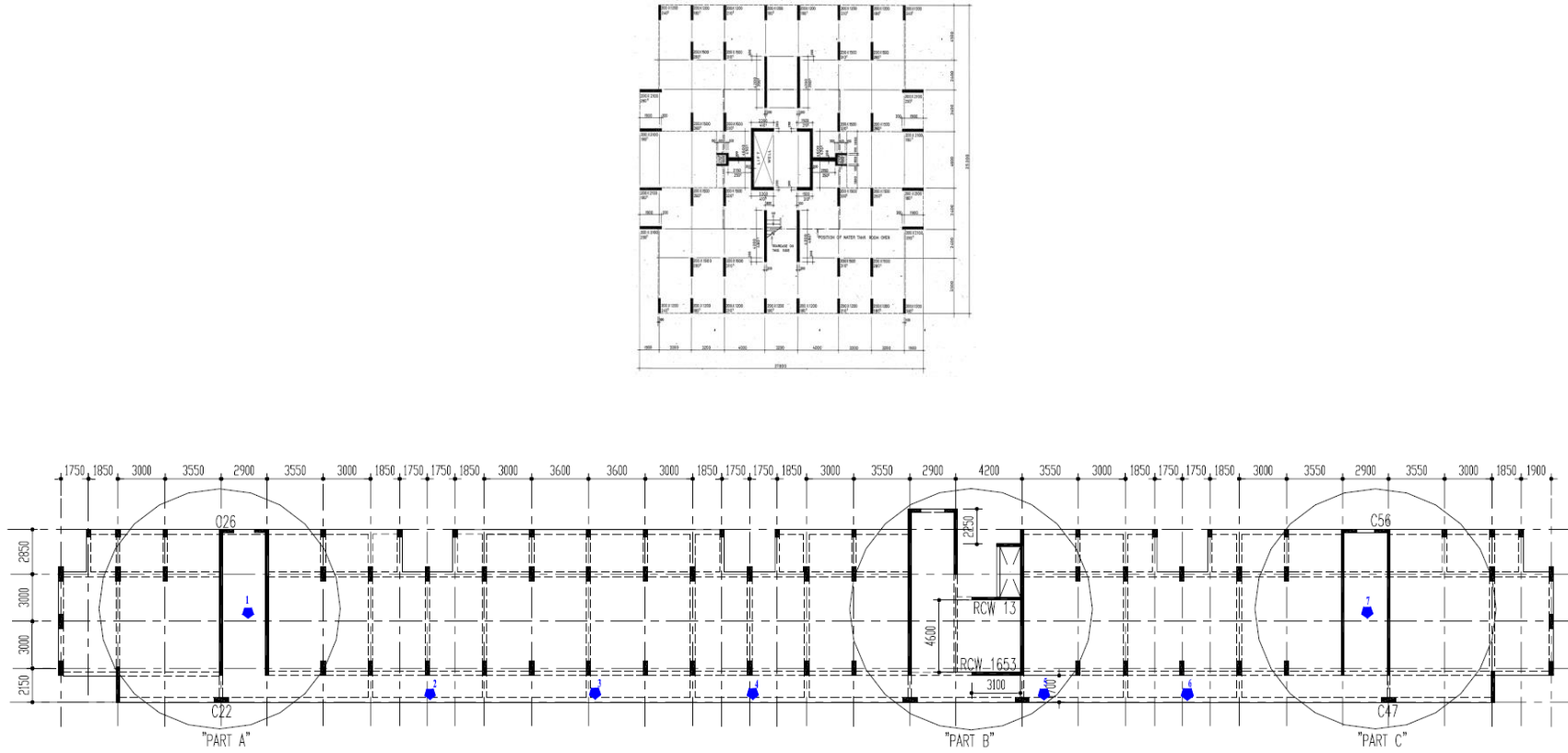


Figure 3-2 Typical floor plan of a point block and a slab block

The components of the generic models and the way they are represented in *OpenSEEs* are summarized as follows:

- (a) Beam and Column elements: The beam and column elements are modeled using fiber elements. The fiber element allows for the interaction of the axial force, bending moment, and flexural shear to be accounted for. It is assumed that the shear deformation is small and the shear effect is not significant in the modeling of the column elements. The *OpenSEEs* commands used are: *nonlinearBeamColumn element, Steel02 material, Concrete02 material*.
- (b) Beam-column joint elements: A joint panel model is used to account for the response of the beam-column joints. The joint panel model accounts for the geometry of the joint and the shear panel behavior. The backbone curve of the shear panel is modeled using bilinear stress-strain curve with pinching hysteretic response. The *OpenSEEs* commands used are: *joint2D element, Hysteretic material*.
- (c) Infilled wall: The infilled wall is simulated using compression only diagonal struts. The *OpenSEEs* commands used are: *truss element, Hysteretic material*.

Figure 3-3 shows the typical column, slab-beam and lift core wall sections. The sections are modeled using force-based nonlinear beam-column elements with co-rotational geometric transformation. Each element is assigned with five integration points along its length where the nonlinear axial-flexural behavior of the cross section is monitored. The use of fiber element with force-based formulation to model shear wall has been proven to be accurate and efficient (Martinelli and

Filippou, 2009). The fibers in each cross section are assigned with material properties to represent unconfined concrete, confined concrete or steel reinforcement. The modeling of each material will be discussed in section 3.1.2. The slab-beam elements include an effective width of the slab in the section definition. The width of the slab is modeled to be equal to beam width plus three times beam depth, based on work by Pantazapoulou and Moehle (1990).

For the 15-storey model, the columns at the 1st to 3rd storey are shown as column section A1, while the columns at the 4th to 15th storey are shown as column section A2. For the 30-storey model, the columns at the 1st storey to 11th storey are shown as column section A1, while columns at 12th to 30th are shown as column section A2. The 11th and 22nd columns from left for the 15-storey model and 5th column from left for the 30-storey model are lift cores. The masonry walls are modeled as equivalent diagonal struts. Compressive only truss element is used to model the equivalent diagonal struts according to work by Saneinejad and Hobbs (1995).

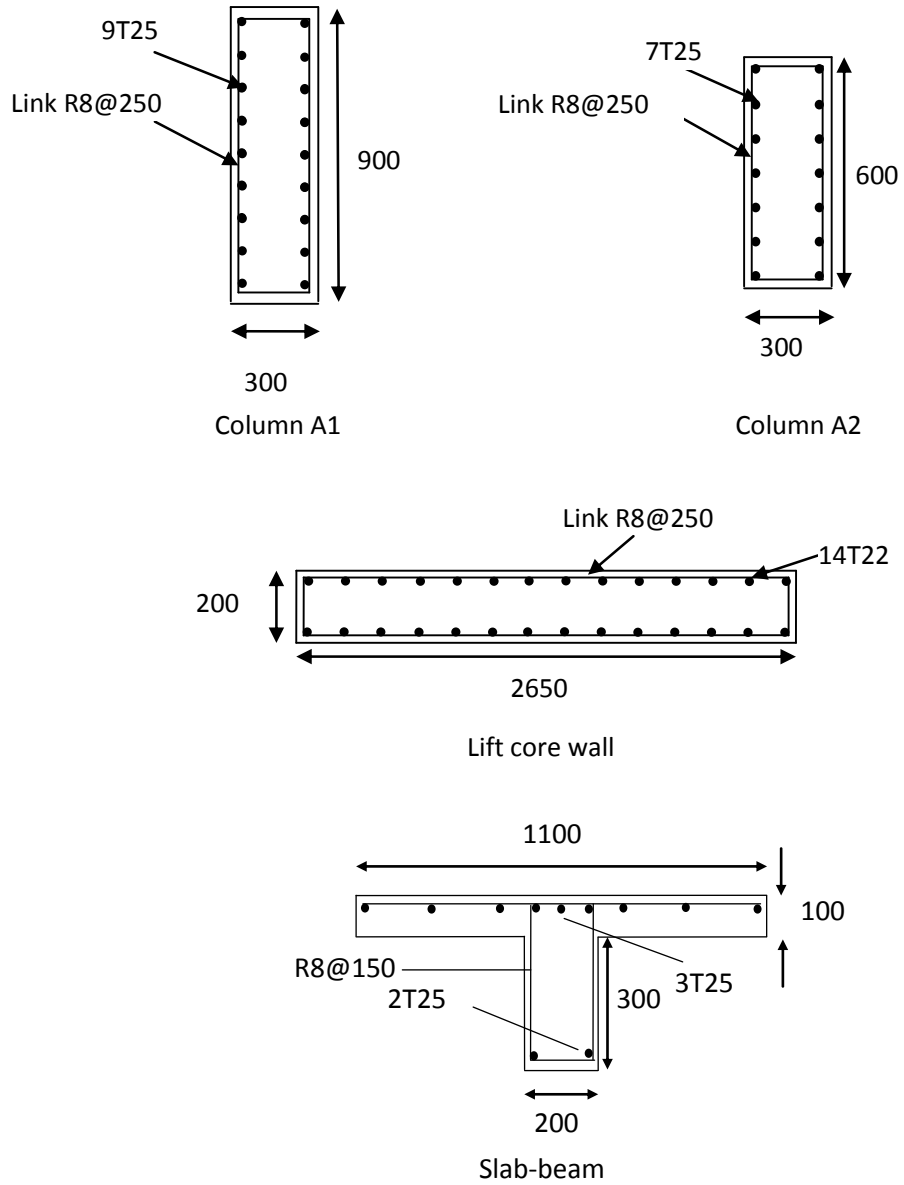


Figure 3-3 Summary of concrete frames elements

3.1.2 MATERIAL PROPERTIES

Concrete Material

In this study, the concrete material model *Concrete02*, which captures the compressive and tensile behavior of concrete, is used. It can be calibrated to include the tension-stiffening effect. To quantify the confinement effects, the confined concrete model by Mander et al. (1988) is used. The confined concrete model accounts for the effects that confinement has on the concrete strength and ductility. The core sections of the beams and columns are assigned with confined concrete properties, while the outer sections are assigned with unconfined concrete properties. Figure 3-4 shows the resulting material backbone curves for confined and unconfined concrete which has an unconfined compressive strength of 30 MPa. The parameters of the unconfined concrete material used in this study are summarized in Table 3-1.

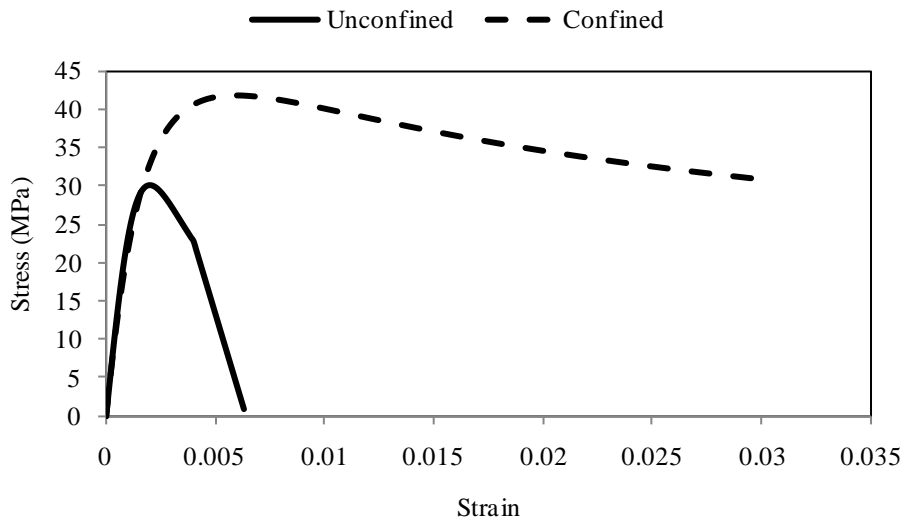


Figure 3-4 Stress-strain relationship for unconfined and confined concrete model according to Mander et al. (1988)

Table 3-1 Material properties for reinforced concrete frame elements

f_c	ε_{sc}	f_{cu}	ε_{su}	f_t	E_{ts}	F_y	E	b
30	0.002	6	0.003	2	500	460	200	0.01

f_c : Unconfined concrete compressive strength (MPa);

ε_{sc} : Unconfined concrete strain at f_c ;

f_{cu} : Unconfined concrete crushing strength (MPa);

ε_{su} : Unconfined concrete strain at f_{cu} ;

f_t : Unconfined concrete tensile strength (MPa);

E_{ts} : Unconfined concrete tension softening slope (MPa);

F_y : Steel yield stress (MPa);

E : Steel modulus of elasticity (GPa);

b : Steel hardening ratio

Steel Material

In this study, the Guiffre-Menegotto-Pinto steel material (*Steel02*) is used. This model is capable of capturing both kinematic and isotropic hardening. The parameters of the steel material used in this study are summarized in Table 3-1.

Masonry Walls

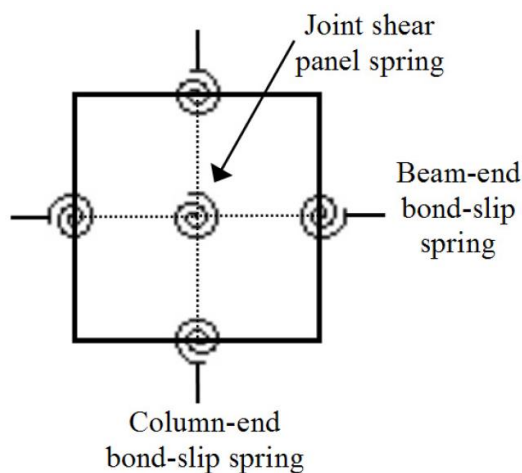
The masonry walls are modeled using equivalent diagonal compression struts. The parameters of the stress-strain relationships of the masonry wall are based on the experimental data by Kaushik et al. (2007). The lateral force-deformation relationship for the masonry infilled wall is modeled based on the methods proposed by Saneinejad and Hobbs (1995). The parameters of the masonry infilled wall are presented in Table 3-2.

Table 3-2 Summary of masonry wall properties

Compressive strength, f_{cm} (MPa)	Strain at f_{cm} , ε_{scm}	Crushing strength, f_{cum} (MPa)	Strain at f_{cum} , ε_{sum}
4.1	0.004	2.5	0.003

3.1.3 BEAM-COLUMN JOINT MODEL

The buildings in Singapore are usually designed according to BS8110 (BSI, 1997). The beam-column joints of the buildings are usually nonseismically detailed. The beam-column joints may have shear failure when subjected to lateral load due to the lack of seismic reinforcement in the joints. In this study, the two-dimensional joint model developed by Altoontash (2004) is employed to model the beam-column joints. This model is named *Joint2D* in *OpenSEEs* scripting language. This model accounts for the finite joint size, and uses rotational springs and systems of constraints to model the shear panel behavior and the bond-slip behavior. Figure 3-5 shows the schematic diagram of this model.

Figure 3-5 Schematic diagram of *Joint2D* element (Altoontash, 2004)

The backbone curve of the joint shear panel is calibrated using the procedure proposed by Mitra and Lowes (2007). Comparison between the simulated and observed response histories have been done, which indicated that the joint model represents well stiffness and strength response parameters for beam-column joints with a wide range of design parameters. Mitra and Lowes (2007) assumed that the joint shear load is transferred via a concrete compression strut. Figure 3-6 shows an idealization of the strut model that employed the following assumptions (Mitra and Lowes, 2007):

- The orientation and in-plane width of the strut are assumed to be constant and defined by the depth of the column and beam flexural compression zones, at a load level corresponding to the beams developing nominal flexural strength on the opposite sides of the joints.
- Strut depth is defined as the maximum of the out-of-plane depth of the beam and column.
- The confined concrete model presented by Mander et al. (1988) defines the stress-strain response of the strut.
- Column longitudinal and joint horizontal reinforcing steel act to confine the joint core concrete; only the component of the confining force acting perpendicular to the orientation of the compression strut is considered.
- The joint carries shear only through the compression strut. By equating the horizontal (or vertical) load carried by the strut with that carried by a joint panel with uniform shear stress, panel shear stress may be related to strut stress as follows:

$$\tau_{strut} = f_{c_strut} \frac{w_{strut} \cos \alpha_{strut}}{w} = f_{c_strut} \frac{w_{strut} \sin \alpha_{strut}}{h} \quad \text{Eq. 3-1}$$

where τ_{strut} = shear stress in the shear-panel component; f_{c_strut} = strut stress; w_{strut} = in-plane width of the strut; α_{strut} = angle of inclination of the strut with the horizontal; and w and h = in-plane width and height of the joint, respectively (Figure 3-6).

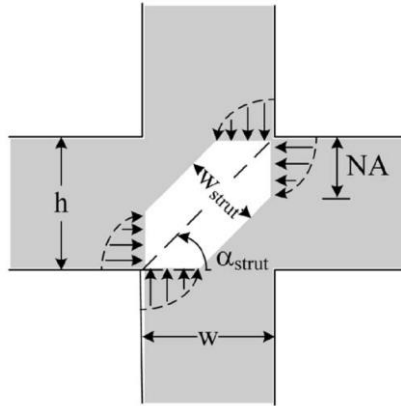


Figure 3-6 Compression strut model for calibration of joint-element shear panel component (Mitra and Lowes, 2007)

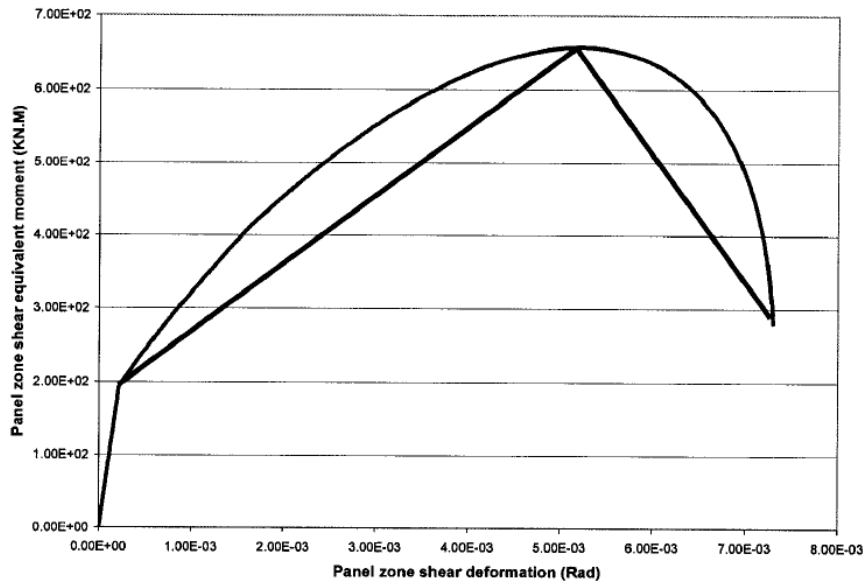


Figure 3-7 Calibrated shear panel backbone curve and multilinear idealization by Altontash (2004)

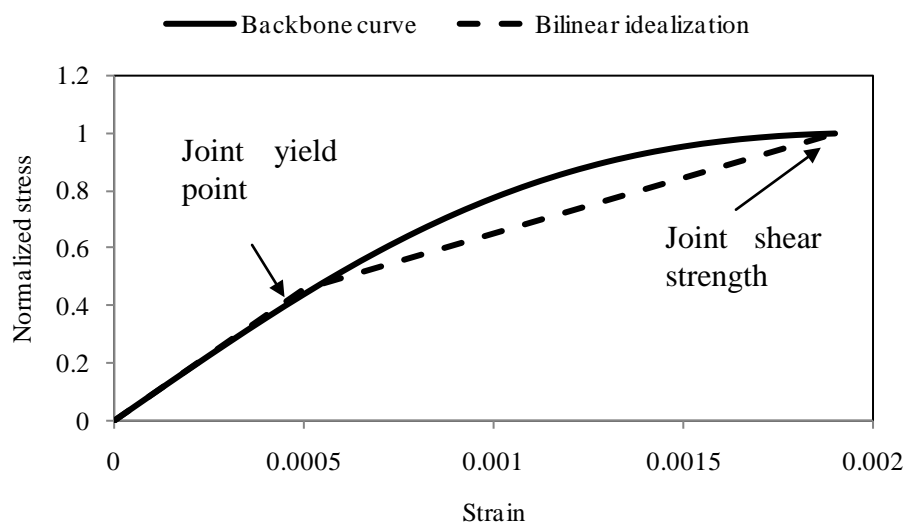


Figure 3-8 Calibrated shear panel backbone curve and bilinear idealization
(present study)

A modification factor of 0.7 is used on the basis of empirical data from Mitra and Lowes (2007), which reflects the differences in shear strength between seismically and nonseismically detailed joints. Altonash (2004) defined the joint panel stress-strain relationship using multi-linear backbone curve, as shown in Figure 3-7. Similar approach is used in current study. In current study, bilinear backbone curve is used to represent the stress-strain behavior of the shear panel model, as shown in Figure 3-8. The yield point of the bilinear stress-strain curve is shown in Figure 3-8. The backbone curve has a maximum point at the shear strength of the joint. Joint shear failure is assumed to occur once the shear stress induced in the joint reaches the predefined shear strength. The cyclic behavior of the joint shear panel is based on recommendations by Altonash (2004), who proposed that the hysteretic behavior to be pinched and have a pinch-point at 25% of the maximum historic stress and 25% of the maximum historic rotation.

3.1.4 CALIBRATION OF JOINT MODEL

In this section, the joint model is calibrated with the experimental tests conducted by Li et al. (2002).

3.1.4.1 *Experimental Set Up (Li et al., 2002)*

Four full-scale reinforced concrete interior beam-wide column joints with nonseismic detailing and limited seismic detailing were designed and tested by Li et al. (2002). Figure 3-8 shows the reinforcing details of the four tested specimen, namely specimens A1, M1, A2 and M2. Figure 3-10 shows the cyclic lateral loading and displacement history used in the tests (Li et al., 2002).

3.1.4.2 *Simulation of Beam-Column Joints*

The numerical simulations are conducted using *OpenSEEs* (OpenSEEs, 2009). Figure 3-11 shows an illustration of the numerical model. Lateral loading is applied using force control and after that displacement control (Figure 3-9). The boundary conditions are representative of those used in the experimental tests. The nonlinear response of beams and columns is simulated using force-based nonlinear beam-column elements with co-rotational geometric transformation. Each element is assigned with five integration points along its length where the nonlinear axial-flexural behavior of the cross section is monitored. The parameters of the unconfined and confined concrete and the steel materials are calculated using the same procedure described in section 3.1.2. The *Joint2D* element is used to simulate the behavior of the beam-wide column joint. The backbone curve of the joint panel model is described in section 3.1.3.

3.1.4.3 Comparison between Experimental and Simulation Results

The story shear force versus horizontal displacement relationships of the four test specimens obtained from experimental testing and *OpenSEEs* simulations are compared in Figure 3-13. From Figure 3-13, it can be seen that the simulation of the joint panel model can accurately predict the behavior of the beam-wide column joints. Pinching can be found in the simulated results, and this is very similar to the behavior of the beam-column joints from the experiment.

The stiffness and column shear force in each cycles obtained from experiment and simulation is compared in Figure 3-13 and Figure 3-14. The maximum joint shear stress in the beam-column joints obtained from experiment and simulation is compared in Figure 3-15. The strength loss at last cycle obtained from experiment and simulation is compared in Figure 3-16. The ratio of experiment and simulation for column shear force, as shown in Figure 3-14, is equal to unity for the first two cycles. This is because the first two cyclic loadings are force-controlled and thus the column shear force obtained from experiment and simulation are the same. It can be concluded that the joint panel model prediction is reasonably well-matched with the experimental results. The differences between the experimental and simulated results are less than 30%. Thus it is concluded that the joint model can be used to predict the behavior of the nonseismically detailed beam-wide column joints.

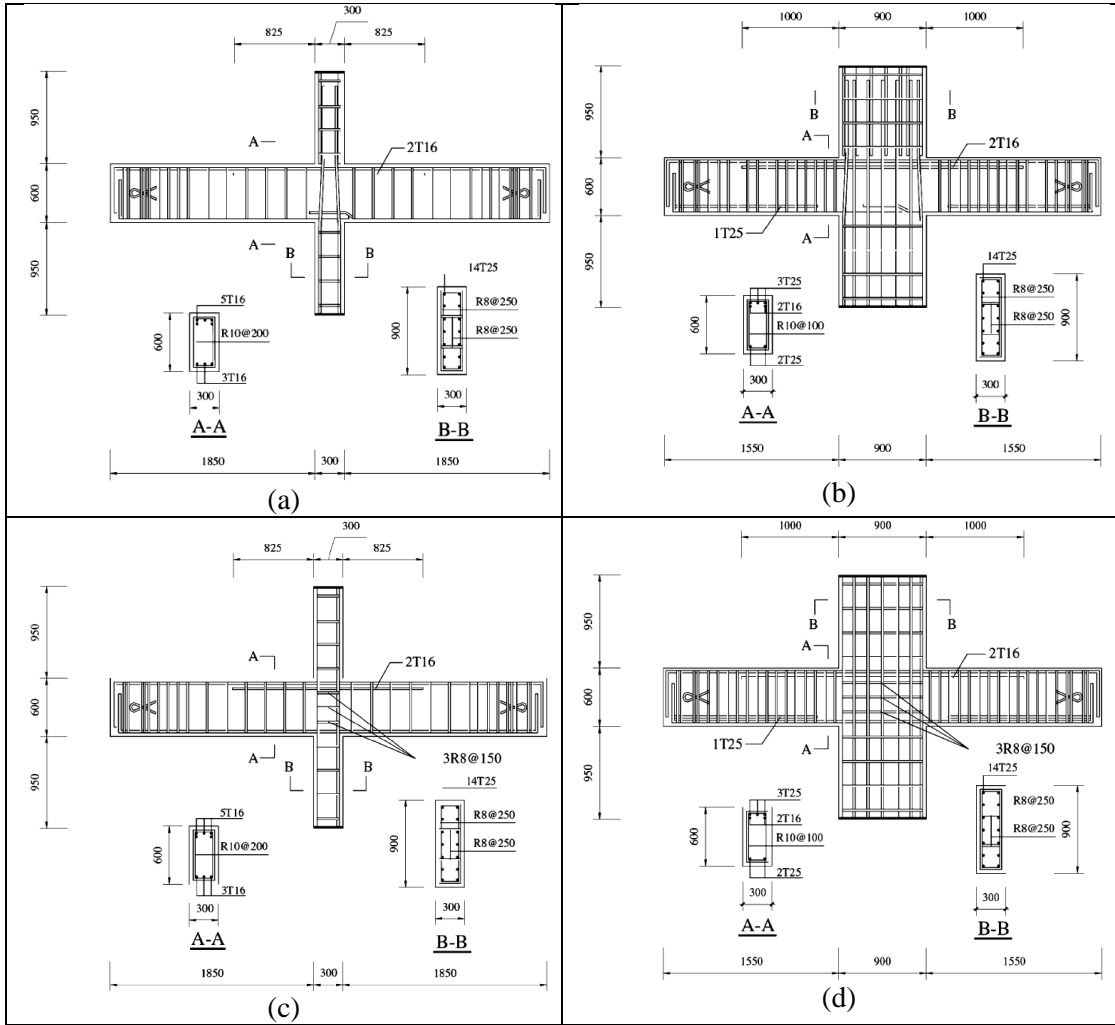


Figure 3-9 Reinforcing detailing of specimens: (a) A1; (b) M1; (c) A2; and (d) M2 (Li et al., 2002)

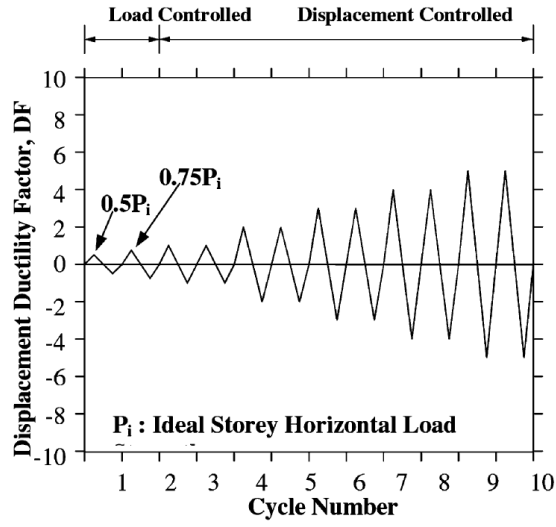


Figure 3-10 Cyclic lateral loading and displacement history (Li et al., 2002)

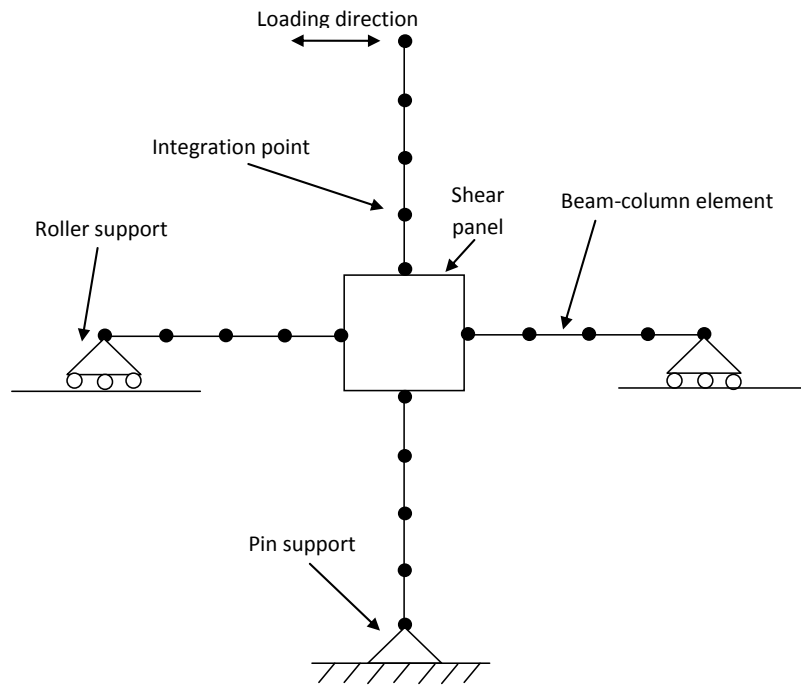


Figure 3-11 Graphical illustration of the numerical simulation of beam-column joint model

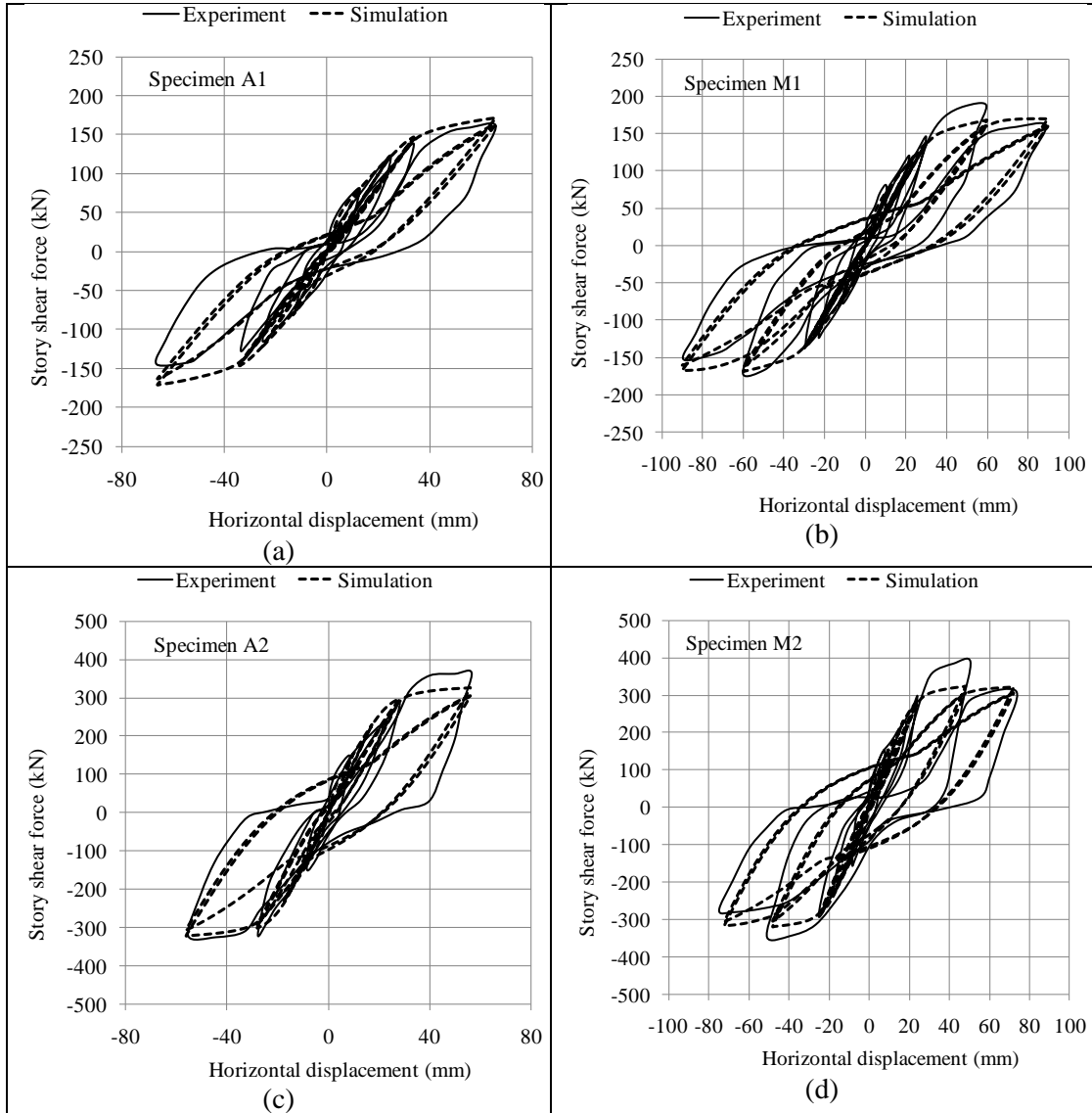


Figure 3-12 Comparison between experiment and simulation results for specimens: (a) A1; (b) M1; (c) A1; and (d) M2.

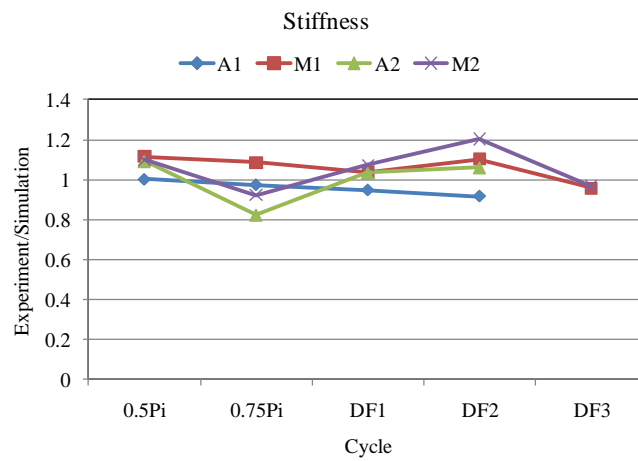


Figure 3-13 Comparison of stiffness in each cycles obtained from experiment and simulation

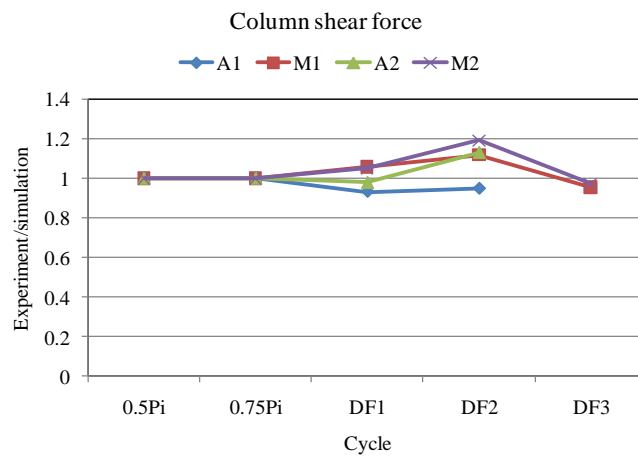


Figure 3-14 Comparison of column shear forces in each cycles obtained from experiment and simulation

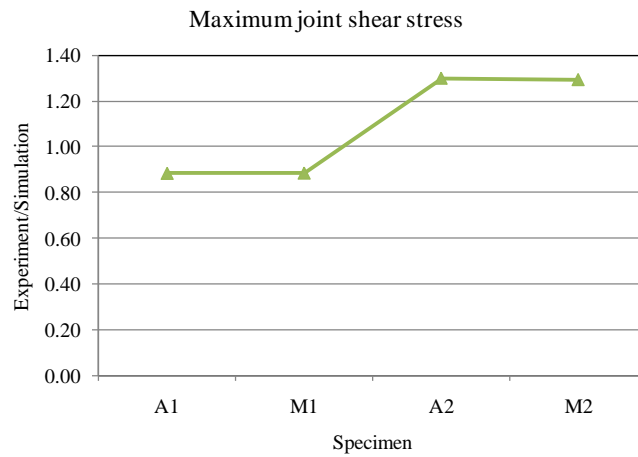


Figure 3-15 Comparison of maximum joint shear stress for each specimen obtained from experiment and simulation

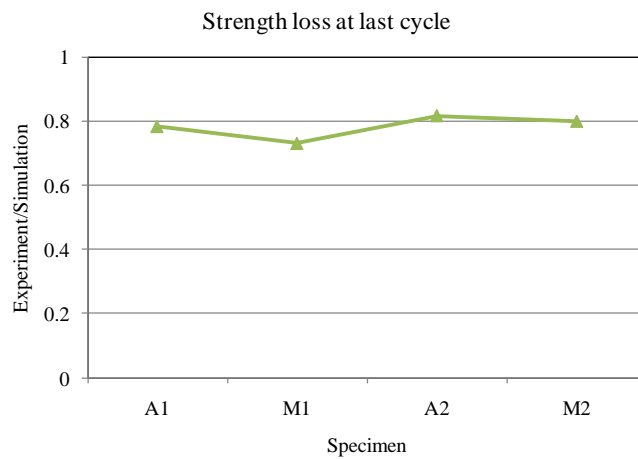


Figure 3-16 Comparison of strength loss at last cycle for each specimen obtained from experiment and simulation

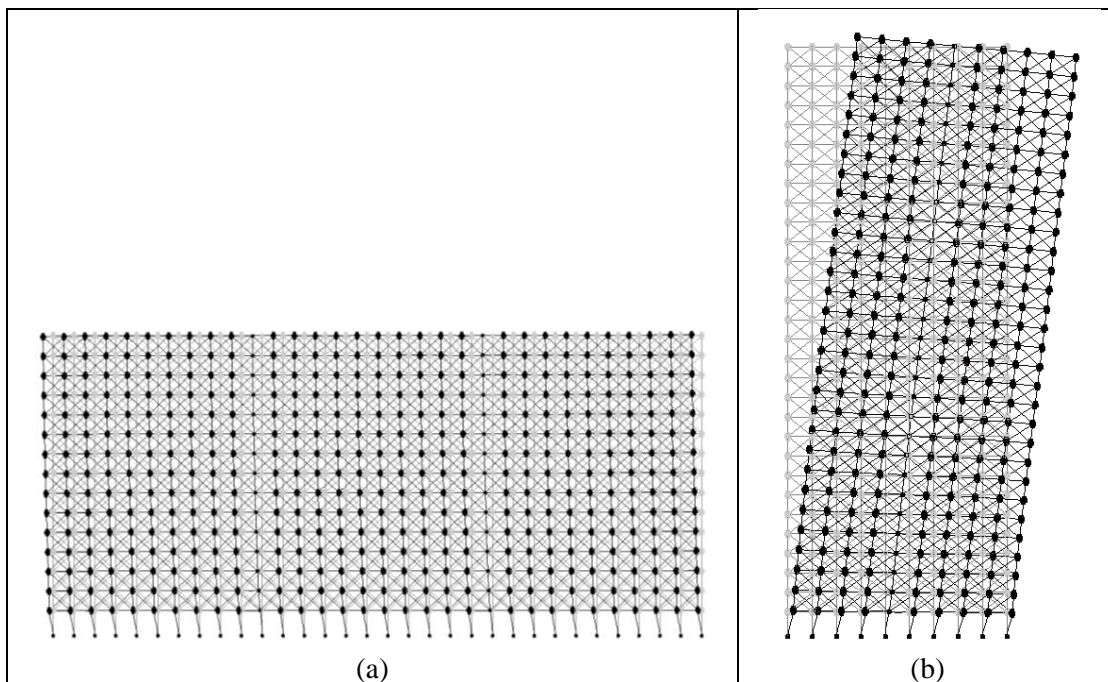


Figure 3-17 Mode shape of the 1st vibration mode of the: (a) 15-storey generic model, $T= 0.67$ sec; (b) 30-storey generic model, $T= 1.31$ sec

3.2 NATURAL VIBRATION PERIOD OF GENERIC MODELS

Table 3-3 presents the natural vibration periods of first mode computed for 15-storey and 30-storey generic models using standard eigenvalue analyses in *OpenSEEs* (2009). The natural vibration periods are computed after the application of gravity loads. Figure 3-18 shows the mode shape of the first natural vibration period of the 15-storey and 30-storey generic models. The natural vibration periods are compared with the natural vibration periods calculated using the period-height relationship derived in Chapter 2, as shown in Table 3-3. From Table 3-3, it can be seen that the absolute differences between the natural vibration periods calculated from *OpenSEEs* and the natural vibration periods estimated using Eq. 2-10 to Eq.2-13 are very small, which are 6.50% for the 15-storey generic model and -1.47% for

the 30-storey generic model. Thus it is reasonable to use the generic models to represent typical 15-storey slab block and 30-storey point block in Singapore.

Table 3-3 Summary of natural vibration period of the generic models computed from *OpenSEEs* and Eq. 2-10 to Eq.2-13

Generic models	Natural vibration period computed from <i>OpenSEEs</i> (sec)	Natural vibration period estimated from Eq. 2-12 to Eq.2-15 (sec)	Percentage difference (%)
15-storey	0.67	0.68	-1.47
30-storey	1.31	1.23	6.50

3.3 CHAPTER SUMMARY

In this chapter, 15-storey and 30-storey generic models which represent typical 15-storey slab block and 30-storey point block buildings in Singapore have been constructed using *OpenSEEs*. The generic models are representative of reinforced concrete infilled frame with shear wall buildings, which are typically found in Singapore. The first-storey of the generic model is not modeled with infilled walls. *NonlinearBeamColumn* element implemented in *OpenSEEs* has been used to model the beam, column and shear wall sections. Special attentions have been paid on the modeling of beam-column joints. A joint panel model, namely *Joint2D* element implemented in *OpenSEEs* has been used to model the beam-wide column joints. Experimental results on beam-wide column joints have been compared with the simulation results using the joint panel model. It is found that the joint panel model can represent well the behavior of nonseismically detailed beam-wide column joints. The natural vibration period of the generic models computed from *OpenSEEs* have been compared with those estimated using the proposed empirical period-height relationships and the differences are very small. It is thus

CHAPTER 3: GENERIC STRUCTURAL MODELS

concluded that the generic models are representative of typical high-rise buildings in Singapore.

CHAPTER 4

METHODOLOGY FOR ESTIMATING HUMAN PERCEPTION TO TREMORS IN HIGH-RISE BUILDINGS

In the seismological point of view, human perception to tremors is usually associated with the macroseismic intensity scale, such as MMI (Wald et al., 1999a) or JMA (1996). Omote et al. (1990) investigated the intensity distribution in high-rise buildings in Tokyo, with number of stories ranging from 30 to 60 aboveground, by means of questionnaire surveys after three earthquakes (Miyagi-ken-Ogi 1978, Kanagawa-Yamanashi Border 1983, Nagano Ken Seibu 1984). It was observed that the intensity tended to increase slightly with height. It also showed that people in these buildings were sensitive to building vibration. Musson (2005) presented a method to approximate the number of people likely to feel any earthquake assuming a uniform population distribution. The method was based on the regional intensity attenuation combined with average earthquake recurrence rates.

For modern cities, especially those located at low-to-moderate seismicity region, where earthquake events are not frequent or the tremors are only caused by long-distance earthquake events, the human perception to weak tremors may cause significant social impacts. Due to the increasing number of tremor events reportedly felt in Singapore (Figure 1-2), there is a need to develop a methodology to estimate the level of perception to tremors of occupants living in high-rise public residential buildings subjected to ground motion excitations, which forms the core content of the present work. This methodology will play an important role in the development of emergency response plan in the event of tremors due to long-distance earthquakes originated from Sumatra. Besides, this methodology will also form a

basis for development of seismic intensity for modern cities where majority of the population lives in high-rise residential buildings. This chapter proposes a methodology for estimating the perception level of occupants living in high-rise buildings given the ground motions intensity. Singapore, an island country located at southern tips of Malay Peninsula, is used as illustrations. The procedure does not rely on empirical nor historical data. Instead, the level of perception to tremors is estimated by quantifying the response of generic models subjected to characterized ground motions. For this purpose, guideline for threshold of human perception to vibration is used to define the threshold motion corresponding to estimated level of perception. The recorded ground motions in Singapore during past Sumatran earthquake events are used as the input ground motions. The ground motions are characterized using the average response spectral acceleration (ARSA) over period band corresponding to the period range of high-rise public residential buildings in Singapore. Two generic models of 15 and 30 stories, which represent typical high-rise residential buildings in Singapore, are constructed and subsequently used for the time-history analysis. The responses of the generic models subjected to the input ground motions characterized to different levels of ground motion intensity are compared with the threshold of human perception to vibrations. Subsequently, the relationships between the level of perception to tremors and the ground motion intensity are established using regression analysis. Three tremor events reportedly felt in Singapore are used to validate the proposed methodology. The proposed methodology will form the basis for defining the lower level of seismic intensity scale applicable for modern cities, which are dominated by high-rise residential buildings.

4.1 METHODOLOGY

The relationships between the human perception to tremors and ground motion intensity can be used to estimate the perception level to tremors of

CHAPTER 4: METHODOLOGY FOR ESTIMATING HUMAN PERCEPTION TO TREMORS IN HIGH-RISE BUILDINGS

occupants living in high-rise buildings as a function of ground motion parameters. The perception level is defined by estimated percentage of occupants living in certain story of a high-rise building to perceive tremors when subjected to ground motion excitation. The AIJ guideline used to define the threshold of perception to vibrations will be discussed in the later part of the chapter. For the ground motion, ARSA in period band 0.1 to 2.0 sec with 5% damping ratio, which corresponds to period range of high-rise public residential buildings in Singapore, will be used. The relationship relating the level of perception to tremors and ground motion intensity can be expressed as follows:

$$P_{\%,i} = f(y_{ARSA}) \quad \text{Eq. 4-1}$$

where $P_{\%,i}$ is the estimated percentage of occupants to perceive tremors at i th storey of the building; y_{ARSA} is the ARSA value of the ground motion. In this study, the function f , which relates the level of perception to tremors and ground motion parameters, is assumed to be natural logarithmic function.

The basic concept involved in the proposed methodology is to quantify the response of a generic model subjected to characterized ground motion, which is scaled linearly to certain ground motion intensity. The generic model used, in this case, is representative of the existing typical buildings. For this purpose, 15-storey and 30-storey generic models which are modeled as closely as possible to the existing high-rise public residential buildings in Singapore are used for the analysis. Thus the response of the models is representative of the expected response of typical buildings in Singapore subjected to ground motion excitations. The quantification of the response of the models can be done by comparing the response (in this study, peak floor acceleration is used) at a particular storey of interest with the threshold of perception to vibrations when subjected to the characterized ground

CHAPTER 4: METHODOLOGY FOR ESTIMATING HUMAN PERCEPTION TO TREMORS IN HIGH-RISE BUILDINGS

motion. Relationships between the estimated level of perception to tremors and the ground motion intensity with structural response exceeding the corresponding perception threshold can then be established using regression analysis. The general framework of this methodology is shown in Figure 4-1.

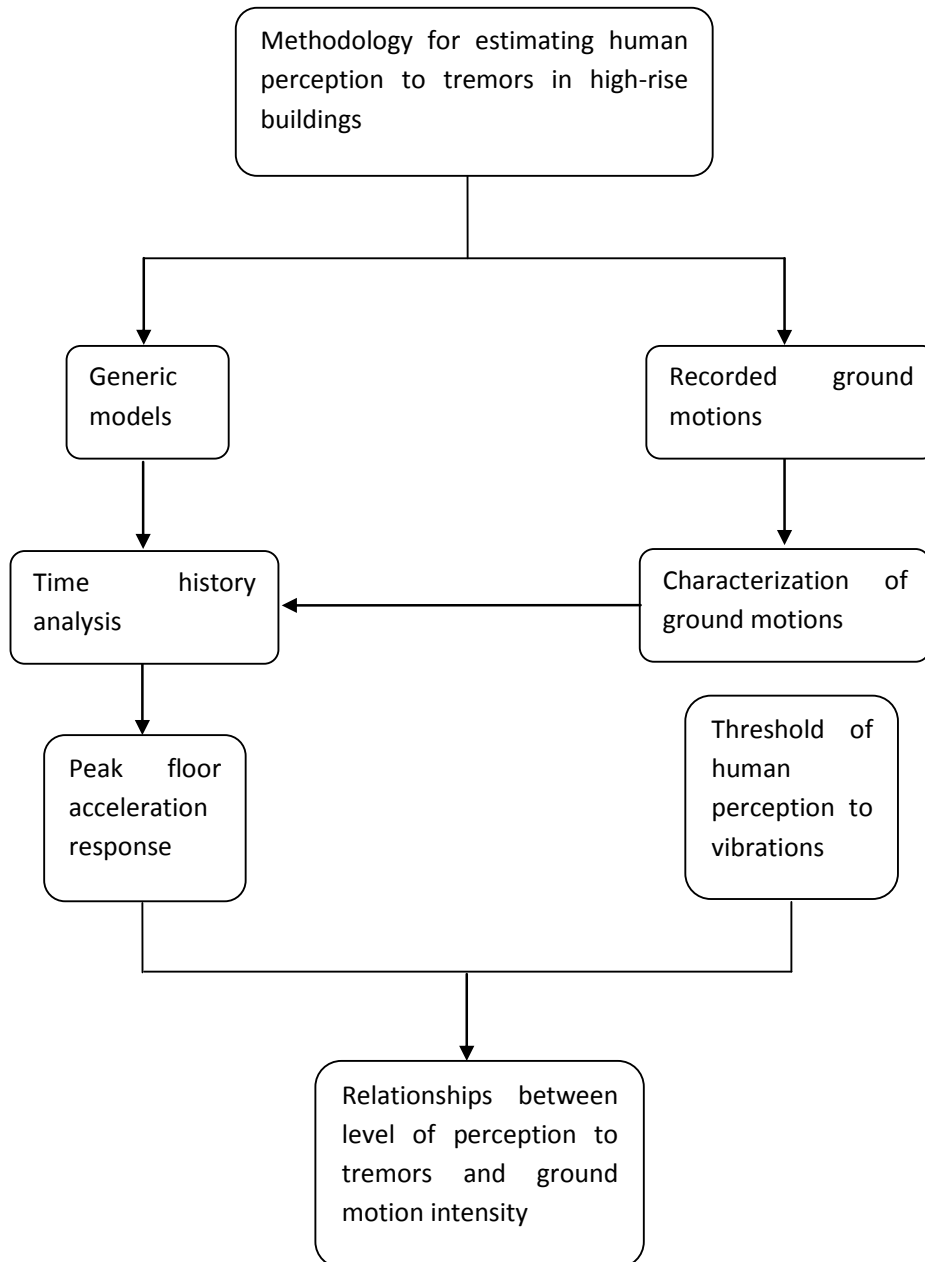


Figure 4-1 Framework for evaluating human perception to tremors

4.2 CHARACTERIZATION OF GROUND MOTION

4.2.1 RECORDED GROUND MOTION

A network of seismic stations in Singapore was established by The Meteorological Service Singapore (MSS) in September 1996. The network comprises one broadband Global Seismographic Network (GSN) station, four teleseismic stations and two borehole arrays. The GSN station, situated on a very hard rock site, at the centre of Singapore island, is equipped with a comprehensive set of sensors to record ground tremors continuously, whereas the other stations operate based on a triggering system (Pan and Lee, 2002).

During last decade, 10 Sumatran earthquakes had generated substantial ground tremors with perceptible levels in Singapore. These earthquakes are listed in Table 4-1. The magnitude of the earthquakes range from $M_w=5.4$ to $M_w=9.1$ while the distances between the epicenters and Singapore range from 460 km to 1600 km. The recorded ground motions of these 10 earthquake events will be used in this study.

4.2.2 SCALING OF GROUND MOTIONS

There is a common practice to use peak ground acceleration (*PGA*) or peak ground velocity (*PGV*) as the ground motion parameters in defining the structural response or the level of human perception to tremors and indoor nonstructural observations, such as those adopted in MMI (Wald et al., 1999a; Wald et al., 1999b) and JMA (JMA, 1996). This may be good for estimating the response of low-rise buildings which are relatively stiff. However, it has been shown that peak ground motion parameters provide poor or fair correlation with structural response, whereas

CHAPTER 4: METHODOLOGY FOR ESTIMATING HUMAN PERCEPTION TO TREMORS IN HIGH-RISE BUILDINGS

spectral and energy parameters provide good correlation (Elenas and Meskouris, 2001). Besides, average response spectral acceleration (ARSA) in period bands have also been used as parameters of constructing fragility curves for structural systems (Singhal and Kiremidjian, 1996). Thus, ARSA of 5% damping ratio is used in this study to define different levels of ground motion intensity.

Table 4-1 Ten significant Sumatran subduction earthquakes that caused perceivable tremors in Singapore during the last 10 years

No	Date	Time (GMT)	Epicentre		Depth (km)	M _w	R (km)	PGA (gal)
			Latitude	Longitude				
1	04 June 2000	16:28:47	4.730°S	101.940°E	43.9	7.9	704	0.35
2	07 June 2000	23:45:35	4.630°S	101.820°E	16.6	6.7	697	0.09
3	11 May 2004	08:28:48	0.415°N	97.825°E	21.0	6.1	670	0.03
4	26 Dec 2004	00:58:50	3.090°N	94.260°E	28.6	9.1	1600	0.30
5	28 Mar 2005	16:09:37	1.670°N	97.070°E	25.8	8.6	747	0.77
6	10 Apr 2005	10:29:11	1.680°S	99.540°E	12.0	6.7	579	0.11
7	17 Apr 2005	21:23:51	1.660°S	99.540°E	23.0	5.4	578	0.013
8	14 May 2005	05:05:19	0.420°N	98.250°E	39.0	6.7	625	0.10
9	12 Sep 2007	11:10:27	4.438°S	101.367°E	34.0	8.4	619	1.2
10	30 Sep 2009	10:16:09	0.789°S	99.961°E	80.0	7.6	460	0.36

The ARSA is calculated by averaging the response spectral acceleration of a ground motion over a period band with 0.1 second interval. In order to have ground motions with different ARSA values, the 10 sets of recorded ground motions (Table 4-1) are scaled linearly to target ARSA in period band 0.1 sec to 2.0 sec, which corresponds to period range of existing high-rise public residential buildings in Singapore. Each set of ground motions has two horizontal ground motions; so there are in total 20 ground motions. The target ARSA are set to a range from 1.0 gal to 7.0 gal. The lower bound of target ARSA is set when the occupants in the buildings start to perceive the tremors, while the upper bound value is set when all the occupants in the buildings perceive the tremors. To obtain the scaled ground motions, the recorded ground motions are multiplied by a scaling factor, which is calculated by taking the ratio of target ARSA to ARSA of the recorded ground

CHAPTER 4: METHODOLOGY FOR ESTIMATING HUMAN PERCEPTION TO TREMORS IN HIGH-RISE BUILDINGS

motions in period band 0.1 sec to 2.0 sec. The scaled ground motions will be used as the input excitations for time history analysis. For illustration purpose, the mean and standard deviation of the spectral accelerations (5% damping ratio) of the 10 sets of recorded ground motions scaled to ARSA of 1.5 gal in period band 0.1 sec to 2.0 sec are shown in Figure 4-2.

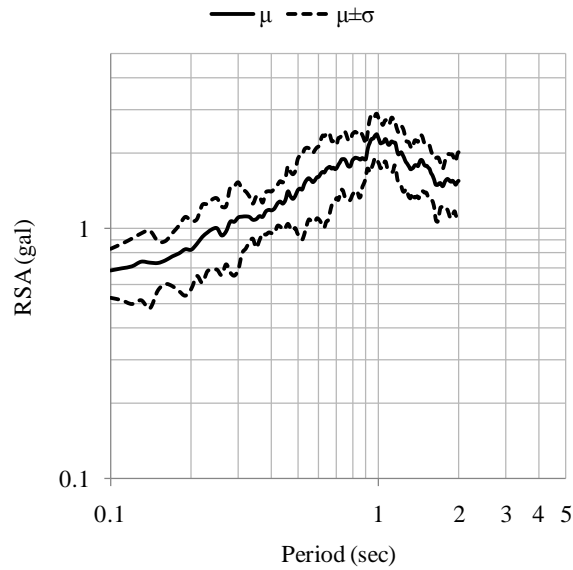


Figure 4-2 Mean and standard deviation of the 10 sets of recorded ground motions scaled to ARSA value of 1.5 gal in period band 0.1 sec to 2.0 sec

4.3 GUIDELINE FOR THRESHOLD OF HUMAN PERCEPTION TO VIBRATION

In 2004, Guidelines for Evaluation of Habitability to Building Vibration was published by Architectural Institute of Japan (AIJ, 2004) (Figure 4-3). The guidelines were formed based on the works by Kanda et al. (1994). The objective of these guidelines is to provide performance assessment to different environmental vibration such as transportation, wind, earthquake and machinery. The tests were

CHAPTER 4: METHODOLOGY FOR ESTIMATING HUMAN PERCEPTION TO TREMORS IN HIGH-RISE BUILDINGS

carried out based on people sitting and subjected to uniaxial sinusoidal vibration. The level of human perception to vibration is presented in the form of estimated percentage of occupants to perceive vibration, while the threshold is expressed in terms of the peak acceleration of the motion. The curves H-10, H-30, H-50, H-70 and H-90, as presented in Figure 4-3, represent the level of perception where 10%, 30%, 50%, 70% and 90% of the occupants may feel the vibration. To obtain the level of perception between these curves, logarithmic interpolation is used.

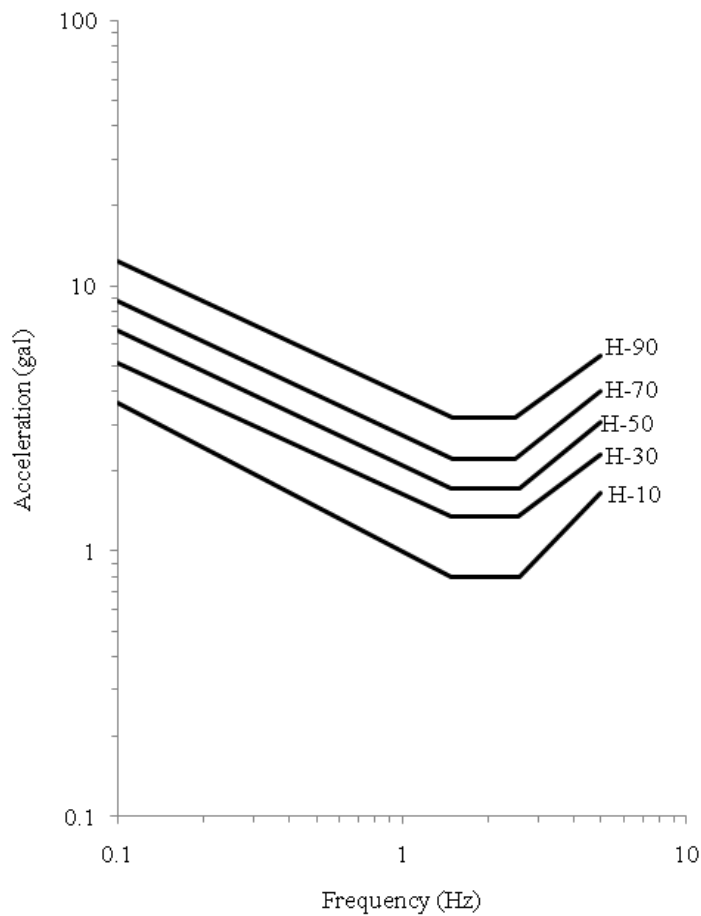


Figure 4-3 Summary of human perception threshold to vibration specified by AIJ-GEH-2004

The human perception to vibration is presented as a function of frequency of the motion. From Figure 4-3, it can be seen that the threshold of perception to vibration decreases when the frequency increases from 0.1 Hz to 1.5 Hz. For vibration frequency ranges from 1.5 Hz to 2.5 Hz, the perception threshold to vibration remains the same, and the perception threshold increases again with increase in vibration frequency for frequency higher than 2.5 Hz. This suggests that people may be more sensitive to vibration with frequency ranges from 1.5 Hz to 2.5 Hz, which coincides with the period range of high-rise residential buildings in Singapore. In the present study, it is assumed that the responses of the generic models are mainly governed by the 1st mode of vibrations. Thus, the threshold acceleration for estimating the level of perception to vibration for the 15-storey and 30-storey generic models can be defined from Figure 4-3 using frequency (period) values of 1.49 Hz (0.67 sec) and 0.76 Hz (1.31 sec), respectively.

4.4 RELATIONSHIPS BETWEEN LEVEL OF PERCEPTION TO TREMORS AND GROUND MOTION INTENSITY

The analyses are conducted using *OpenSEEs* (2009). Newmark integrator is used in the time history analysis. The scaled ground motions are used as input excitations. There are in total 10 sets of recorded ground motions used, and for each set of ground motions there are two components (N-S and E-W). Thus, for each target ARSA value, there are 20 analyses conducted. The peak floor acceleration response of the generic models subjected to ground motion characterized to certain ARSA value is compared with the threshold of human perception to vibrations corresponding to the 15-storey and 30-storey generic models, respectively. For the 15-storey generic model, the peak floor acceleration responses at top and the 7th storey are used. For the 30-storey generic model, the responses at the top and 15th storey are used. The ARSA of the input ground motion will be associated with the level of perception to vibration if the peak floor acceleration exceeds the

CHAPTER 4: METHODOLOGY FOR ESTIMATING HUMAN PERCEPTION TO TREMORS IN HIGH-RISE BUILDINGS

corresponding perception threshold. Thus, for each ARSA value, there will be 20 data points corresponding to 20 perception levels with the perception threshold exceeded by the peak floor acceleration response.

The perception levels corresponding to each ARSA value is assumed to have a lognormal distribution function. The regression analysis is performed between the mean of the perception levels and the ARSA assuming a natural logarithmic function. Thus, the regression equations relating the ARSA with the perception level are expressed as

For 15-storey model,

$$p = 61.56 \ln ARSA + 11.17 \quad \text{for 15}^{\text{th}} \text{ storey} \quad \text{Eq. 4-2}$$

$$p = 61.51 \ln ARSA + 5.48 \quad \text{for 7}^{\text{th}} \text{ storey} \quad \text{Eq. 4-3}$$

For 30-storey model,

$$p = 69.38 \ln ARSA + 5.32 \quad \text{for 30}^{\text{th}} \text{ storey} \quad \text{Eq. 4-4}$$

$$p = 67.12 \ln ARSA - 41.51 \quad \text{for 15}^{\text{th}} \text{ storey} \quad \text{Eq. 4-5}$$

where p is the perception level, which is expressed in terms of estimated percentage of occupants to perceive tremors; and $ARSA$ is the ground motion intensity in gal. The curves representing the above mentioned relationships are presented in Figures 4-4 and 4-5 for 15-storey and 30-storey generic models, respectively. Also plotted in the figures are the lognormal distributions of the perception levels in

CHAPTER 4: METHODOLOGY FOR ESTIMATING HUMAN PERCEPTION TO TREMORS IN HIGH-RISE BUILDINGS

corresponding ARSA values. The relationships shown in Eq. 4-2 to 4-5 can be used to estimate the percentage of occupants in high-rise buildings who may perceive tremors given the ARSA value of the ground motion.

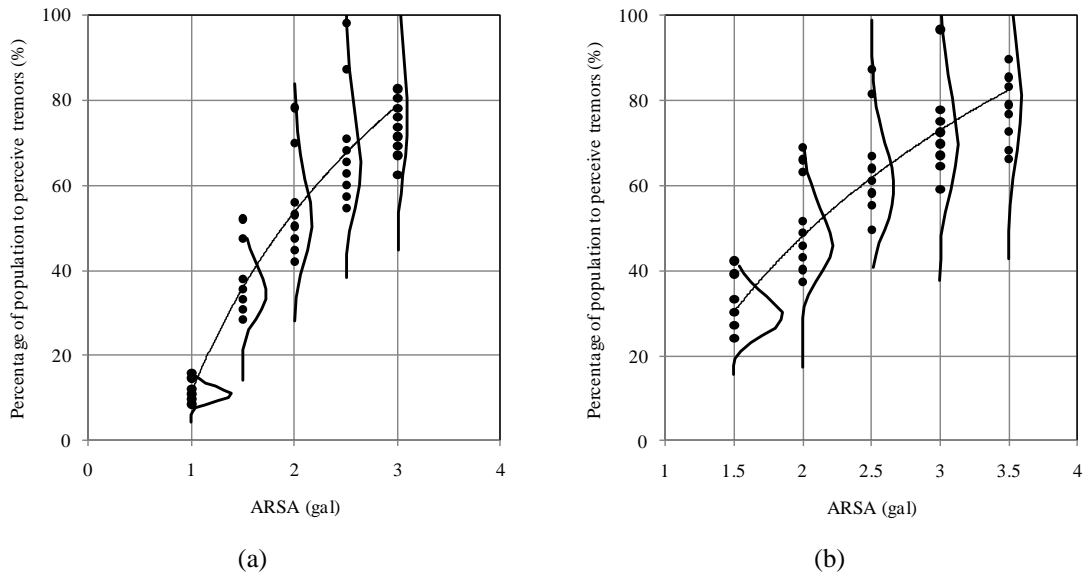


Figure 4-4 Regression relationships between perception level and ARSA for the 15-storey generic model at (a) 15th storey; and (b) 7th storey

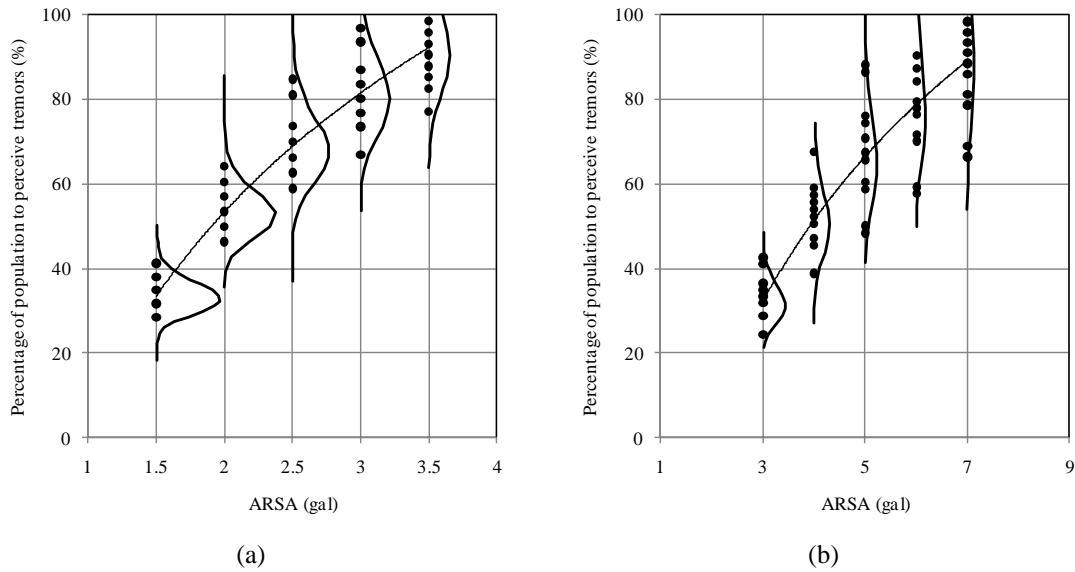


Figure 4-5 Regression relationships between perception level and ARSA for the 30-storey generic model at (a) 30th storey; and (b) 15th storey

4.5 VALIDATIONS

The proposed methodology is used to estimate the level of perception to tremors due to three Sumatran earthquakes which caused perceptible tremors in Singapore. The ground motions in Singapore due to the three earthquake events were captured by the seismic stations situated at soft-soil site (Kallang Formation) and firm-soil site (Bukit Timah Granite). The ARSA values in period band 0.1 sec to 2.0 of the recorded ground motions during the three earthquake events at firm-soil site and soft-soil site are presented in Table 4-2. The details of the three tremor events reportedly felt and the reports from the local newspaper and the authorities are as follows:

Case study 1: December 26, 2004 event

A great earthquake with a magnitude of $M_w=9.1$ according to the United States Geological Survey (USGS) occurred in Sumatra-Andaman Islands, Indonesia, on December 26, 2004, at 00:58:50 (UTC). The main tremors were reportedly felt in several areas of Singapore, 1600 km south-east to the epicenter. A local Singapore newspaper reported that the areas where the tremors were felt are Tanjong Rhu, Marine Parade, Toa Payoh, Siglap, Clementi, Meyer Road, and Beach Road (*Today*, December 27, 2004). From the distribution of the locations, the reported locations where tremors were felt are at the southern part of Singapore which is largely overlain by Quaternary marine clay deposits (soft-soil site).

Case study 2: March 28, 2005 event

On March 28, 2005, tremors felt in Singapore at around 16:09:37 (UTC) were due to an earthquake with a magnitude of $M_w=8.6$ that occurred in Northern Sumatra, Indonesia, approximately 747 km away from Singapore. There were around 200 reportedly felt tremors cases in Singapore due to the earthquake event. It was reported by a local newspaper (*The New Paper*, March 30, 2005) that tremors lasted for about two minutes. The tremors were felt in many parts of Singapore including Bedok, Farrer Park, Hougang, Marine Parade, Potong Pasir, Punggol, Sengkang, Serangoon, Teban Gardens, Toa Payoh and Whampoa. Another local newspaper (*The Straits Times*, March 29, 2005) reported additional locations that felt the tremor, which were Bradell, Bukit Batok, Choa Chu Kang, East Coast, Fort Road, Geylang and Zion Road. The locations of the reported felt tremors cases were located island wide, both on firm-soil site and soft-soil site.

Case study 3: September 30, 2009 event

The September 30, 2009 event occurred just off the southern coast of Sumatra, Indonesia. The major shock hit at 10:16:09 (UTC) and had a moment magnitude of 7.6. The epicenter was 45 km west-northwest of Padang, Sumatra, and 220 km southwest of Pekanbaru, Sumatra. It was reported by a local Chinese newspaper (*Lienhe Zao Bao*, October 1, 2009) that tremors were felt in many parts of Singapore including Woodlands, Sembawang, Yishun, Bukit Panjang, Bukit Batok, Chuo Chu Kang, Bedok Reservoir, Aljunied, Clarke Quay, Marina Square and Toa Payoh. The reported felt cases in Singapore were island wide, both on firm-soil site and soft-soil site.

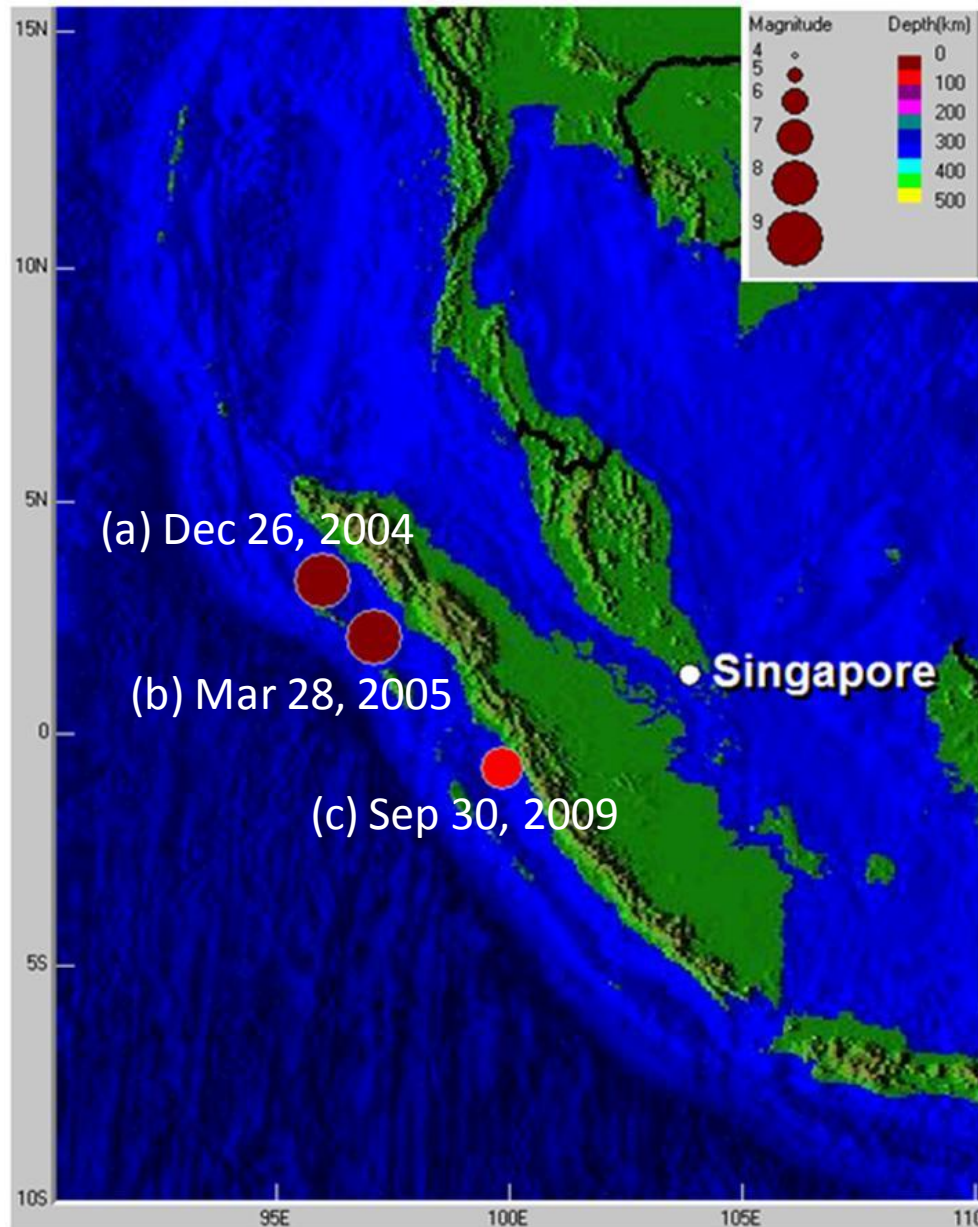


Figure 4-6 Epicenters of the (a) December 26, 2004; (b) March 28, 2005; and (c) September 30, 2009 Sumatran earthquake events

Figure 4-6 shows the epicenters of the three earthquake events. Figure 4-7 shows the surface geology of Singapore (DSTA, 2009) overlaid with the locations

CHAPTER 4: METHODOLOGY FOR ESTIMATING HUMAN PERCEPTION TO TREMORS IN HIGH-RISE BUILDINGS

where the tremors reportedly felt due to the three earthquake events. The maximum values of ARSA of the N-S and E-W components of each event, as shown in Table 4-2, are substituted into Eq. 4-2 to 4-5 to estimate the perception level due to the three earthquake events. The results of the estimations are summarized in Table 4-3. From Table 4-3, it can be seen that for December 26, 2004 event, it is estimated that the occupants living in buildings located at firm-soil site are unlikely to perceive the tremors, while there are a few people living in buildings located at soft-soil site may perceive the tremors. These match well with the reports for this event (Figure 4-6), where there were only cases reported felt from the southern part of Singapore which is mainly covered by soft-soil site.

For March 28, 2005 event, it is estimated that up to 35 % and 75% of the occupants living in buildings located at firm-soil site and soft-soil site, respectively, may perceive the tremors. These match well with the reports from the newspaper and authorities, that there were large numbers of cases reported felt from island wide, both on firm-soil site and soft-soil site.

For September 30, 2009 event, it is estimated that about 16% of the occupants living in buildings located at firm-soil site may perceive the tremor, while the occupants living in higher story of the buildings at soft-soil site are very likely to perceive the tremor. These agree well with the reports from the newspaper and authorities, that most of the reported felt cases were located on soft-soil site. There were, but relatively fewer cases (compared with March 28, 2005 event) reported from occupants living in buildings located at firm-soil site.

CHAPTER 4: METHODOLOGY FOR ESTIMATING HUMAN PERCEPTION TO TREMORS IN HIGH-RISE BUILDINGS

Table 4-2 The ARSA values of the recorded ground motions during the three earthquake events at firm-soil site and soft-soil site

Earthquake events		ARSA (gal)	
		Firm-soil	Soft-soil
December 26, 2004	N-S	0.49	0.94
	E-W	0.32	0.81
March 28, 2005	N-S	1.46	2.72
	E-W	0.80	2.28
September 30, 2009	N-S	1.08	5.06
	E-W	0.89	4.52

Table 4-3 Estimated percentage of occupants to perceive tremors during December 26, 2004, March 28, 2005 and September 30, 2009 Sumatran earthquake events in (a) 15-storey; (b) 30-storey buildings

(a)

Storey	December 26, 2004		March 28, 2005		September 30, 2009	
	Firm-soil	Soft-soil	Firm-soil	Soft-soil	Firm-soil	Soft-soil
15 th	0%	7.36%	34.47%	72.77	15.91%	100%
7 th	0%	1.67%	28.76%	67.03	10.21%	100%

(b)

Storey	December 26, 2004		March 28, 2005		September 30, 2009	
	Firm-soil	Soft-soil	Firm-soil	Soft-soil	Firm-soil	Soft-soil
30 th	0%	1.03%	31.58%	74.74%	10.66%	100%
15 th	0%	0%	0% %	25.65%	0%	67.32

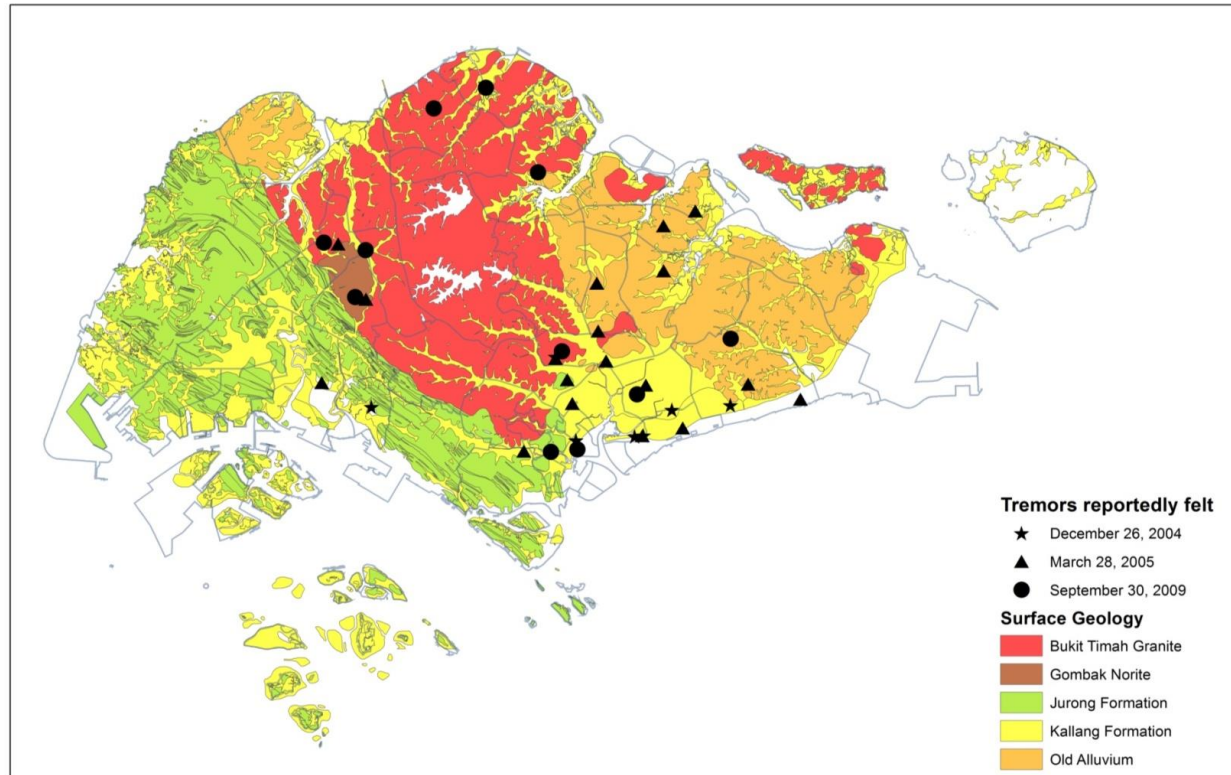


Figure 4-7 The surface geology of Singapore (DSTA, 2009) overlaid with the location of tremors reportedly felt in Singapore during December 26th, 2004, March 28th, 2005 and September 30th, 2009 Sumatran earthquake events

4.6 CHAPTER SUMMARY

This chapter proposed a methodology for estimating the level of perception to tremors of occupants living in high-rise residential buildings subjected to ground motion excitations. Singapore, where majority of the population lives in high-rise residential buildings, has been used as illustrations. In contrast with previous approaches, which were based on empirical or historical data, the proposed methodology is based on statistical analysis of analytical results of seismic response of generic models to recorded ground motions. Guideline for threshold of human perception to vibration has been used to define the threshold motion corresponding to the perception level, which is expressed in terms of estimated percentage of occupants to perceive tremors. The ground motions have been characterized using average response spectral acceleration (ARSA) in period band 0.1 sec to 2.0 sec corresponding to period range of high-rise residential buildings in Singapore. The period band coincides with the frequency band of lowest perception threshold. The 15-storey and 30-storey generic models have been used for the analysis. Relationships between the estimated level of perception to tremors and ARSA of the input ground motions with structural response exceeding the corresponding perception threshold have been established using regression analysis. The relationships can be used to estimate the percentage of occupants living in high-rise buildings who may perceive the tremors given ground motion intensity. The proposed methodology has been validated with three tremor events reportedly felt in Singapore. It has been found that the estimated results match well with the reports from the local newspapers and the authorities.

CHAPTER 5

SEISMIC PERFORMANCE OF TYPICAL BUILDINGS IN SINGAPORE TO MAXIMUM CREDIBLE EARTHQUAKE GROUND MOTIONS

In this chapter, the seismic performances of the 15-storey and 30-storey generic models subjected to ground motions due to maximum credible earthquakes in the Sumatran fault and subduction zone are assessed.

5.1 POTENTIAL FAILURE MODES

For lightly reinforced concrete frame building, as represented by the 15-storey and 30-storey generic models, the potential failure modes of structures when subjected to seismic loading include:

- (a) Beam-column joint shear failure:

The nonseismically detailed beam-wide column joints may have shear failure when subjected to seismic loading. Joint shear failure occurs when the induced joint shear stress reaches the joint shear strength. The shear strength of the beam-wide column joints in the generic models are modeled as $0.95\sqrt{f'_c}$. The details of the modeling of beam-wide column joints have been presented in Chapter 3.

- (b) Column shear failure

Sezen and Moehle (2004) reported a model for shear strength of columns that initially yield in flexure. The empirical model is based on theoretical concepts of shear resistance but is calibrated to test data. The shear strength is defined as

$$V_n = V_s + V_c = k \frac{A_{st} f_{yt} d}{s} + k \left(\frac{0.5 \sqrt{f'_c}}{a/d} \sqrt{1 + \frac{P}{0.5 \sqrt{f'_c} A_g}} \right) 0.8 A_g \quad \text{Eq. 5-1}$$

where V_s and V_c are the shear contributions assigned to steel and concrete, respectively; k is a parameter equal to 1 for $\mu_\delta \leq 2$, equal to 0.7 for $\mu_\delta \geq 6$, and varies linearly for intermediate μ_δ values; μ_δ = displacement ductility; A_{st} = area of shear reinforcement parallel to the horizontal shear force within spacing s ; f_{yt} = yield strength of transverse reinforcement; d = effective depth (= $0.8h$, where h = section depth parallel shear force); P = axial compression force; f'_c = concrete compressive strength (MPa); A_g = gross section, and a/d = shear span/ effective depth (value limited between 2 and 4). The shear strength of the columns of the 15-storey and 30-storey generic models is estimated at 359.2 kN and 430.7 kN, respectively, based on Eq. 5-1.

5.2 STATIC PUSHOVER ANALYSIS

Nonlinear static pushover analysis is conducted to determine the overstrength, ductility and possible failure modes of the 15-storey and 30-storey generic models. In seismic codes, the design base shear is defined as

$$V_d = \frac{V_e}{\Omega\mu} \quad \text{Eq. 5-2}$$

where V_e is the elastic base shear; and Ω is the overstrength ratio defined as

$$\Omega = \frac{V_y}{V_d} \quad \text{Eq. 5-3}$$

μ is the ductility factor defined as

$$\mu = \frac{\Delta_u}{\Delta_y} \quad \text{Eq. 5-4}$$

where V_y is the base shear at significant yield point; V_d is design base shear; Δ_u is the ultimate displacement, and Δ_y is the significant yield displacement. Figure 5-1 shows the overstrength ratio and displacement ductility factor for a typical frame building (Balendra et al., 1999).

5.2.1 STATIC LATERAL LOAD

For tall buildings, the contribution from the higher modes could be more important. Thus a nonlinear contribution of static lateral loads is adopted. In this study, the distribution of lateral load recommended by FEMA 356 (FEMA, 2000) is adopted:

$$F_x = C_{vx} V \quad \text{Eq. 5-5}$$

$$C_{vx} = \frac{w_x h_x^k}{\sum_{i=1}^n w_i h_i^k} \quad \text{Eq. 5-6}$$

where C_{vx} is the vertical distribution factor; k is 2.0 for $T \geq 2.5$; $k=1.0$ for $T \leq 0.5$; k is interpolated linearly to calculate values of k for intermediate values of T . In this study, for the 15-storey generic model, $T=0.67$ sec, thus $k=1.085$; for the 30-storey generic model, $T=1.32$ sec, thus $k=1.41$; V is the total horizontal earthquake base shear force; w_i is the portion of the total building weight W located on or assigned to floor level i ; w_x is the portion of the total building weight W located on or assigned to floor level x ; h_i is the height from the base to floor level i ; and h_x is the height from the base to floor level x .

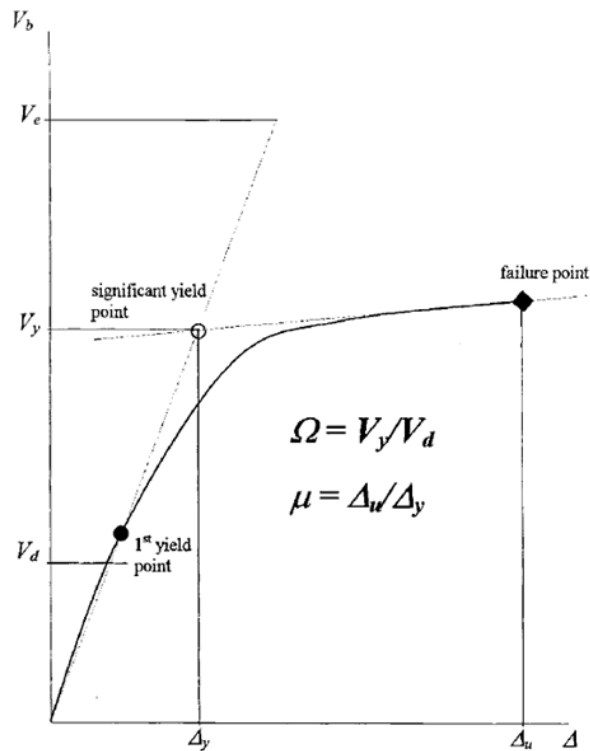
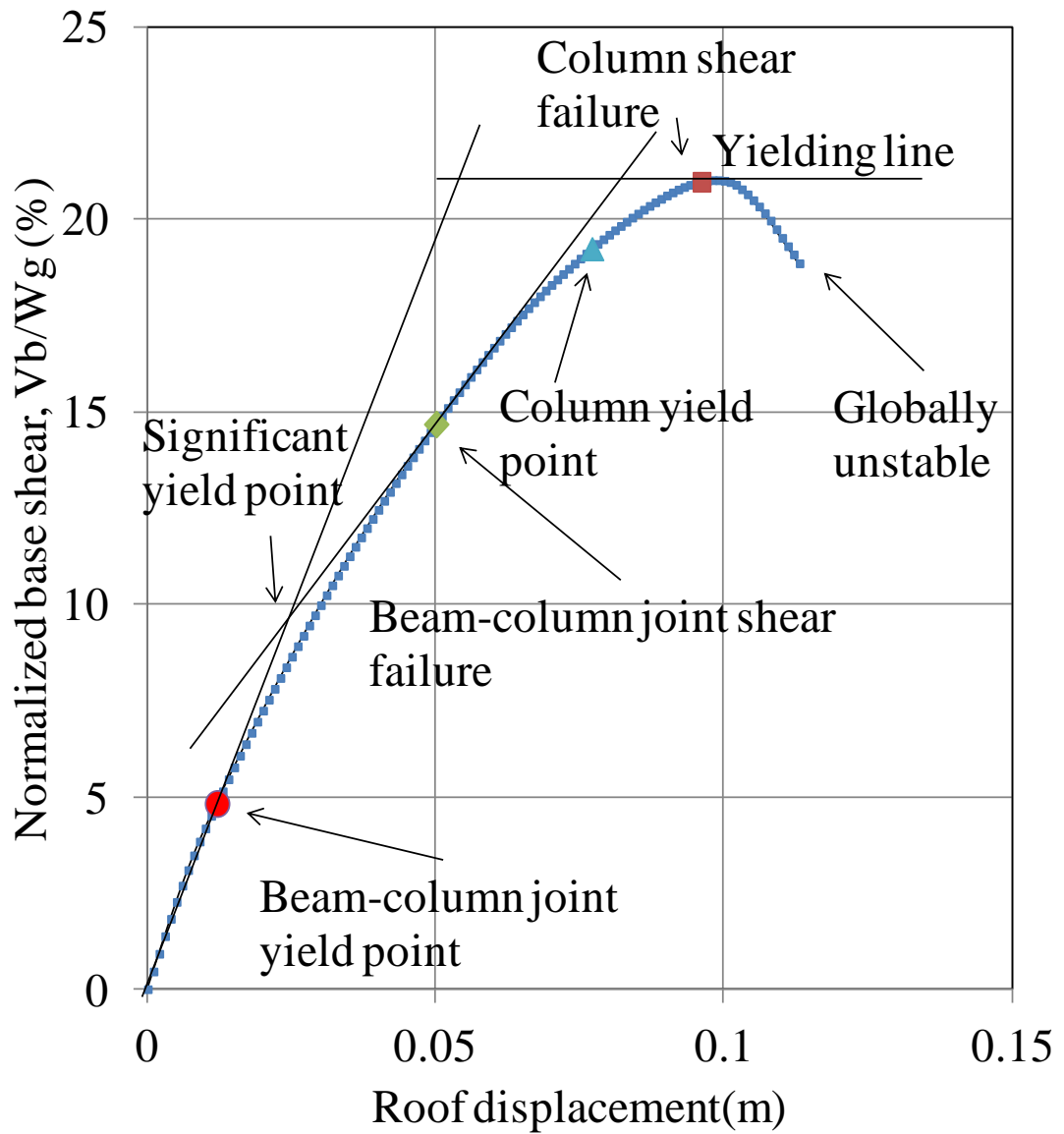


Figure 5-1 Overstrength ratio and displacement ductility factor (reprinted from work by Balendra et al., 1999)

5.2.2 RESULTS

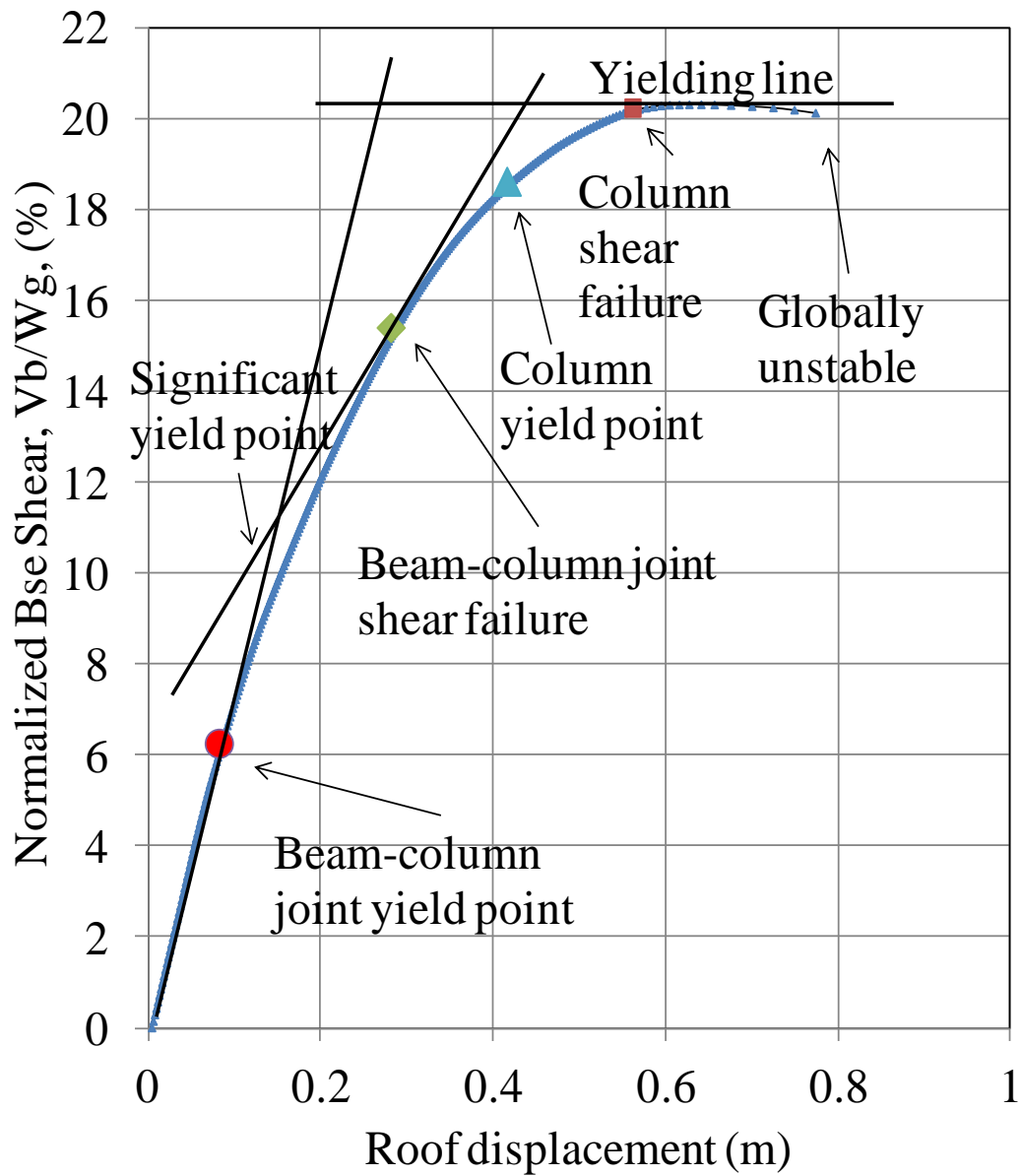
Figure 5-2 shows the results from the pushover analysis for the 15-storey and the 30-storey generic model.

For the 15-storey generic model (Figure 5-2a), the first beam-column joint yield point occurs when the roof displacement reaches 0.016 m, and the corresponding base shear force is 4.7% weight. The first beam-column joint shear failure occurs at roof displacement of 0.05 m, which corresponds to base shear force of 14.75% weight. The first column yield point occurs at roof displacement of 0.07 m, which corresponds to base shear force of 19.23% weight. The first failure of column in shear occurs at roof displacement of 0.096 m, which corresponds to base shear force of 20.96% weight. Beyond the first column shear failure point, more columns fail in shear as the roof displacement increases. This causes the base shear force decreases as the roof displacement increases. The 15-storey generic model is globally unstable at roof displacement of 0.113 m, which corresponds to base shear force of 18.86% weight, due to shear failure of multiple beam-column joints and columns. The pushover analysis is then terminated. Comparing with the behavior of a typical ductile structure (Figure 5-1), it can be concluded that the 15-storey generic model is a nonductile structure. Considering the point where first beam-column joint shear failure occurs, the significant yield point occurs at roof displacement of 0.028 m, which corresponds to base shear force of 8.2% weight. The overstrength ratio is calculated as 5.47 for a design base shear force of 1.5% weight.



(a)

Figure 5-2 Base shear versus roof displacement for: (a) 15-storey generic model; (b) 30-storey generic model



(b)
 Figure 5-2 Con't

For the 30-storey generic model (Figure 5-2b), the first beam-column joint yield point occurs when the roof displacement reaches 0.08 m, and the corresponding base shear force is 5.4% weight. The first beam-column joint shear failure occurs at roof displacement of 0.28 m, which corresponds to base shear force

of 15.4% weight. The first column yield point occurs at roof displacement of 0.42 m, which corresponds to base shear force of 18.62% weight. The first failure of column in shear occurs at roof displacement of 0.56 m, which corresponds to base shear force of 20.24% weight. Beyond the first column shear failure point, the base shear force continues to increase slightly as roof displacement increases. At roof displacement of 0.61 m, more columns fail in shear. The base shear force starts to decrease as the roof displacement increases. The 30-storey generic model is globally unstable when at roof displacement of 0.77 m, which corresponds to base shear force of 19.85% weight, due to shear failure of multiple beam-column joints and columns. The pushover analysis is then terminated. Comparing with the behavior of a typical ductile structure (Figure 5-1), it can be concluded that the 30-storey generic model is a nonductile structure. Considering the point where first beam-column joint shear failure occurs, the significant yield point occurs at roof displacement of 0.13 m, which corresponds to base shear force of 10.35% weight. The overstrength ratio, Ω , is calculated as 6.90 for a design base shear force of 1.5% weight.

At the point where first beam-column joint shear failure occurs, the ratio of column shear force to column shear strength for 15-storey and 30-storey generic model are $V/V_n = 0.49$ and $V/V_n = 0.66$, respectively. This shows that the structures are likely to have beam-column joint shear failure prior to column shear failure.

5.3 MAXIMUM CREDIBLE GROUND MOTIONS

5.3.1 TARGET SPECTRA

Megawati and Pan (2002) have identified that the maximum credible ground motions in Singapore are likely to be caused by two large earthquakes with different

source mechanism. One is the Sumatran fault earthquake with an epicentral distance of around 425 km and a moment magnitude of 7.5 ($M_w=7.5$, $R=425$ km). The other one is the Sumatran subduction earthquake with an epicentral distance of 700 km and a moment magnitude of 9.0 ($M_w=9.0$, $R=700$ km).

The acceleration response spectrum for maximum credible Sumatran fault earthquake is predicted using the attenuation relationship for the horizontal component of Sumatran fault earthquakes (personal communication with Kusnowidjaja Megawati). The attenuation relationship is presented as

$$\ln(Y) = a_0 + a_1(M_w - 6) + a_2(M_w - 6)^2 + a_3 \ln(R) + (a_4 + a_5 M_w)R + \varepsilon_{\ln(Y)} \quad \text{Eq. 5-6}$$

where Y is the geometric mean of the horizontal PGA, PGV or RSA values (5% damping ratio) at various natural periods. The unit for the acceleration values is cm/s^2 and that for velocity is cm/s . M_w is the moment magnitude and R is the distance from the station to the centre of the corresponding fault plane, in km.

The acceleration response spectrum for maximum credible Sumatran subduction earthquake is predicted using attenuation relationship for Sumatran megathrust earthquakes derived by Megawati and Pan (Megawati and Pan, 2010). The attenuation relationship is presented as

$$\ln(Y) = a_0 + a_1(M_w - 6) + a_2(M_w - 6)^2 + a_3 \ln(R) + (a_4 + a_5 M_w)R + \varepsilon_{\ln(Y)} \quad \text{Eq. 5-7}$$

where Y is the geometric mean of the horizontal PGA, PGV or RSA values (5% damping ratio) at various natural periods. The unit for the acceleration values is cm/s^2 and that for velocity is cm/s . M_w is the moment magnitude and R is the

distance from the station to the centre of the corresponding fault plane, in km. The regression coefficients of the attenuation relationships with 5% damping ratio for Sumatran megathrust earthquakes can be found in work by Megawati and Pan. (2010).

Figure 5-3 shows the predicted pseudo-acceleration response spectra (5% damping ratio) in Singapore resulting from the maximum credible Sumatran fault earthquake ($M_w=7.5$, $R= 425$ km) and the maximum credible Sumatran subduction earthquake ($M_w=9.0$, $R= 700$ km).

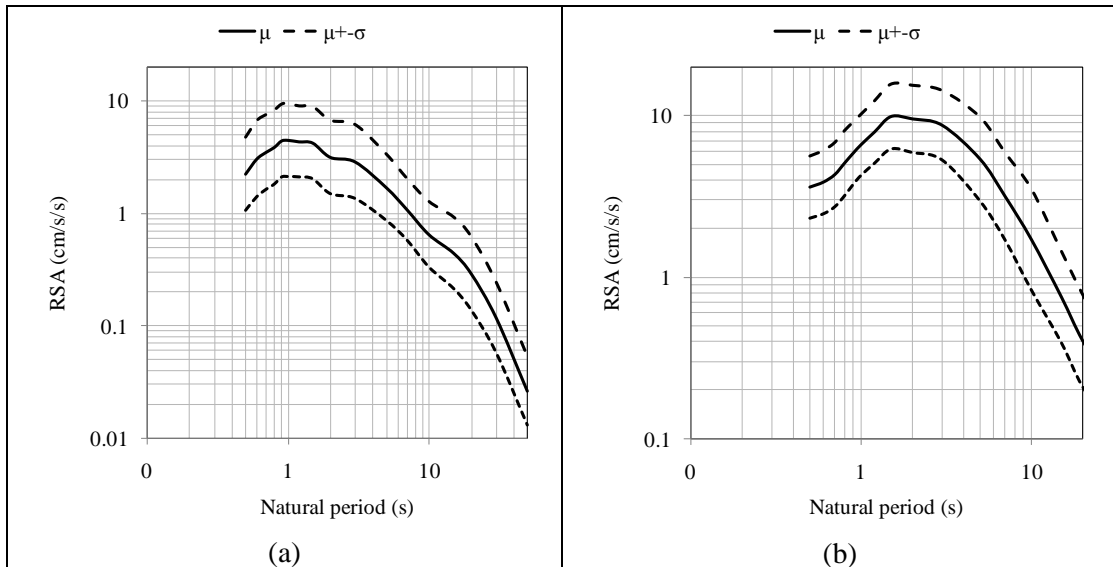


Figure 5-3 Pseudo-acceleration response spectrum (5% damping ratio) at rock site in Singapore resulting from: (a) the maximum credible Sumatran fault earthquake ($M_w=7.5$, $R= 425$ km); (b) the maximum credible Sumatran subduction earthquake ($M_w=9.0$, $R= 700$ km).

5.3.2 RECORDED GROUND MOTIONS

A network of seismic stations in Singapore was established by The Meteorological Service Singapore (MSS) in September 1996. The network comprises one broadband Global Seismographic Network (GSN) station, four teleseismic stations and two borehole arrays. The GSN station, situated on a very hard rock site, at the centre of Singapore Island, is equipped with a comprehensive set of sensors to record ground tremors continuously, whereas the other stations operate based on a triggering system.

Table 5-1 Summary of the 6 recorded Sumatran fault earthquakes

No	Date	Time (GMT)	Epicentre		Depth (km)	M_w	R (km)
			Latitude	Longitude			
1	10 Oct 1996	15:21:05	3.445°N	97.943	22.8	6.2	697
2	22 Apr 1997	5:55:59	3.37S	102.14E	107	5.9	526
3	20 Aug 1997	7:15:15	4.36N	96.49E	33	6	864
4	24 May 1998	2:32:53	6.51S	104.91E	52	5.6	865
5	18 Sept 1999	12:52:35	4.03S	103.32E	33	5.4	576
6	17 Dec 2006	21:39:18	0.57N	99.83E	18.2	5.8	454

In this study, 6 sets of recorded Sumatran fault earthquake ground motions and 10 sets of recorded Sumatran subduction earthquake ground motions in Singapore are used. Each set of ground motions consist of N-S and E-W components. The magnitude of the Sumatran fault earthquakes range from $M_w=5.4$ to $M_w=6.2$, and the distances between the epicenter and Singapore range from 526 km to 865 km. The magnitude of the Sumatran subduction earthquakes range from $M_w=5.4$ to $M_w=9.1$, and the distances between the epicenter and Singapore range from 460 km to 1600 km. The details of the Sumatran fault earthquakes and the Sumatran subduction earthquakes are summarized in Table 5-1 and Table 4-1 (Chapter 4), respectively.

5.3.3 SCALING OF GROUND MOTIONS

The recorded Sumatran fault ground motions in Singapore (Table 5-1) are scaled to match the predicted $\mu+\sigma$ acceleration response spectrum due to maximum credible fault earthquake, while the recorded Sumatran subduction ground motions in Singapore (Table 4-1) are scaled to match the predicted $\mu+\sigma$ acceleration response spectrum due to maximum credible Sumatran subduction earthquake. The method used for scaling is based on trial-and-error and Fourier Transformation (Karabalis et al., 1994). This method is based on the concept of using actual records to generate time histories that fit a given target response spectrum. The physical characteristics of the earthquake motion are retained throughout the procedure, which makes the technique powerful in comparison with the classical artificial record generation. In this method, an actual record is scaled in frequency domain by its spectral ratio with the design target spectrum. Firstly, the target spectrum and the recorded ground motion used for scaling are selected. The ratio R between the target spectrum and the spectrum of the recorded ground motion in each frequency window is calculated. The Fourier Spectrum Amplitude of the recorded ground motion is computed using Fast Fourier Transform (FFT). Subsequently, the time history in each frequency window is generated using inverse FFT. The time history generated from inverse FFT is then multiplied by the ratio R . The scaled time histories in all frequency window are summed up to generate a new ground motion. The process is iterated until desired difference between the target spectrum and the spectrum of the scaled ground motion is achieved. The summary of the scaling procedure is shown in Figure 5-4. The recorded ground motions are scaled to match the target response spectrum, so that: (1) the average error between the scaled spectrum and the target spectrum is less than 10%, and (2) the ratio of standard deviation to mean of the scaled response spectra is less than 10%. Figure 5-5 shows the comparison between the target spectrum and the spectrum of the scaled ground motion with number of iterations of 1, 2, 5, and 10. Good match

between the target spectrum and the spectrum of the scaled ground motion is obtained after 10 iterations, as shown in Figure 5-5.

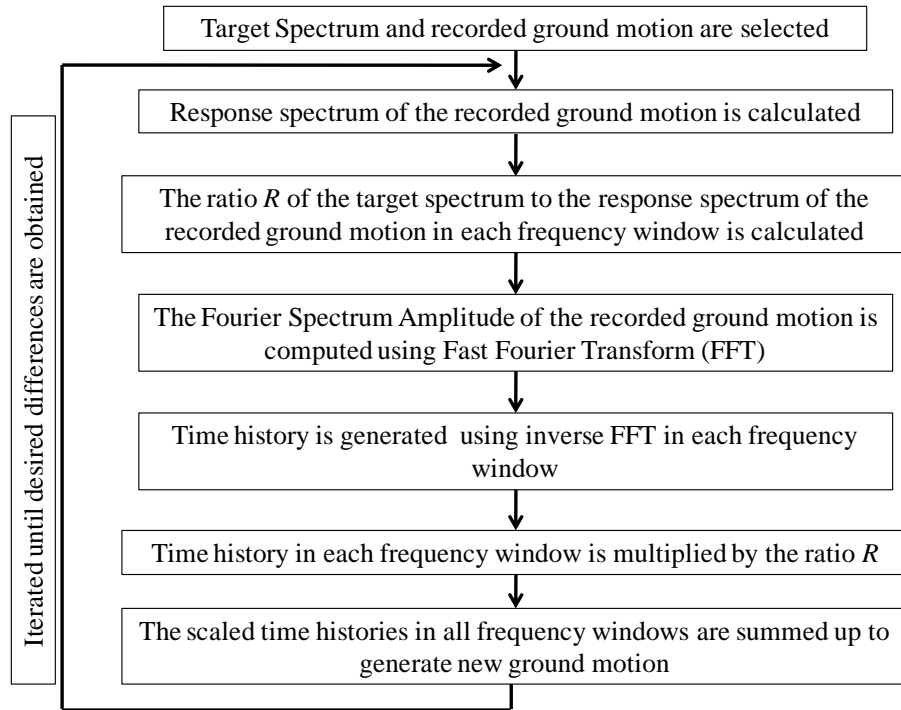


Figure 5-4 Procedure of ground motion scaling in frequency domain

Figure 5-6 shows the comparison between the predicted $\mu+\sigma$ response spectrum (5% damping ratio) for the maximum credible Sumatran fault earthquake ($M_w=7.5$, $R= 425$ km) and response spectra of the 6 sets of scaled ground motions. Figure 5-7 shows the comparison between the predicted $\mu+\sigma$ response spectrum (5% damping ratio) for the maximum credible Sumatran fault earthquake ($M_w=7.5$, $R= 425$ km), and the mean and standard deviation of response spectra of the 6 sets of scaled ground motions. Figure 5-8 shows the comparison between the predicted $\mu+\sigma$ response spectrum (5% damping ratio) for the maximum credible Sumatran subduction earthquake ($M_w=9.0$, $R= 700$ km), and response spectra of the 10 sets of scaled ground motions. Figure 5-9 shows the comparison between the predicted

$\mu+\sigma$ response spectrum (5% damping ratio) for the maximum credible Sumatran subduction earthquake ($M_w=9.0$, $R=700$ km), and the mean and standard deviation of response spectra of the 10 sets of scaled ground motions. Figure 5-10 shows a set of recorded and scaled Sumatran fault earthquake ground motions. Figure 5-11 shows a set of recorded and scaled Sumatran subduction earthquake ground motions.

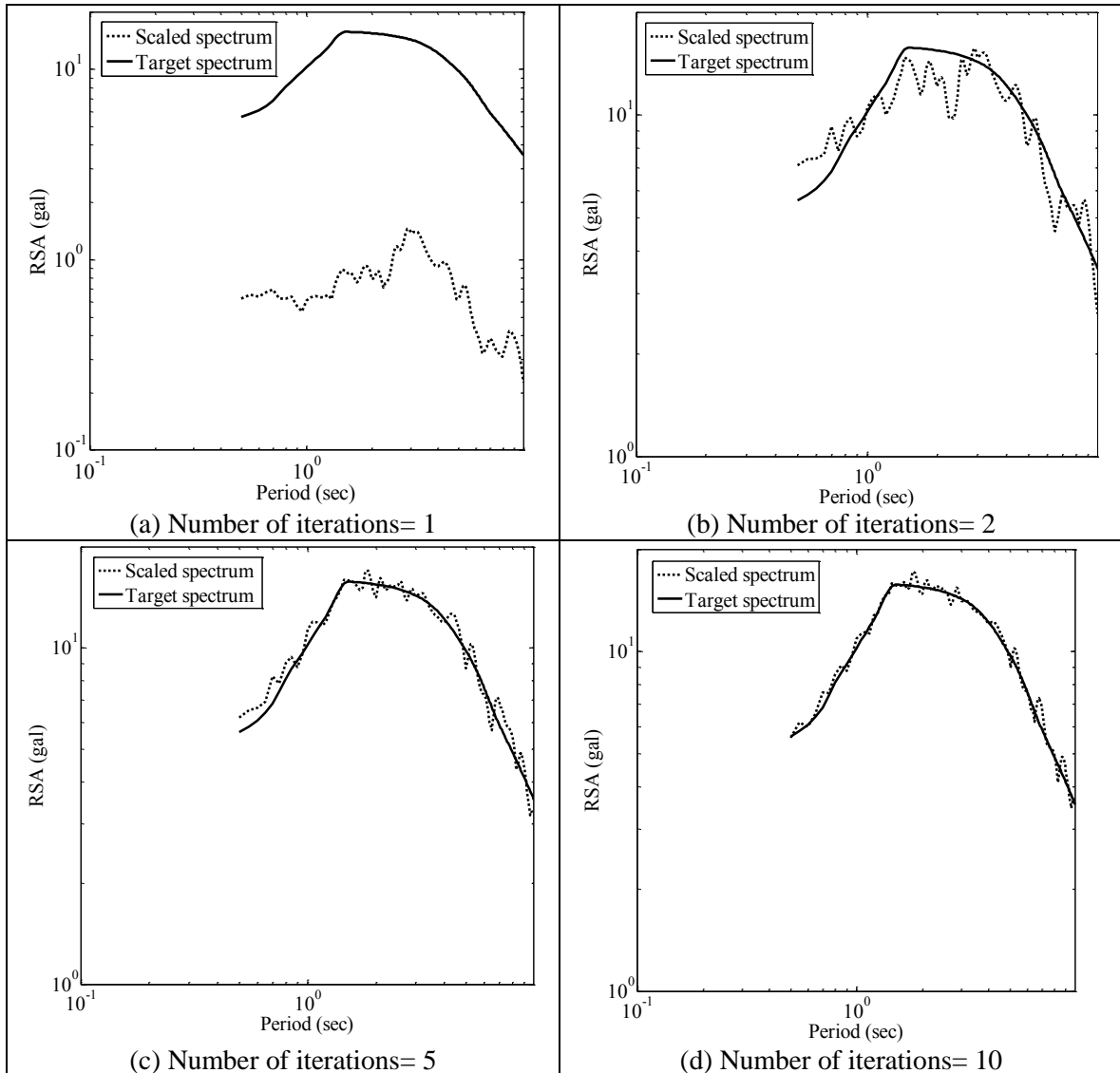


Figure 5-5 Comparison between the target spectrum and the spectrum of scaled ground motion with number of iterations equal to (a) 1; (b) 2; (c) 5; (d) 10

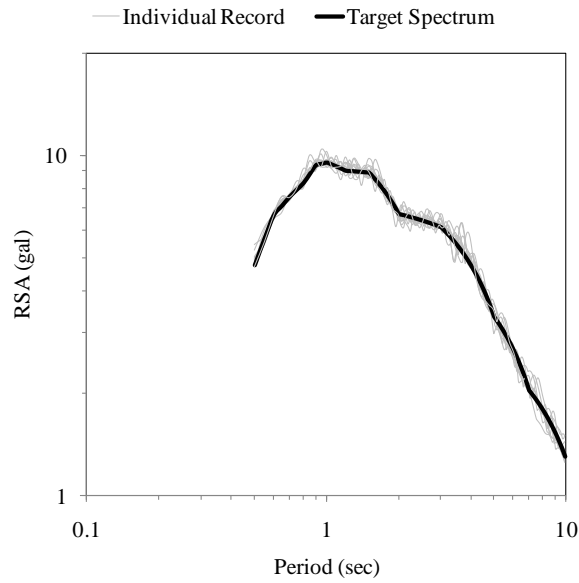


Figure 5-6 Predicted $\mu+\sigma$ response spectrum (5% damping ratio) for the maximum credible fault earthquake ($M_w=7.5$, $R= 425$ km) and the acceleration response spectra of the 6 sets of scaled ground motions

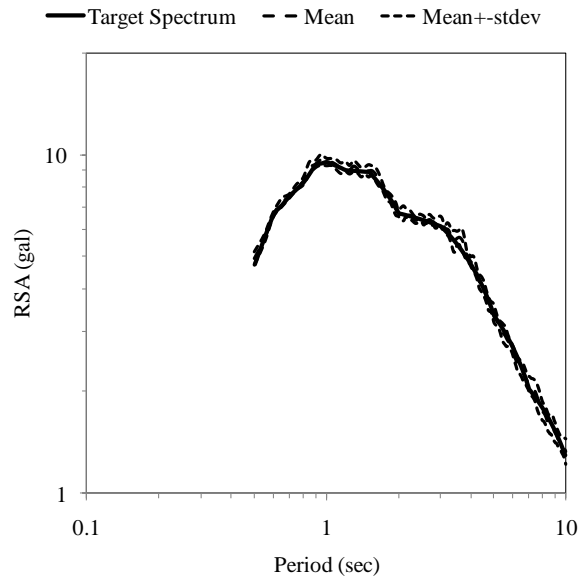


Figure 5-7 Predicted $\mu+\sigma$ response spectrum (5% damping ratio) for the maximum credible fault earthquake ($M_w=7.5$, $R= 425$ km), and the mean and mean plus one standard deviation of the acceleration response spectra of the 6 sets of scaled ground motions

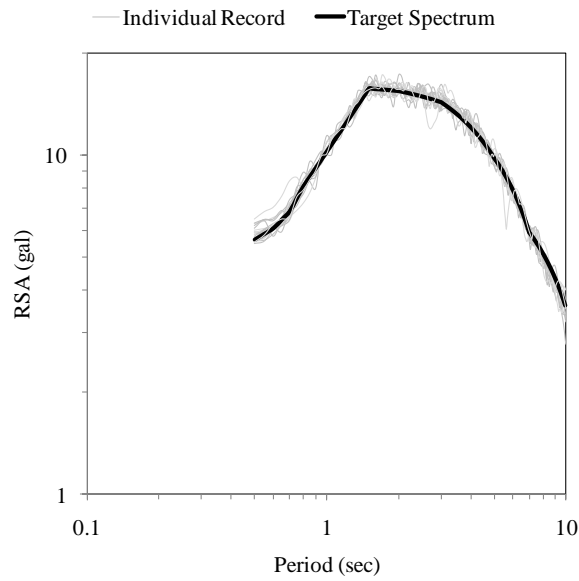


Figure 5-8 Predicted $\mu+\sigma$ response spectrum (5% damping ratio) for the maximum credible subduction earthquake ($M_w=9.0$, $R=700$ km), and the acceleration response spectra of the 10 sets of scaled ground motions

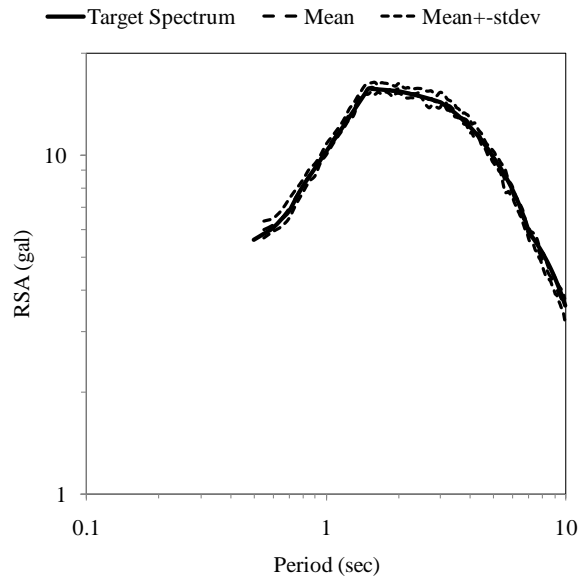


Figure 5-9 Predicted $\mu+\sigma$ response spectrum (5% damping ratio) for the maximum credible subduction earthquake ($M_w=9.0$, $R=700$ km), and the mean and mean plus one standard deviation of the acceleration response spectra of the 10 sets of scaled ground motions

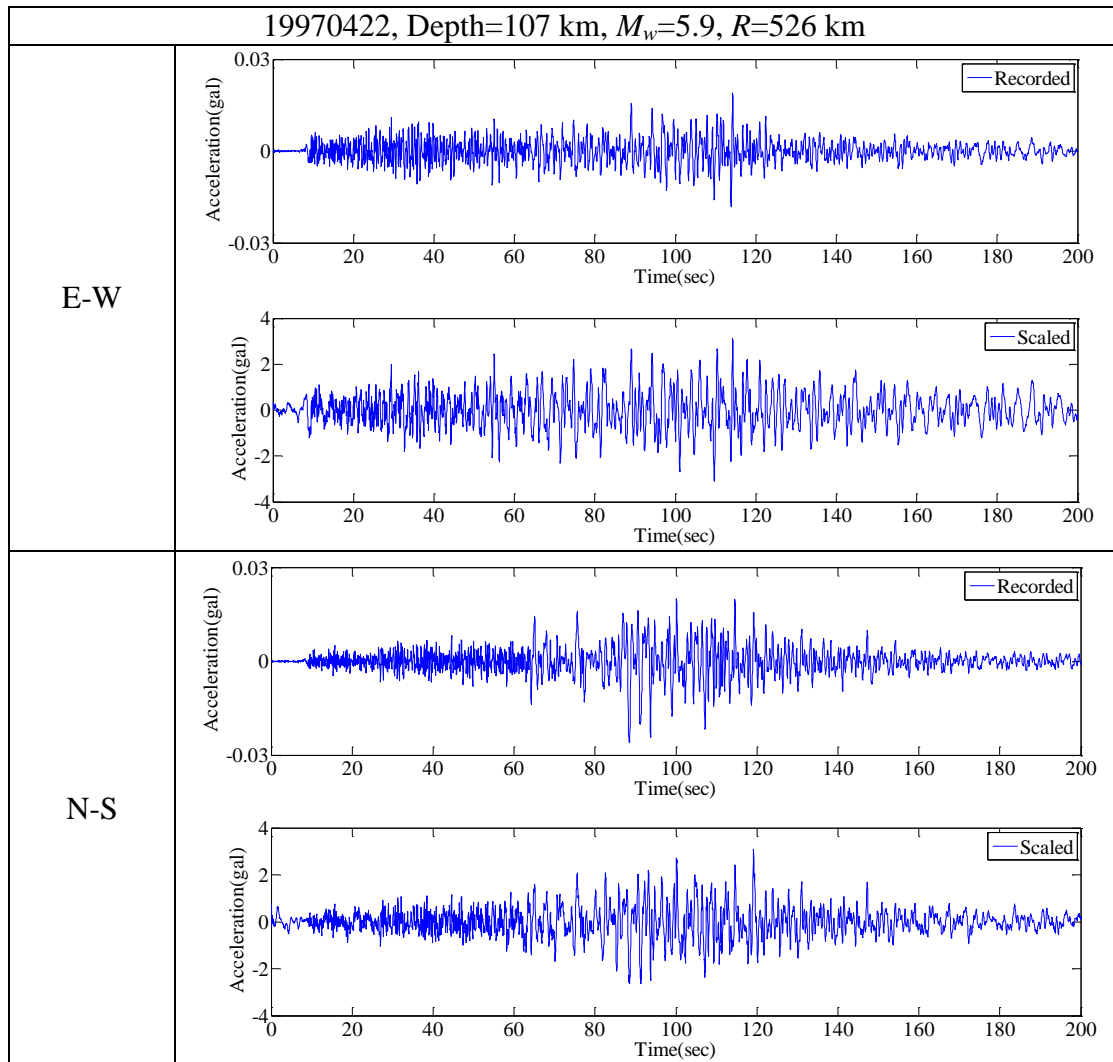


Figure 5-10 Recorded and scaled ground motions in Singapore during 22nd Apr
1997 Sumatran fault earthquake in E-W and N-S direction

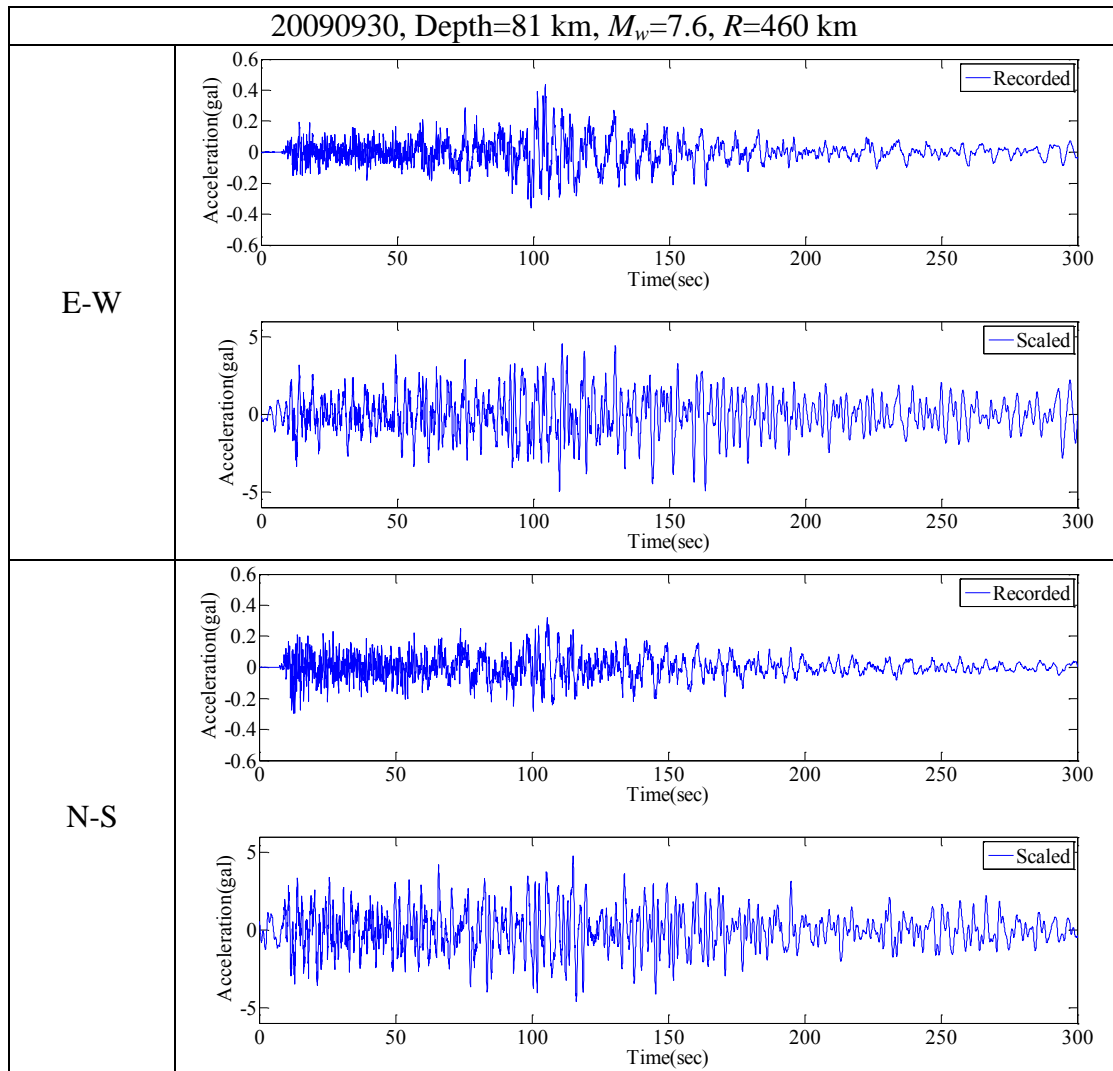


Figure 5-11 Recorded and scaled ground motions during 30 Sept 2009 Sumatran subduction earthquake event in E-W and N-S direction

5.4 EFFECT OF SOFT-SOIL AMPLIFICATION

It should be noted that the ground motions generated in section 5.3 are for rock site. The central and southeastern parts of Singapore Island are largely overlain by Quaternary marine clay deposits, and a significant portion of the southern coastal area is reclaimed land (Pitts, 1984). The soft-soil deposits can significantly amplify the bedrock motion, as confirmed by recent Sumatran earthquakes where tremors were largely felt by residents of high-rise buildings in these areas and not in other areas with better ground conditions. Since seismic-resistant design is not required in Singapore, buildings on soft-soil and rock site are designed against the same lateral loads, resulting in buildings with the same seismic capacity. The seismic risk to structures on soft-soil sites is, therefore, higher than those on firm-soil or rock site, simply because the seismic hazard level is higher at the soft-soil site.

Table 5-2 Soil profiles of the soft-soil site, which is overlain by marine clay deposit

Formation	D (m)	V_S (m/s)	ρ (t/m ³)	PI
Fill (sandy soil)	6.5	120	1.67	Low
Upper marine clay	13	120	1.61	30
Clay	2	190	1.94	30
Lower marine clay	9	145	1.69	30
Organic clay	4	225	1.62	30
Residual soil	5	235	2.07	15
Slightly weathered silty sand	5.9	225	2.07	15
Slightly weathered silt	4.6	440	2.11	Low

Table 5-2 shows the soil profile at a soft-soil site, which is overlain by marine clay deposit (located at the Kallang formation), in the southern part of Singapore (Pan and Lee, 2002). The shear-wave velocity profiles were obtained by crosshole PS logging. These are typical soft-soil profiles in Singapore, having average shear-wave velocity values of the upper 30 m ($V_{S,30}$) of 130 m/s. According

to the 2012 edition of the International Building Code (ICC, 2012), the soft-soil site is classified as soft-soil (Site Class E) based on the value of $V_{S,30}$.

The site response analysis is carried out using the equivalent linear model of the horizontally-layered soil deposit, as implemented in the widely-used computer program called *SHAKE91* (Schnabel et al., 1972; Idriss and Sun, 1992). In the equivalent linear method, nonlinear behavior of soil is accounted for by the use of strain-dependent stiffness and damping parameters. The stiffness of the soil is characterized by the maximum shear modulus G_{\max} and a modulus reduction curve, showing how the shear modulus G decreases from G_{\max} at larger strain. Damping behavior is characterized by the damping ratio, which increases with increasing strain amplitude. The present study uses the G/G_{\max} and damping ratio curves developed by Seed and Idriss (1970) for cohesionless soils, and the curves proposed by Vucetic and Dobry (1991) for cohesive soils. More details about the soft-soil site amplification can be found in the work by Megawati and Pan (2009). The maximum shear strain level and the damping ratio in the soft-soil site during MCE event are 0.03% and 4%, respectively.

Figures 5-12 and 5-13 show the acceleration response spectra at the soft-soil site due to the maximum credible Sumatran fault earthquake ground motions and the corresponding spectral amplifications, respectively. Figures 5-14 and 5-15 show the acceleration response spectra at the soft-soil site due to the maximum credible Sumatran subduction earthquake ground motions and the corresponding spectral amplifications, respectively. The amplification factors, as shown in Figures 5-13 and 5-15, indicate that the soft-soil deposit amplify the ground motion significantly within natural period of 0.5 sec to 3 sec. The soft-soil site has a predominant period of $T=1.20$ sec. The spectral acceleration at $T=1.20$ sec for maximum credible Sumatran subduction earthquake (mean RSA \approx 70 gal) are slightly larger than the spectral acceleration at $T=1.20$ sec for maximum credible Sumatran fault

earthquake (mean RSA \approx 60 gal). The largest amplification factor of about 7.0 ($T=1.20$ sec) is found in Figure 5-13 for maximum credible Sumatran fault earthquake. The largest amplification factor of about 6.0 ($T=1.20$ sec) is found in Figure 5-15 for maximum credible Sumatran subduction earthquake. Example of the generated ground motions at the soft-soil site due to the maximum credible Sumatran fault earthquake and Sumatran subduction earthquake are shown in Figures 5-16 and 5-17, respectively.

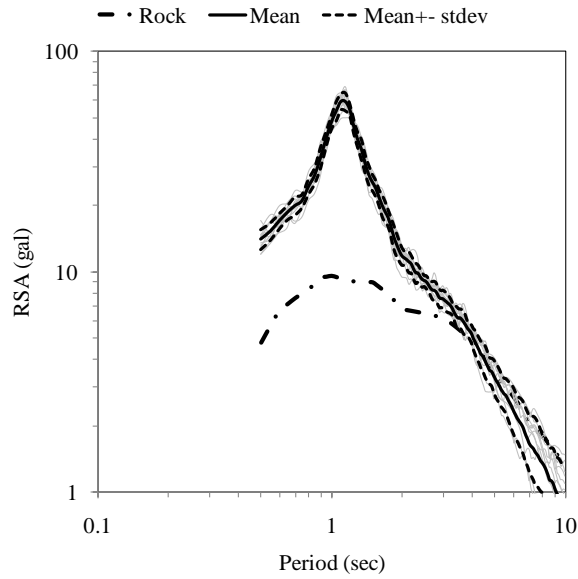


Figure 5-12 Pseudo-acceleration response spectra (5% damping ratio) of the maximum credible Sumatran fault earthquake ground motions at soft-soil site and the corresponding mean and mean plus one standard deviation

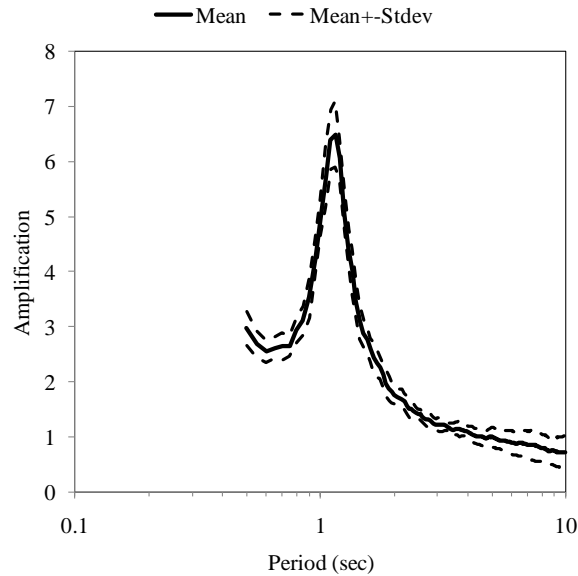


Figure 5-13 Spectral amplification factors of ground motions at soft-soil site due to maximum credible Sumatran fault earthquake with respect to rock site

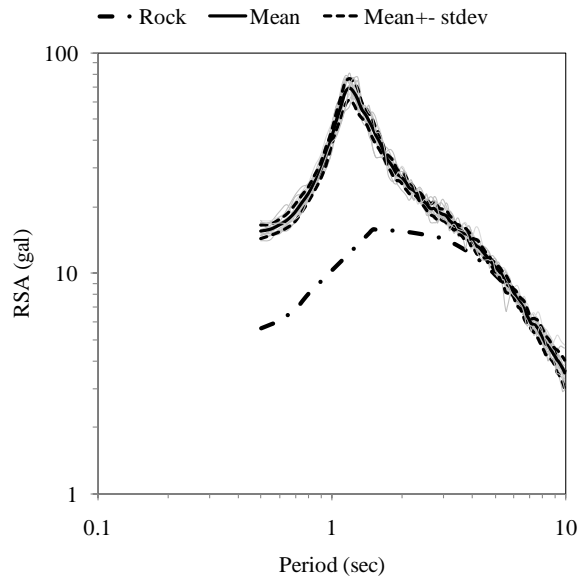


Figure 5-14 Pseudo-acceleration response spectra (5% damping ratio) of the maximum credible Sumatran subduction earthquake ground motions at soft-soil site and the corresponding mean and mean plus one standard deviation

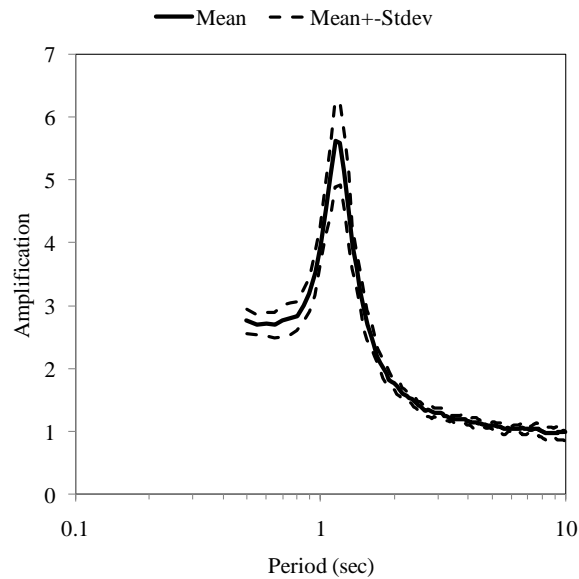


Figure 5-15 Spectral amplification factors of ground motions at soft-soil site due to maximum credible Sumatran subduction earthquake with respect to rock site

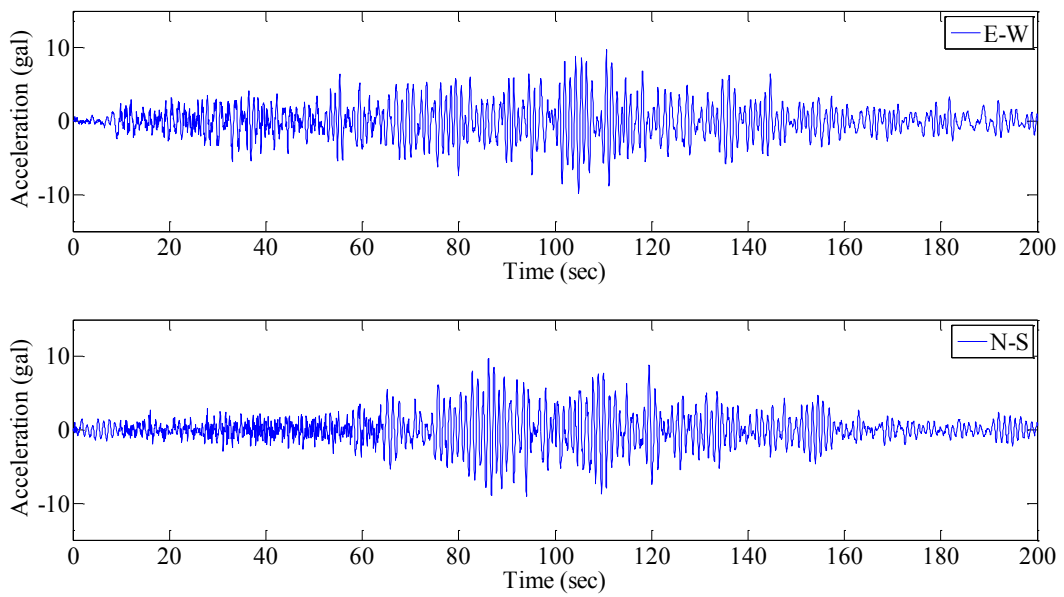


Figure 5-16 Simulated ground acceleration at the soft-soil site from the scaled 22 Apr 1997 Sumatran fault earthquake event in E-W and N-S direction

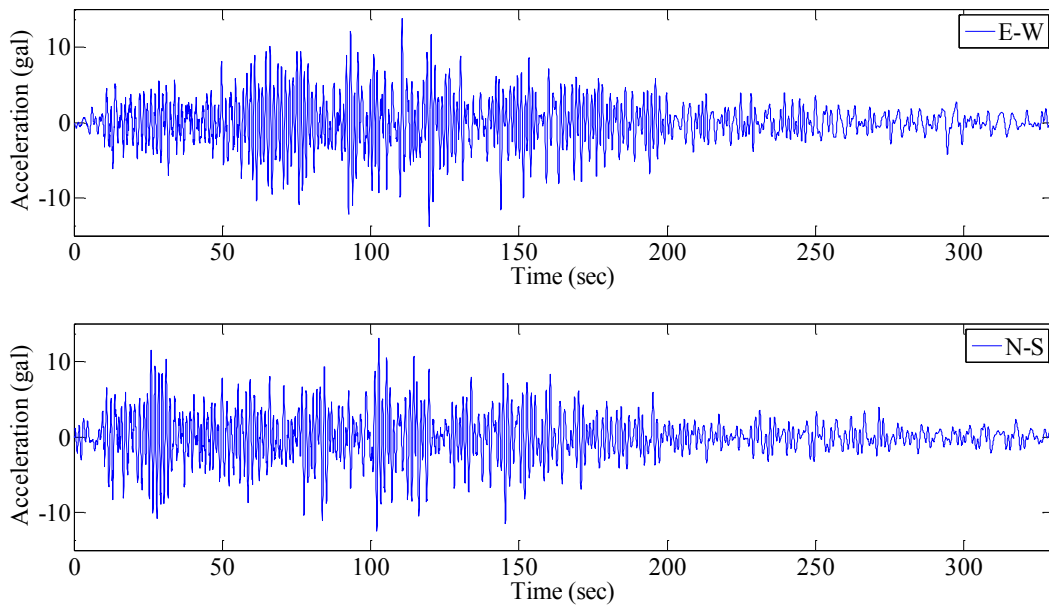


Figure 5-17 Simulated ground acceleration at the soft-soil site from the scaled 30 Sept 2009 Sumatran subduction earthquake event in E-W and N-S direction

5.4.1 STRUCTURAL ANALYSIS RESULTS

The nonlinear dynamic analyses are conducted using *OpenSEEs* (2009). The 6 sets of simulated ground motions for maximum credible Sumatran fault earthquake and 10 sets of simulated ground motions for maximum credible Sumatran subduction earthquake are used as input ground motions. The 15-storey and 30-storey generic models described in Chapter 3 are used for the analysis. Standard Rayleigh damping is utilized, proportional to the initial stiffness and mass matrices, with 5% of critical damping.

Figures 5-18 and 5-19 show the maximum interstorey drift ratio profile of the 15-storey and 30-storey generic models, respectively, when subjected to maximum credible ground motions at both rock and soft-soil sites. Due to soft-first-storey effect, the maximum inter-storey drift ratio is always located at the first-storey. In general, the two generic models have larger responses when subjected to maximum credible Sumatran subduction earthquake ground motions at the soft-soil site compared with those when subjected to maximum credible Sumatran fault earthquake ground motions at the soft-soil site. However, the maximum inter-storey drift ratio of the generic models is less than 0.1%.

Figure 5-20 shows the normalized induced joint shear stress in the 15-storey and 30-storey generic models subjected to maximum credible earthquake ground motions. The induced joint shear stresses are below the joint shear strength for both structures. This implies that the joint shear failure is unlikely to occur in the joints when the generic models are subjected to MCE ground motions. However, torsional effects, which may significantly amplify the response of structures, are not considered in this study. The torsional effects of buildings with soft-first-storey will be discussed in next chapter.

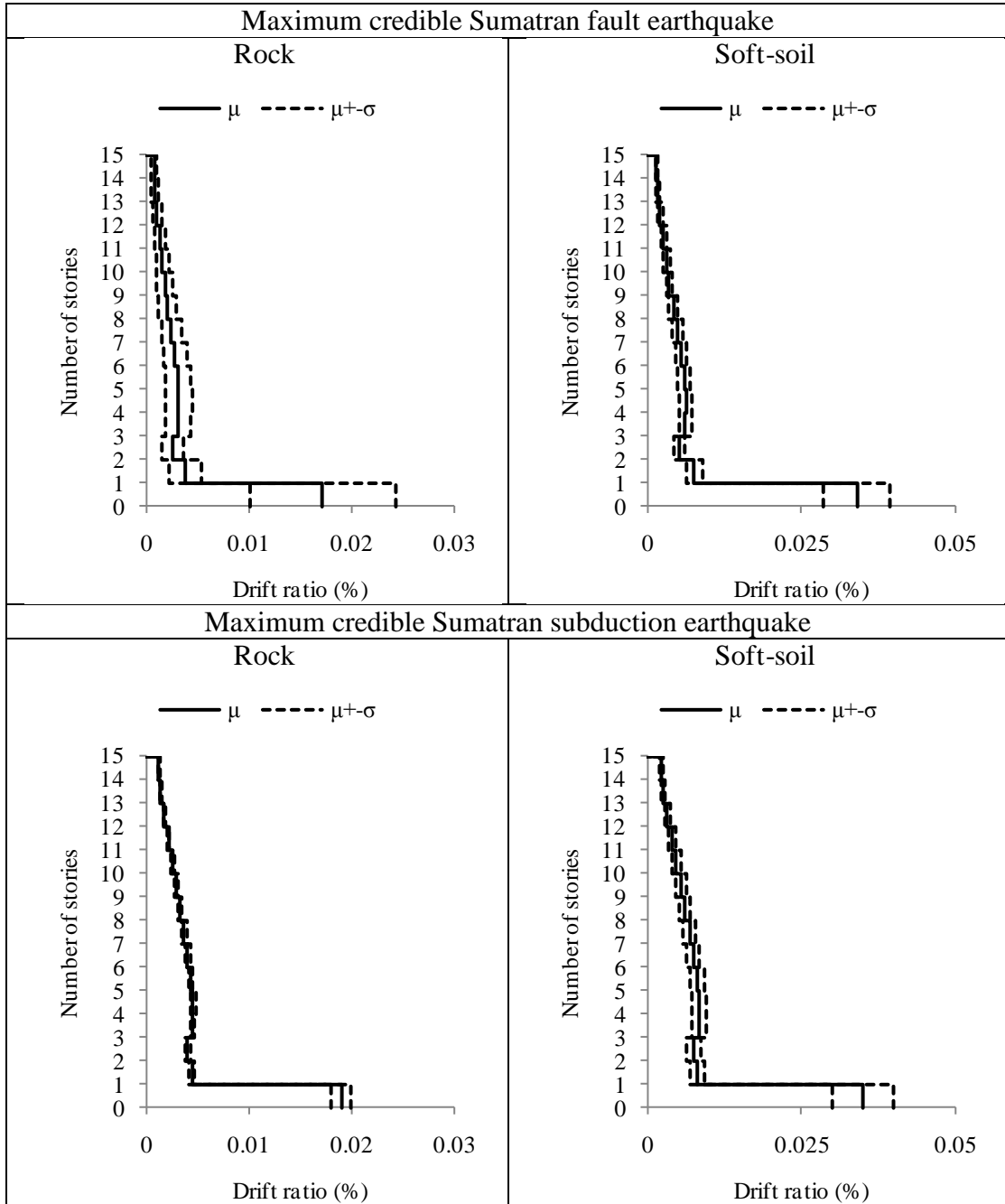


Figure 5-18 Maximum interstorey drift profile in the 15-storey generic model due to maximum credible Sumatran fault and subduction earthquakes

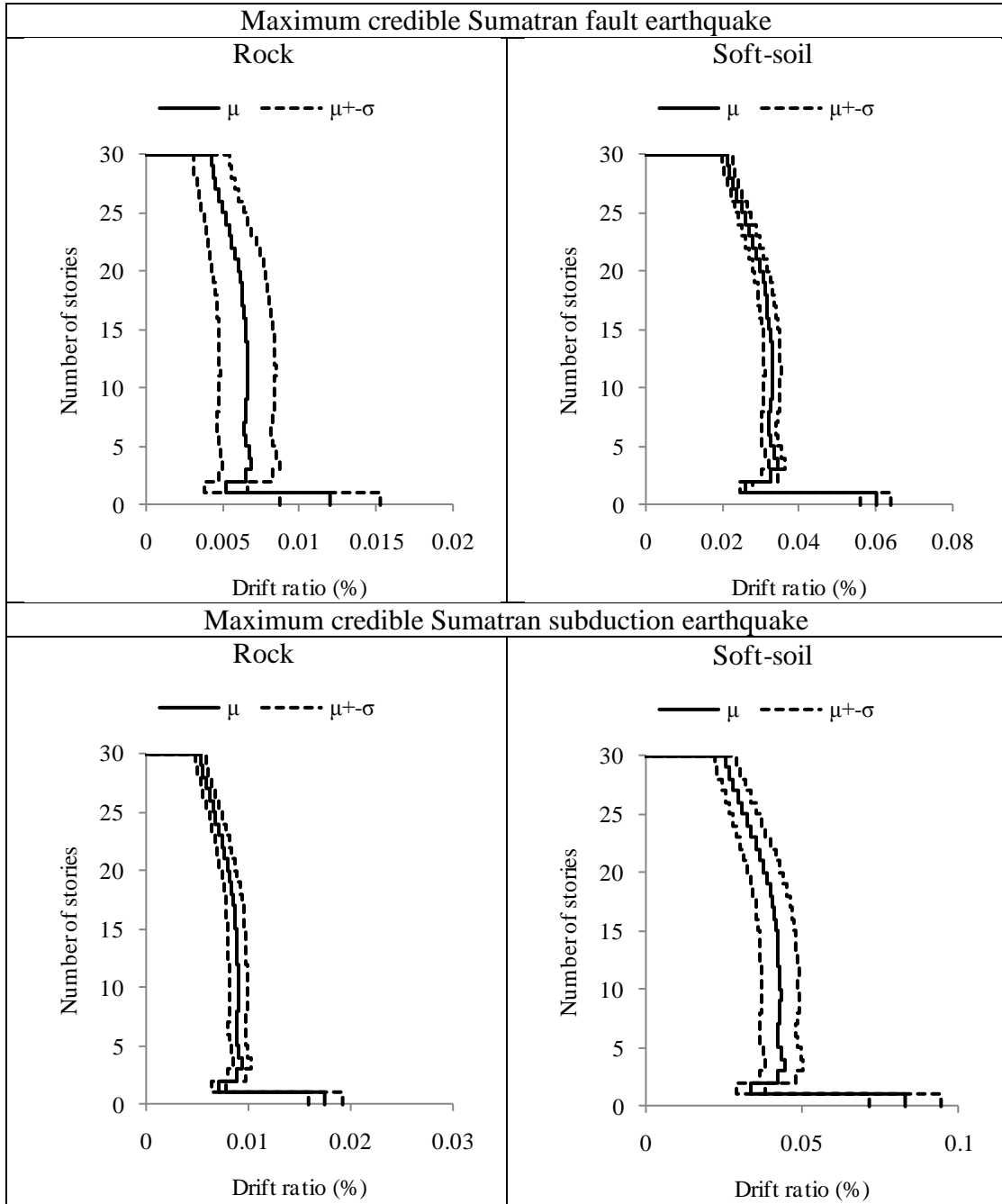


Figure 5-19 Maximum interstorey drift ratio profile in the 30-storey generic model due to maximum credible Sumatran fault and subduction earthquakes

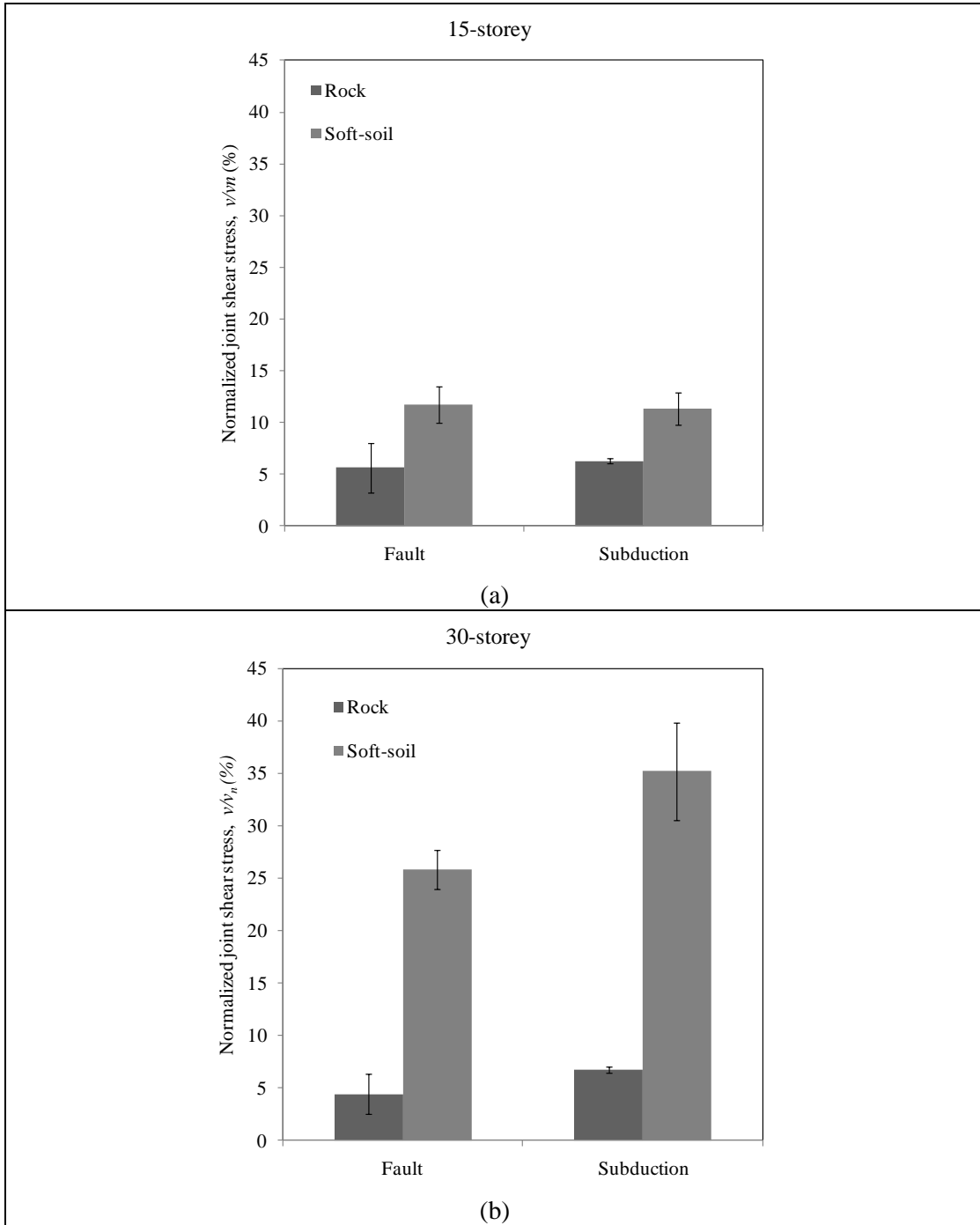


Figure 5-20 Maximum induced joint shear stress in the: (a) 15-storey generic model and (b) 30-storey generic model subjected to maximum credible Sumatran earthquake ground motions at rock and soft-soil site. Error bars represent standard deviations of the results

5.5 CHAPTER SUMMARY

In this chapter, the seismic performances of the 15-storey and 30-storey generic models subjected to maximum credible Sumatran earthquake ground motions have been assessed. Static pushover analysis has been conducted to determine the potential failure modes of the models. It has been found that beam-column joint shear failure may occur prior to column shear failure. The overstrength ratios of the 15-storey and 30-storey generic models are found to be 5.47 and 6.9, respectively. Acceleration response spectra due to maximum credible Sumatran fault and subduction earthquakes have been computed using the attenuation relationships for Sumatran fault and megathrust earthquakes, respectively. Six sets of recorded Sumatran fault earthquake ground motions and ten sets of recorded Sumatran subduction earthquake ground motions have been scaled to match the predicted acceleration response spectra. The ground motions due to maximum credible Sumatran fault and subduction earthquakes at a typical soft-soil site in Singapore have been generated using equivalent linear model of the horizontally-layered soil deposit, which is implemented in the widely-used computer program called *SHAKE91*. Nonlinear time history analyses have been conducted using the generic models subjected to the ground motions at the soft-soil site. The maximum inter-storey drift ratio of the generic models is found to be less than 0.1%. It is found that beam-column joint shear failure is unlikely to occur in the generic models due to maximum credible Sumatran earthquake ground motions at soft-soil site. However, torsional effects are not taken into account in the analysis.

CHAPTER 6

TORSIONAL RESPONSE OF NONDUCTILE STRUCTURES WITH SOFT-FIRST-STOREY

In Singapore, high-rise residential buildings are usually designed with irregular plan and open first-storey. It is concerned that the potential giant Sumatran earthquakes may cause damages in the buildings due to effects of structural irregularities, such as torsional and soft-first-storey effects. Although there are large number of investigations regarding the torsional effect of buildings and seismic performance of soft-first-storey structure (De Stefano and Pintucchi, 2008), to the best knowledge of the author, study on the coupling of torsional and soft-first-storey effects is very rare. In this chapter, torsional response of nonductile structure with soft-first-storey is studied using simplified two-storey model with two-way eccentricities considering element strength deterioration and stiffness degradation.

6.1 LITERATURE REVIEW

The effects of structural irregularities, such as torsional and soft-first-storey effects, are the critical factors which cause damages in building structures during earthquakes. Torsional response is caused primarily by asymmetry in mass, stiffness or strength, while soft-first-storey effect is usually caused by the reduction in lateral stiffness in the first-storey compared with the storey above.

6.1.1 TORSIONAL RESPONSE

According to International Building Code (ICC, 2012), the definitions of horizontal structural irregularities are as follows:

- (a) Torsional irregularities (considered when diaphragms are rigid or semi-rigid):
 - (i) Torsional irregularity exists when the maximum storey drift at one end of the structure transverse to an axis, computed with accidental torsion included, is more than 1.2 times the average of the storey drifts at the two ends of the structure.

- (b) Extreme torsional irregularity (considered when diaphragms are rigid or semi-rigid):
 - (i) Extreme torsional irregularity exists when the maximum storey drift at one end of the structure transverse to an axis, computed with accidental torsion included, is more than 1.4 times the average of the storey drifts at the two ends of the structure.

Torsional response of asymmetric building structures has been widely investigated in the past few decades. Bozorgnia and Tso (1986) studied the inelastic seismic response of a class of one-way torsionally unbalanced structures, which consisted of a single mass supported by bilinear hysteretic elements. It was found that the effect of asymmetry was most pronounced for stiff structures with low yield strength and the uncoupled torsional-to-lateral frequency ratio was insignificant in

affecting the responses. Chandler et al. (1991) conducted parametric study of torsional coupling effects in the response of asymmetric buildings. Forty five strong motion earthquakes from Europe, North America, the Middle East and Southern Pacific were selected. It was found that the torsional response was relatively insensitive to the ratio of peak ground acceleration to velocity. It was also shown that the effect of torsional coupling was more pronounced in stiff, short period structures. De la Llera and Chopra (1996) studied the inelastic seismic behavior and design of asymmetric multistory buildings emphasizing the use of storey shear and torque histories. They found that the torsional capacity of the system could be increased by introducing resisting planes in the orthogonal direction, and the stiffness and strength distribution could be modified to localize yielding in selected resisting planes. Tso and Myslimaj (2003, 2005) studied the problem of the resisting elements of a one-storey model under bi-directional excitations, focusing on the implications on seismic design of the interdependence between strength and stiffness in lateral resisting elements. They found that, in order to reduce torsional response, the centre of stiffness and the centre of strength should be located on the opposite sides of the centre of mass. Perus and Fajfar (2005) tackled the torsional issue of a general nature, such as the effects of plastic excursions on torsional response in comparison with the corresponding elastic response. They also pointed out that large plastic deformations caused a flattening of the displacement envelopes in the horizontal plane, which indicates that torsional effects in the inelastic range are generally smaller than that in the elastic range. They found that inelastic torsional response was generally similar to elastic torsional response. Lucchini et al. (2009) identified the critical parameters that influence the nonlinear seismic response of asymmetric-plan buildings. They found that the building response changes when moving from linear to nonlinear range. An extensive review of the progress in research regarding seismic response of irregular plan building structures since year 2002 was done by De Stefano and Pintucchi (2008).

6.1.2 SOFT-STOREY EFFECT

According to the International Building Code (ICC, 2012), vertical stiffness and strength irregularities exist when:

- (a) Stiffness irregularity:
 - (i) Soft-storey: A soft-storey is one in which the lateral stiffness is less than 70% of that in the storey above or less than 80% of the average stiffness of the three stories above.
 - (ii) Extreme soft-storey: An extreme soft-storey is one in which the lateral stiffness is less than 60% of that in the storey above or less than 70% of the average stiffness of the three stories above.
- (b) Discontinuity in capacity:
 - (i) Weak storey: A weak storey is one in which the storey lateral strength is less than 80% of that in the storey above.

Valmundsson and Nau (1997) evaluated stiffness-strength limits for 5-, 10-, and 20-storey buildings designed according to the Equivalent Static Method of the 1994 Uniform Building Code (UBC) with strong beams and weak columns. It was found that the mass and stiffness criteria of UBC result in moderate increases in response quantities of irregular structures compared to regular structures. Several modification to the criteria were proposed based on the findings. Chintanapakdee and Chopra (2004) conducted study to compare the seismic demands for vertically

irregular and regular frames determined by nonlinear response history analysis due to an ensemble of 20 ground motions. The results from modal pushover analysis were compared with those from the nonlinear response history analysis. They found that the modal pushover analysis estimated the largest drift demands to a sufficient degree of accuracy. Fragiadakis et al. (2006) studied four types of storey irregularities: stiffness, strength, combined stiffness and strength, and mass irregularities. They found that the drift demand of a storey with reduced stiffness sometimes decreased depending on the intensity of shaking, and the position of maximum demand was not always at the location of irregularity. Sadashiva et al. (2012) analyzed the structures with 3, 5, 9 and 15 storeys with the floor mass at all levels kept the same. The maximum interstorey ratio demands of the regular and irregular structures were compared. Simple equations were then developed to estimate possible variations in demand due to vertical stiffness-strength irregularity applied at critical locations in structures. An extensive review of the progress in research regarding seismic response of vertically irregular building structures since year 2002 was done by De Stefano and Pintucchi (2008).

6.2 MATHEMATICAL MODEL

Traditionally, simplified single-storey model is used to study the torsional response of a structure (Chandler et al., 1991; Peruš and Fajfar, 2005; Lucchini et al., 2009). In this study, the problem is tackled using a simplified two-storey model. The validation of using simplified two-storey model to represent the multi-storey model is presented in Appendix B. By varying the stiffness ratio of second-storey to first-storey and the stiffness eccentricity, the effect of horizontal as well as vertical irregularity can be taken into account. Figure 6-1 shows the 3-dimensional illustration of the simplified two-storey model with two-way eccentricities. The floor diaphragm is assumed to be rigid. The floor diaphragm is square in plan with edge length D . The masses are lumped at the centre nodes of each storey. Each

storey has x-direction, y-direction and rotational degree of freedoms. Thus the model has six degree of freedoms. The ground motions are applied in x-direction and y-direction simultaneously.

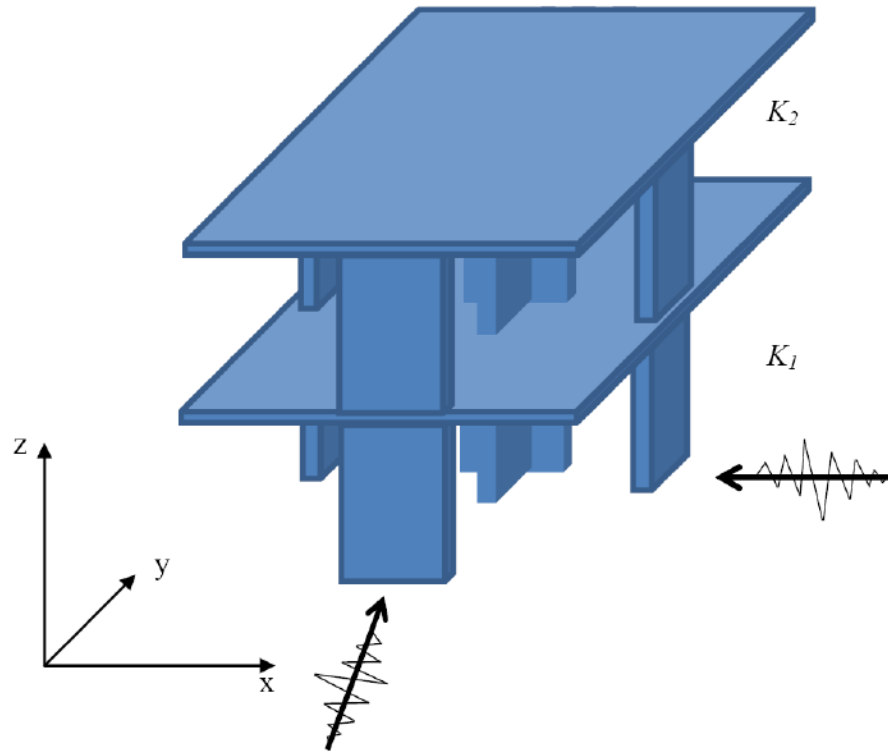


Figure 6-1 3-Dimensional illustration of a simplified two-storey model with two-way eccentricities subjected to bidirectional ground motions

6.2.1 STIFFNESS AND STRENGTH RATIOS

The total stiffness in the first-storey is denoted as K_1 , while the total stiffness in the second-storey is denoted as K_2 . In order to create soft-first-storey effect, the ratio of K_2 to K_1 is varied. The stiffness ratio, α_k , is defined as

$$\alpha_k = \frac{K_2}{K_1} \quad \text{Eq. 6-1}$$

For a soft-first-storey structure, α_k will always be equal to or greater than unity:

$$\alpha_k \geq 1 \quad \text{Eq. 6-2}$$

In most of the practical scenarios, a change in stiffness is always accompanied with a change in strength. Therefore, the stiffness ratio of the second-storey to the first-storey is assumed to be equal to the strength ratio of the second-storey to the first-storey:

$$\alpha_k = \alpha_R \quad \text{Eq. 6-3}$$

where α_R is the strength ratio of the second-storey to the first-storey.

The stiffness ratio of the upper-storeys to the first-storey of the 15 and 30-storey generic models presented in Chapter 3 is calculated. The storey stiffness can be calculated by displacing the storey of interest by a constant unit displacement. It is found that the stiffness ratios of the 15-storey and 30-storey generic models are 7.3 and 5.6, respectively. In this study, the stiffness ratio, and thus strength ratio, of the simplified two-storey model is assigned to have values of 1, 1.2, 1.5, 2.0, 5.0, 10.0, and 50.0 to examine the effect of increasing stiffness ratio (i.e. effect of “softer” and “weaker” first-storey). It should be noted that for most of the soft-storey structures, the stiffness ratio usually does not reach extreme value of 50.0. According to IBC (ICC, 2012), a structure can be classified as extreme soft-storey if the lateral stiffness is less than 60% of that in the storey above or less than 70% of

the average stiffness of the three stories above. It seems that stiffness ratio with extreme value of 50.0 is not reasonable and unrealistic. However, stiffness ratio of 50.0 is used in this study to examine the worst case that could be found in a soft-first-storey structure.

6.2.2 OVERSTRENGTH RATIO

To examine the coupling of torsional and soft-storey effects in structure with different structural capacity, the overstrength ratio of the two-storey model is varied. The overstrength ratio is defined as

$$\Omega = \frac{V_y}{V_d} \quad \text{Eq. 6-4}$$

where V_y is the base shear force at yield of the model, and V_d is the design base shear force of the model. The larger the overstrength ratio, the lesser will the model displace into inelastic range when subjected to force exceeding the yield strength. In Singapore, buildings are mainly designed according to BS8110 (BSI, 1997), which requires that all buildings to be capable of resisting a notional ultimate lateral design load applied at each floor level simultaneously for structural robustness. These static lateral loads are equal to 1.5% of the characteristic dead weight of the structure. Thus V_d is taken as 1.5% weight of the model. In this study, overstrength ratios of 5.0, 2.5 and 1.5 are used to study the response of models with different structural capacity. In addition to the assigned overstrength ratio, an elastic model is also included to represent structures which remain fully elastic during the earthquake excitations.

6.2.3 STIFFNESS AND STRENGTH ECCENTRICITY

Figure 6-2 shows the plan view of the first-storey and second-storey of the mathematical model. In each storey, there are four edge elements and two centre elements. The masses are lumped at the centre. The centre of stiffness (CS) is defined as the point in the structure at which a resultant elastic resisting force must be applied to induce a purely translational response of the floor diaphragm (Chandler et al., 1991). The stiffness eccentricity, e_s , is defined as the distance between the centre of mass (CM) and CS. In this study, normalized stiffness eccentricity, e_s/D , where D is the length of the edge parallel to the direction of stiffness eccentricity is used. The centre of strength (CR) is defined as the point at which a resultant lateral force must be applied in order to induce simultaneous yielding of all the lateral load-resisting elements (Chandler et al., 1991). The resistance eccentricity, e_R , is defined as the distance between the CM and CR. In this study, normalized resistance eccentricity, e_R/D , where D is the length of the edge parallel to the direction of resistance eccentricity is used. In most of the practical scenario, a change in stiffness is always accompanied by a change in strength. In this study, CS is assumed to coincide with CR, and thus

$$\frac{e_R}{D} = \frac{e_s}{D} = \frac{e}{D} \quad \text{Eq. 6-5}$$

As the ground motions are used in both x-direction and y-direction, stiffness eccentricities and thus strength eccentricities are created in both directions. In this study, the stiffness eccentricity in x-direction is assumed to be equal to stiffness eccentricity in y-direction,

$$\frac{e_x}{D} = \frac{e_y}{D} \quad \text{Eq. 6-6}$$

where e_x/D and e_y/D are the normalized stiffness eccentricity in x-direction and y-direction, respectively. The stiffness eccentricity in the second-storey is assumed to be equal to the stiffness eccentricity in the first-storey. In this study, stiffness and strength eccentricities of 0%, 10% and 20% are used.

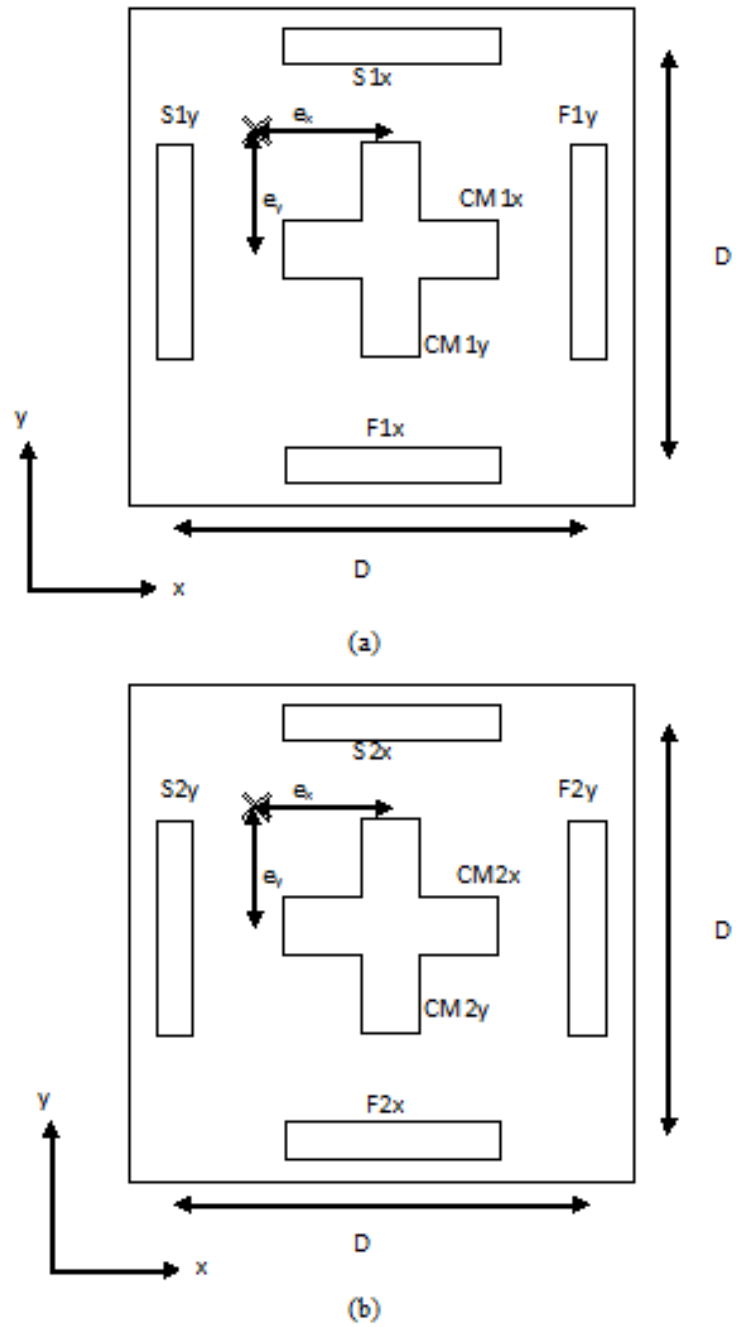


Figure 6-2 Plan view of the mathematical model in 1st and 2nd storey

6.2.4 RESISTING ELEMENTS

As shown in Figure 6-2, in each storey there are two edge resisting elements and one centre resisting element in each direction. In each direction, the side at which the CR and CS located is called stiff edge, while the opposite side is called flexible edge. Each resisting element has only stiffness and resistance in one direction. The elements are named after the location of the elements and the direction of resistance. The resisting elements are axially rigid. The elements have no torsional stiffness. For example, element S1y is the element located at the stiff edge of the first-storey, and it has only resistance in y-direction. Figure 6-2 shows the locations of all the elements. The stiffness and strength of the centre elements (CM1x, CM1y, CM2x, CM2y) are equal to half of the total stiffness and strength of the structure in one direction. In other words, it is equal to the sum of the stiffness of the edge elements, so as to represent the effect of central core wall system which is typically found in high-rise residential buildings in Singapore. The stiffness and strength of the edge elements are then varied to create the eccentricity. For stiffness eccentricity of 0%, the stiffness of the elements located at the stiff and flexible edges are both equal to $0.25K$, where K is the total stiffness at each storey in one direction. For stiffness eccentricity of 10%, the stiffness of the elements located at the stiff and flexible edges are equal to $0.35K$ and $0.15K$, respectively. For stiffness and strength eccentricity of 20%, the stiffness of the elements located at the stiff and flexible edges are equal to $0.45K$ and $0.05K$, respectively. Similar rule applies for strength of the elements with different strength eccentricity.

6.2.5 UNCOUPLED TORSIONAL TO LATERAL FREQUENCY RATIO

The uncoupled torsional to lateral frequency ratio of a system, Ω_θ , is defined as

$$\Omega_\theta = \frac{\omega_\theta}{\omega_l} \quad \text{Eq. 6-7}$$

where ω_θ is the uncoupled torsional frequency of the system, and ω_l is the uncoupled lateral frequency of the system. It should be noted that Eq. 6-7 is typically used to evaluate one-storey plan asymmetric system. In the present study, the frequencies of the first uncoupled lateral modes in each direction and first torsional mode are used to calculate the uncoupled torsional to lateral frequency ratio. Depending on the value of the ratio, the structure can be classified as

- (a) Torsionally stiff, $\Omega_\theta > 1$
- (b) Torsionally flexible, $\Omega_\theta < 1$

The total lateral and torsional stiffness of the models in the x-direction and y-direction in the n th storey ($n=1, 2$) are defined as

$$K_{nx} = \sum k_{nxi} \quad \text{Eq. 6-8}$$

$$K_{ny} = \sum k_{nyi} \quad \text{Eq. 6-9}$$

$$K_{n\theta} = \sum k_{nyi} x_i^2 + \sum k_{nxi} y_i^2 \quad \text{Eq. 6-10}$$

where K_{nx} and K_{ny} are the total lateral stiffness of the models in n th storey in x-direction and y-direction respectively; $K_{n\theta}$ is the total torsional stiffness in the n th storey of the model; k_{nxi} and k_{nyi} are the initial stiffness of the of the i th resisting element in n th storey in the x and y directions, respectively, and x_i , y_i are the distances from the origin (CM) to the i th resisting element. From the equations of motions for 2-DOF system (Paz and Leigh, 2004), the uncoupled lateral and rotational frequencies are

$$\omega_x^2 = \frac{[(K_{1x} + K_{2x})m_{2x} + m_{1x}K_{2x}] \pm \sqrt{\{[(K_{1x} + K_{2x})m_{2x} + m_{1x}K_{2x}]\}^2 - 4m_{1x}m_{2x}K_{1x}K_{2x}}}{2m_{1x}m_{2x}}$$

Eq.6-11

$$\omega_y^2 = \frac{[(K_{1y} + K_{2y})m_{2y} + m_{1y}K_{2y}] \pm \sqrt{\{[(K_{1y} + K_{2y})m_{2y} + m_{1y}K_{2y}]\}^2 - 4m_{1y}m_{2y}K_{1y}K_{2y}}}{2m_{1y}m_{2y}}$$

Eq. 6-12

$$\omega_\theta^2 = \frac{[(K_{1\theta} + K_{2\theta})m_{2\theta} + m_{1\theta}K_{2\theta}] \pm \sqrt{\{[(K_{1\theta} + K_{2\theta})m_{2\theta} + m_{1\theta}K_{2\theta}]\}^2 - 4m_{1\theta}m_{2\theta}K_{1\theta}K_{2\theta}}}{2m_{1\theta}m_{2\theta}}$$

Eq. 6-13

where ω_x and ω_y are the uncoupled lateral frequencies in x-direction and y-direction respectively; ω_θ is the uncoupled torsional frequency; m_{1x} , m_{2x} are the masses in the x-direction in 1st and 2nd storey, respectively; m_{1y} , m_{2y} are the masses in the y-

direction in 1st and 2nd storey, respectively; $m_{1\theta}$, $m_{2\theta}$ are the mass moment of inertia in 1st and 2nd storey, respectively. Thus, the uncoupled periods of the models are

$$T_x = \frac{2\pi}{\omega_x} \quad \text{Eq. 6-14}$$

$$T_y = \frac{2\pi}{\omega_y} \quad \text{Eq. 6-15}$$

$$T_\theta = \frac{2\pi}{\omega_\theta} \quad \text{Eq. 6-16}$$

where T_x , T_y and T_θ are the uncoupled period in x-direction, the uncoupled period in y-direction, and the uncoupled torsional period, respectively.

In this study, three models are constructed as follows:

- (a) Model *F-S*: Torsionally stiff in one direction and torsionally flexible in the orthogonal direction.
- (b) Model *F-F*: Torsionally flexible in both directions.
- (c) Model *S-S*: Torsionally stiff in both directions.

The mass and mass moment of inertia at each storey of the models are shown in Table 6-1. The uncoupled lateral and torsional frequencies of the models are calculated using the equation of motions for two degree of freedom system. The vibration period of first, second and third modes of the three models with different

stiffness eccentricity are shown in Table 6-2. The uncoupled lateral period in the x-direction is set to be longer than the uncoupled lateral period in the y-direction. The uncoupled period of the first vibration mode for the three models are set at 1.20 sec, coinciding with the predominant period of the ground motions used, which will be discussed in the subsequent section.

Table 6-1 Masses at each storey for models *F-S*, *F-F* and *S-S*

	<i>F-S</i>	<i>F-F</i>	<i>S-S</i>
M_x (kg)	4×10^3	4×10^3	4×10^3
M_y (kg)	4×10^3	4×10^3	4×10^3
I (kg.m ²)	4×10^3	7.8×10^3	1.8×10^3

Note: M_x denotes mass in the x-direction at each storey, M_y denotes mass in the y-direction at each storey, I denotes the mass moment of inertia at each storey

Table 6-2 The first three periods for symmetric and asymmetric models, *F-S*, *F-F*, *S-S*

e/D	<i>F-S</i>			<i>F-F</i>			<i>S-S</i>		
	0	0.1	0.2	0	0.1	0.2	0	0.1	0.2
T_1 (sec)	1.20 (T_x)	1.25	1.48	1.20 (T_θ)	1.30	1.62	1.20 (T_x)	1.22	1.36
T_2 (sec)	0.94 (T_θ)	0.99	1.05	0.94 (T_x)	0.92	0.90	0.94 (T_y)	0.85	0.96
T_3 (sec)	0.80 (T_y)	0.76	0.70	0.80 (T_y)	0.79	0.75	0.63 (T_θ)	0.61	0.57

Note: T_θ denotes uncoupled torsional mode, T_x denotes uncoupled lateral mode in x-direction, T_y denotes uncoupled lateral mode in y-direction

6.3 GROUND MOTIONS

In this study, the maximum credible Sumatran subduction earthquake ground motions at soft-soil site, which have been presented in Chapter 5, are used.

There are in total 10 sets of ground motions. Each set of the ground motions consists of N-S and E-W components. The N-S component of each set of ground motions is first applied in the x-direction of the models, and the E-W component is applied in the y-direction. In order to take into account of the effect of direction of ground motion excitations, the N-S component of each set of ground motions is then applied in the y-direction, and the E-W component is applied in the x-direction. Thus, there are in total 20 sets of results.

6.4 HYSTERETIC MODEL

In this study, a simple hysteretic model that includes strength and stiffness deterioration properties developed by Ibarra et al. (2005) is used to capture the deterioration of the element stiffness and strength. Figure 6-3 shows the monotonic trilinear backbone of the hysteretic model. If no deterioration exists, the backbone curve is defined by three parameters: the elastic (initial) stiffness K_e , the yield strength F_y , and the strain hardening stiffness $K_s = \alpha_s K_e$. If deterioration of the backbone curve is included, a softening branch begins at the cap deformation (δ_c), which corresponds to the peak strength (F_c) of the load-deformation curve. If δ_c is normalized by the yield deformation, the resulting ratio may be denoted as ductility capacity,

$$\mu_{cap} = \frac{\delta_c}{\delta_y} \quad \text{Eq. 6-17}$$

where δ_c is cap deformation and δ_y is yield deformation. The softening branch is defined by the post-capping stiffness, $K_c = \alpha_c K_e$, which usually has a negative value. A residual strength can be assigned to the model, $F_r = \lambda F_y$, which represents the fraction of the yield strength of the component that is preserved once a given

deterioration threshold is achieved. In this study, the following parameter values are used: $\alpha_s = 0.05$, $\alpha_c = -0.1$, $\lambda = 0.05$, and $\mu_{cap} = 2.0$. The ductility capacity of 2.0 is chosen as the structures studied are nonductile structures (Ibarra et al., 2005).

The model captures four modes of cyclic deterioration (Ibarra et al., 2005): basic strength deterioration, post-capping strength deterioration, unloading stiffness degradation, and accelerated reloading stiffness degradation. Each mode of cyclic deterioration is based on an energy index that has two parameters: deterioration coefficient (normalized by yield strain and stress) and an exponent term to describe how the rate of cyclic deterioration changes with accumulation of damage. Ibarra et al. (2005) has suggested that the cyclic deterioration parameters can be consolidated into two parameters:

- (a) γ , deterioration coefficient.
- (b) c , an exponent that controls the rate of deterioration.

It has been shown that for ductile structures, the deterioration coefficient, γ ranges from 85 to 130 (Haselton et al., 2009). For nonductile structures, the deterioration coefficient, γ is shown to range from 32 to 82 (Liel et al., 2011). As it is expected that nonductile structures have a lower energy dissipation capacity, thus $\gamma=75$ and $c=1.0$ are used in this study (Figures 6-4 to 6-6). The effect of variation in γ on the response of the models will be discussed in the later section (Figure 6-7).

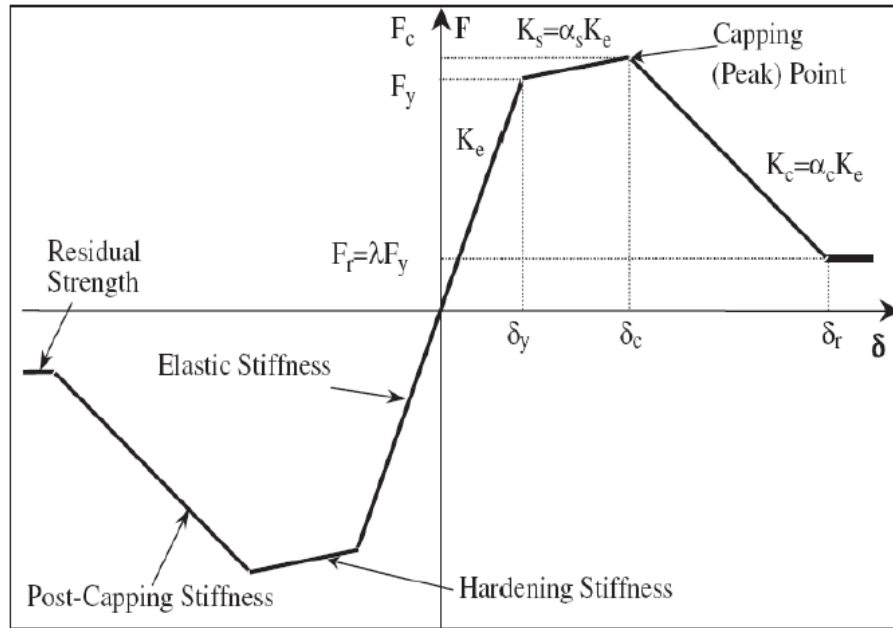


Figure 6-3 Backbone curve for hysteretic model (Ibarra et al., 2005)

6.5 RESULTS AND DISCUSSIONS

The analyses are conducted in *OpenSEEs* (2009). Standard Rayleigh damping is utilized, proportional to the initial stiffness and mass matrices, with 5% of critical damping. The response of the models is presented in a few ways:

- (a) Displacement amplification of irregular model with respect to regular model (henceforth referred to as displacement amplification), u/u_R , where u is the displacement response relative to the ground of irregular model, and u_R is the displacement response relative to the ground of regular model. Regular model is defined as model with stiffness ratio of 1.0 and stiffness eccentricity of 0%.

- (b) Normalized displacement of model with strength deterioration and stiffness degradation with respect to model with no deterioration (henceforth referred to as normalized displacement), $u/u_{\gamma=\infty}$, where u is the displacement response relative to the ground of model with deterioration, and $u_{\gamma=\infty}$ is the displacement response relative to the ground of model with no deterioration, i.e. $\gamma=\infty$.
- (c) Coefficient of variation, which is defined as the ratio of standard deviation to mean of displacement response relative to the ground (henceforth referred to as variation coefficient), σ/\bar{u} (%), where σ is the standard deviation of the displacement response relative to the ground, and \bar{u} is the mean of the displacement response relative to the ground.
- (d) Ductility demand, $\mu_d=\delta_{max}/\delta_y$, where δ_{max} is the maximum displacement response relative to the ground, and δ_y is the yield displacement.

The results presented are the mean displacement response, unless otherwise specified. As it is expected that for a soft-first-storey structure, the damage would more likely to occur at the first-storey where the stiffness and strength are lower than the storey above, thus only the response of the first-storey is presented.

6.5.1 GENERAL OBSERVATIONS

Figures 6-4 to 6-6 show the effect of variation in stiffness ratio and stiffness eccentricity on the displacement amplification for the elastic models, and models with overstrength ratio of 2.5 and 1.5, respectively. The stiffness ratio, α_k of the

models is assigned with values of 1, 1.2, 1.5, 2.0, 5.0, 10.0, and 50.0 to examine the effect of variation in stiffness ratio. Stiffness ratio with values larger than 1.0 imply participation of soft-first-storey effect. The larger stiffness ratio results in “softer” and “weaker” first-storey compared with the second-storey. Coupling of torsional effect is then incorporated by assigning stiffness eccentricity, e/D , of 0%, 10% and 20%. Stiffness eccentricity with values larger than 0% implies participation of torsional effect.

From Figures 6-4 to 6-6, it is found that the displacement amplification in the first-storey generally increases as the stiffness ratio increases, while increase in stiffness eccentricity does not always result in increase in displacement amplification (e.g. element S1x of model *F-S*). No consistent trend of changes in displacement amplification is found with increase in stiffness eccentricity. The trend of changes in displacement amplification as the stiffness eccentricity increases is strongly model-dependent, and it varies for different models.

For models with only soft-first-storey effect (i.e. stiffness eccentricity of 0%), the displacement amplification in the first-storey, as shown in Figures 5 to 7, is always smaller than 1.5 although the stiffness ratio is increased to an extreme value ($\alpha_k=50$). This thus suggests that the displacement amplification can be conservatively taken as 1.5 when assessing structure with only soft-first-storey effect (without coupling of torsional effect). As shown in Figures 6-4 to 6-6, coupling of torsional and soft-first-storey effects (stiffness ratio coupled with stiffness eccentricity) is more significant in affecting the displacement amplification of elements at flexible side. Large change in displacement amplification is found when the torsional and the soft-first-storey effects are coupled for a system. For instance, for element F1y of model *S-S* with overstrength ratio of 1.5 (Figure 6-6i), the displacement amplification is 9.7 times larger than that of the regular model when stiffness ratio of 50.0 is coupled with stiffness eccentricity of 20%. For the

same element, the displacement amplification of model with stiffness eccentricity of 20% increases from 7.1 to 9.7 as stiffness ratio increases from 1.0 to 50.0, while the displacement amplification of model with stiffness ratio of 50.0 increases from 1.38 to 9.7 as stiffness eccentricity increases from 0% to 20%. Similar trend can also be found for models *F-F* and *F-S*. Therefore, coupling of torsional and soft-first-storey effects is a critical factor that must be taken into account when assessing seismic performance of an irregular structure.

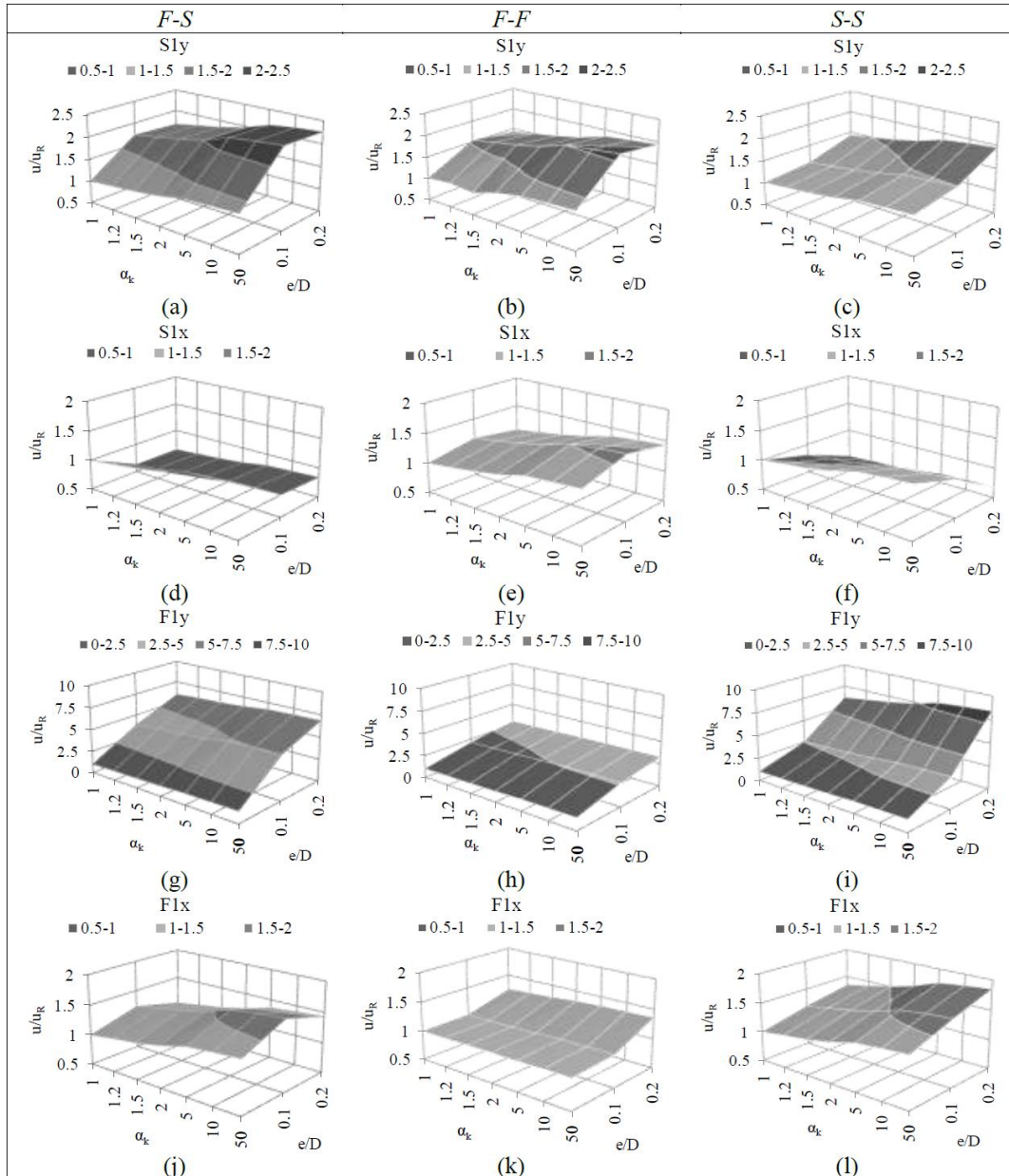


Figure 6-4 Effect of variation in stiffness ratio and stiffness eccentricity on the displacement amplification of irregular elastic models with respect to regular elastic models

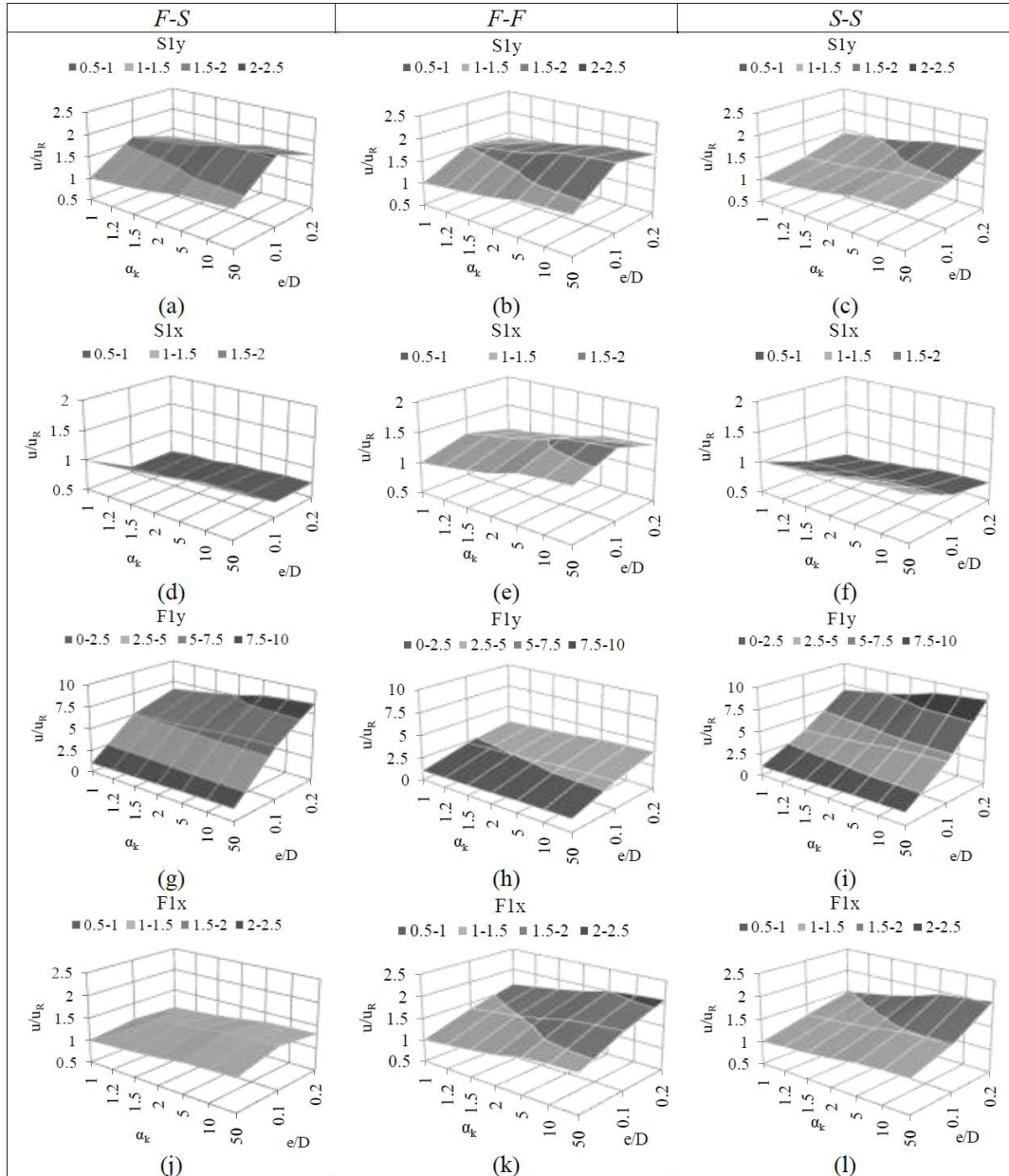


Figure 6-5 Effect of variation in stiffness ratio and stiffness eccentricity on the displacement amplification of irregular models with respect to regular models with overstrength ratio of 2.5

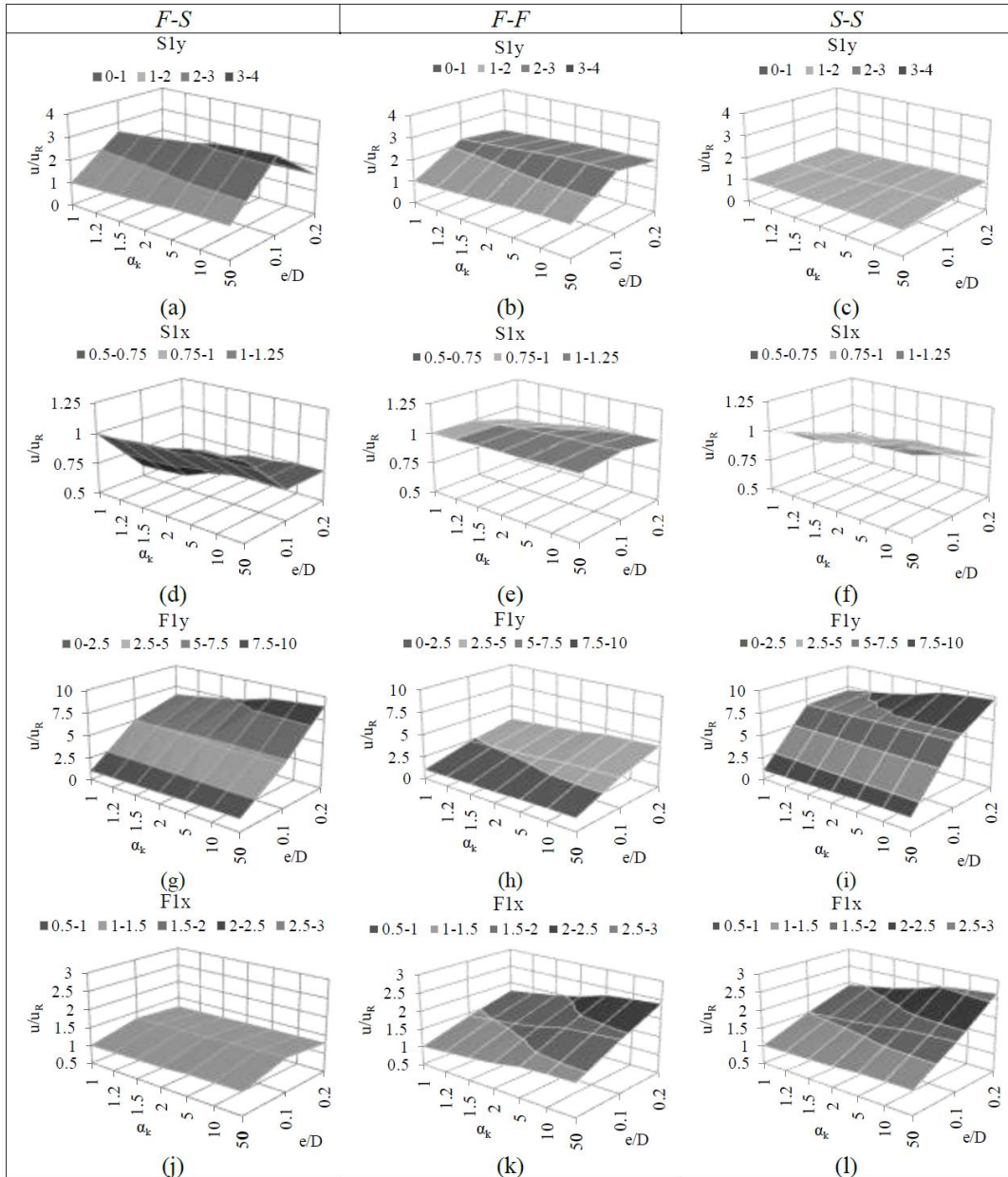


Figure 6-6 Effect of variation in stiffness ratio and stiffness eccentricity on the displacement amplification of irregular models with respect to regular models with overstrength ratio of 1.5

Comparing the displacement amplification of models with different overstrength ratio (Figures 6-4 to 6-6), it is found that the effect of varying

overstrength ratio is insignificant on the trend of changes in displacement amplification. The trend of changes in displacement amplification of elastic system is similar to those of inelastic system. This is similar to the finding by Perus and Fajfar (2005).

From Figures 6-4 to 6-6, it is confirmed that the displacement amplification of elements at the flexible side is larger than those at the stiff side. The displacement amplification of element F1y of the models is larger than those of F1x. This suggests that the elements at the flexible side in the direction of shorter uncoupled lateral period (Table 1) have larger displacement response than the displacement response of the elements in the orthogonal direction. It is also found that the displacement amplification at the flexible side of model *S-S* is generally larger than that of models *F-F* and *F-S*.

6.5.2 EFFECT OF DETERIORATION COEFFICIENT, γ

The results presented in previous sections are based on the assumption of deterioration coefficient, γ , equal to 75. However, the value of γ is not definite, and it may vary for different structures. Thus, the effects of varying deterioration coefficient, γ , on the normalized displacement and variation coefficient of the models are discussed. Smaller deterioration coefficient implies lower cyclic energy-dissipation capacity (Ibarra et al., 2005). The models used for illustrations are models with stiffness ratio of 2.0 coupled with stiffness eccentricity of 20%. The deterioration coefficient is assigned with values of $\gamma=\infty$ (no deterioration), $\gamma=100$ (slow deterioration), $\gamma=75$, $\gamma=50$ and $\gamma=25$ (fast deterioration). Figure 6-7a and 6-7b show the effect of variations in deterioration coefficient, γ on the normalized displacement, $u/u_{\gamma=\infty}$, and the variation coefficient, σ/\bar{u} , respectively.

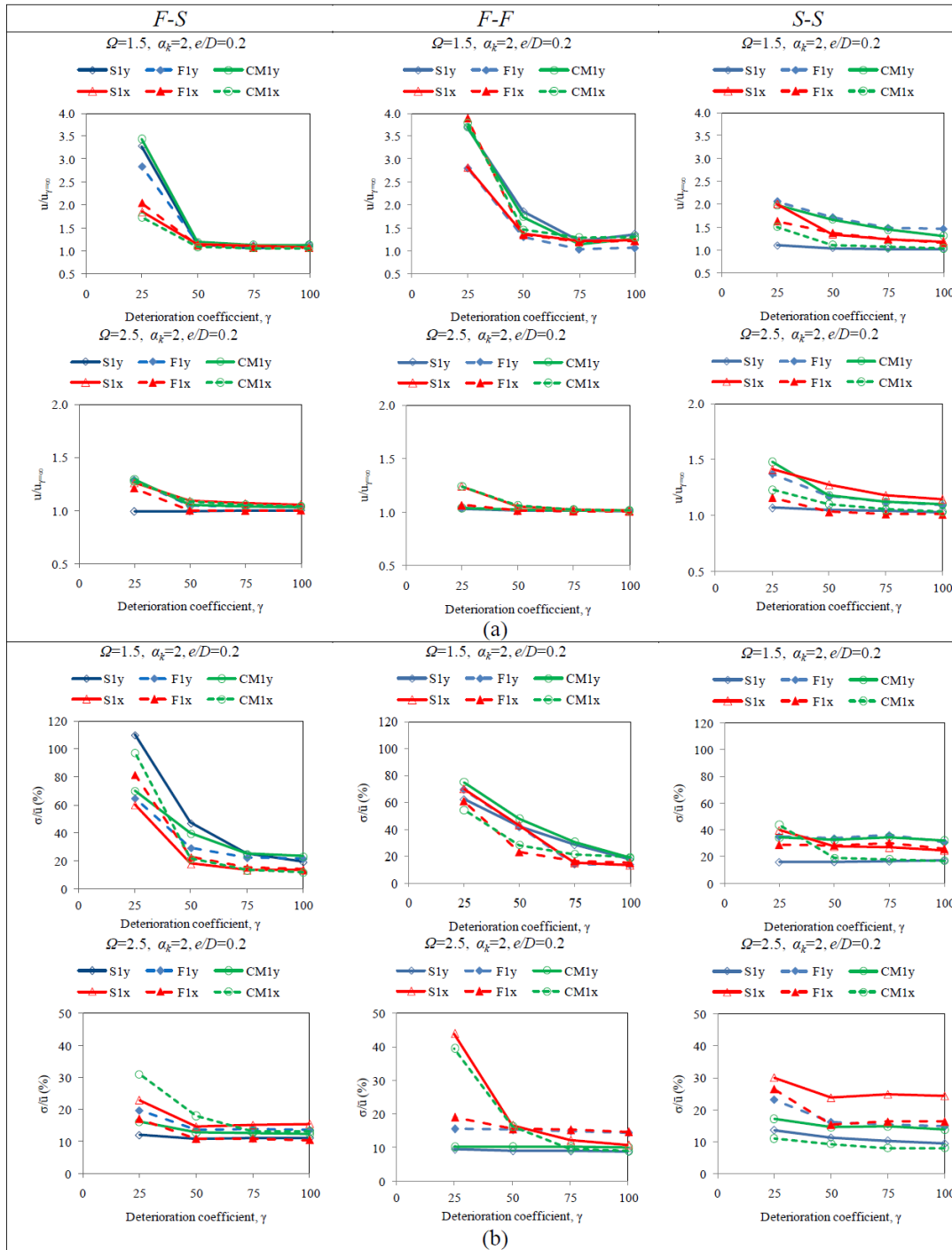


Figure 6-7 Effect of deterioration coefficient, γ on the: (a) normalized displacement $u/u_{\gamma=\infty}$, and (b) coefficient of variation, σ/\bar{u} (%)

From Figure 6-7, it can be seen that the normalized displacement generally increases as the deterioration coefficient decreases from 100 to 25. This implies that the displacement response may be larger for structures with lower cyclic energy-dissipation capacity, which is commonly applicable to nonductile structures. The normalized displacement is less sensitive to change in deterioration coefficient from 100 to 50, while larger change in normalized displacement is found as the deterioration coefficient decreases from 50 to 25. The increase in normalized displacement of models with overstrength ratio of 1.5 is larger than those of models with overstrength ratio of 2.5. This implies that the more the elements displace into inelastic range, the larger is the effect of decrease in deterioration coefficient on the normalized displacement.

Similar observations are also found for the effect of variation in deterioration coefficient on the variation coefficient. The variation coefficient increases as the deterioration coefficient of the elements decreases from 100 to 25. Larger change in variation coefficient is also found as the deterioration coefficient changes from 50 to 25. The variation coefficient for models with overstrength ratio of 1.5 is larger than those with overstrength ratio of 2.5. This implies that the more the elements displace into inelastic range, the larger is the variation coefficient of the response. The variation coefficient for models with deterioration coefficient of 75, which is adopted in this study, is less than 40%. However, a relatively large variation coefficient is found for deterioration coefficient of 25, where the variation coefficient is found to be 110% (model *F-S* with overstrength ratio of 1.5).

6.6 DUCTILITY DEMAND-CAPACITY CURVES

In this study, the ductility capacity, μ_{cap} is defined at the component level as the ratio of the deformation at peak strength to the yield deformation (Ibarra et al., 2005), as shown in Eq. 6-17. The analysis presented in previous section is based on

ductility capacity of 2.0. This is reasonably representative of typical structures in Singapore, which are nonductile structures. The ductility demand, μ_d is defined as the ratio of maximum deformation of an element to yield deformation (Biggs, 1964):

$$\mu_d = \frac{\delta_{max}}{\delta_y} \quad \text{Eq. 6-18}$$

where δ_{max} is the maximum deformation of an element when subjected to excitation, and δ_y is the deformation at yield. Failure is likely to occur when ductility demand exceeds ductility capacity:

$$\mu_d > \mu_{cap} \quad \text{Eq. 6-19}$$

Figure 6-8 shows the ductility demand-capacity curves for models with stiffness ratio of 2.0 coupled with stiffness eccentricity of 20%. The curves are constructed by changing the ductility capacity of the models, and the corresponding ductility demand of each element of the models subjected to the MCE ground motions is plotted against the ductility capacity. The curves can be used to approximately assess the seismic performance of existing structures subjected to the MCE ground motions. It is noted that the models with ductility capacity of 2.0 are less likely to fail when the overstrength ratio is equal to 5.0. The models, with overstrength ratio smaller than 5.0, are more likely to fail due to insufficient ductility capacity. The curves can also be used as a guideline when designing structures considering coupling of torsional and soft-first-storey effects. For example, a ductility capacity of 4.0 is needed for a structure with overstrength ratio of 2.5 to withstand the MCE ground motions. It is suggested that for structure with overstrength ratio smaller than 5.0, ductility capacity needs to be increased in order to withstand the MCE ground motions at soft-soil site in Singapore. From Chapter 5, the overstrength

ratios of the 15-storey and 30-storey generic models have been obtained using pushover analysis. As the overstrength ratio of the two generic models are larger than 5.0, it is thus concluded that the 15-storey and 30-storey generic models are unlikely to fail when subjected to MCE ground motions considering torsional effects.

CHAPTER 6: TORSIONAL RESPONSE OF NONDUCTILE STRUCTURES WITH SOFT-FIRST-STOREY

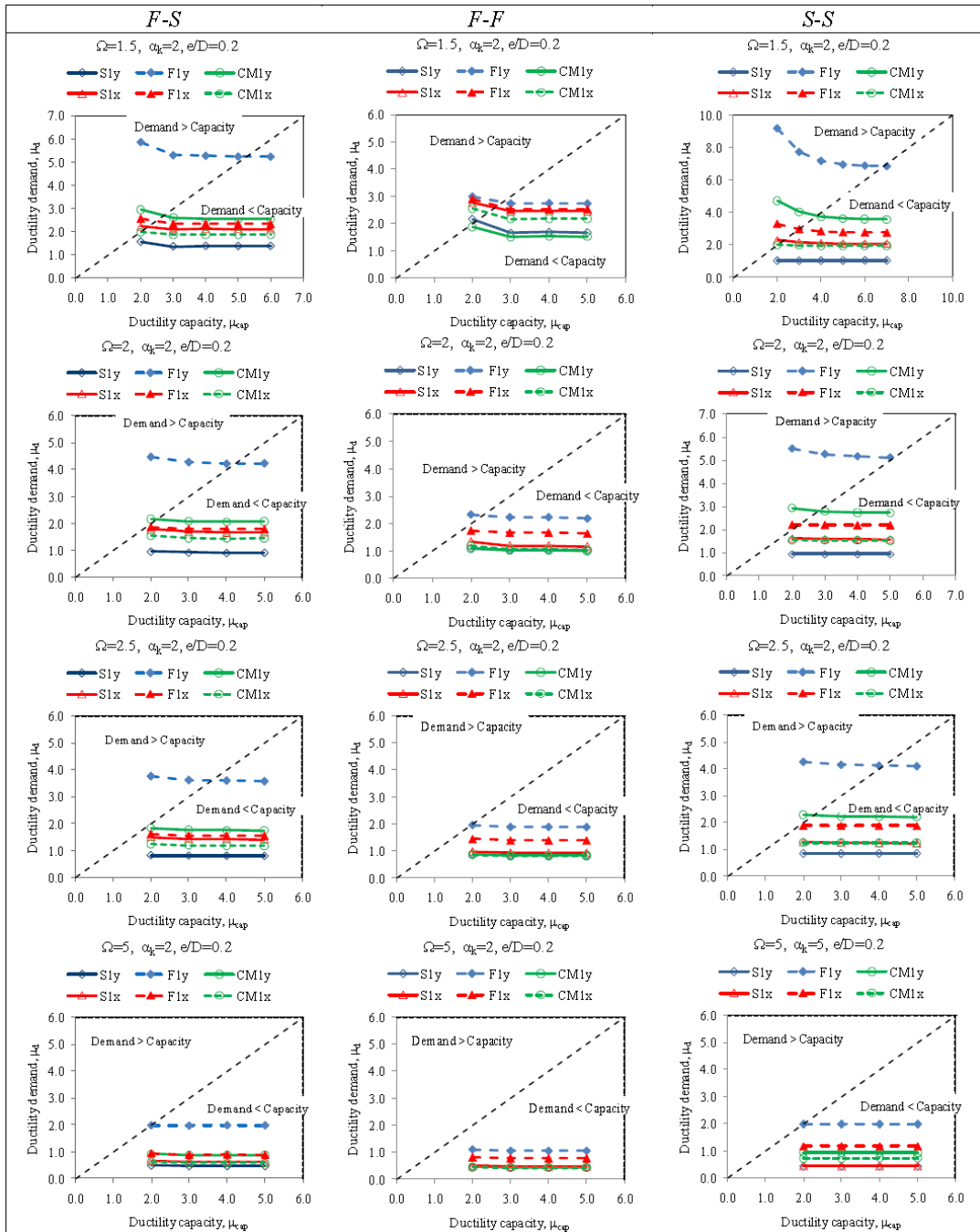


Figure 6-8 Ductility demand-capacity curves

6.7 CHAPTER SUMMARY

In this chapter, the torsional response of nonductile structure with soft-first-storey has been studied. A simplified two-storey model with two-way eccentricities subjected to bidirectional ground motion excitations has been used. The simplified model has been studied using different ratios of uncoupled torsional to lateral frequency: 1. Model *F-S*, torsionally stiff in one direction and torsionally flexible in the orthogonal direction; 2. Model *F-F*, torsionally flexible in both directions; 3. Model *S-S*, torsionally stiff in both directions. The stiffness and strength ratio of second-storey to first-storey has been varied to create different level of soft-first-storey effect, while the stiffness and strength eccentricity has been varied to create torsional effect. The overstrength ratio of the models has been varied to study the response of structures with different structural capacity. Hysteretic model which includes strength deterioration and stiffness degradation properties has been used to capture the deterioration of the element stiffness and strength. The maximum credible Sumatran subduction earthquake ground motions at the typical soft-soil site in Singapore have been used as input excitations. The following conclusions can be drawn from this study:

1. In general, displacement amplification of irregular model with respect to regular model increases as stiffness ratio increases, while no consistent trend of changes in displacement amplification has been found as stiffness eccentricity increases.
2. The displacement amplification of elements at the flexible side is larger than that at the stiff side. The displacement response of elements at the flexible side in the direction of shorter uncoupled lateral period is larger than that in the orthogonal direction. The displacement amplification due to only soft-first-storey effect can be

conservatively taken as 1.5. Coupling of torsional and soft-first-storey effects is more significant in affecting the displacement amplification of element at the flexible side. The displacement amplification of model *S-S* at the flexible side is generally larger than those of models *F-F* and *F-S*. The trend of changes in displacement amplification of elastic system is similar to those of inelastic system.

3. The normalized displacement of model with strength deterioration and stiffness degradation with respect to model with no deterioration, $u/u_{\gamma=\infty}$, and the coefficient of variation, σ/\bar{u} , increase when the deterioration coefficient, γ , of the elements decreases from 100 to 25. However, the normalized displacement and variation coefficient are more sensitive to changes in deterioration coefficient from 50 to 25. The more the elements displace into inelastic range, the larger is the effect of decrease in deterioration coefficient on the normalized displacement and the variation coefficient. The variation coefficient for models with deterioration coefficient of 75, which is adopted in this study, is less than 40%.
4. Ductility demand-capacity curves have been constructed. The curves can be used to approximately assess the seismic performance of existing structures, and as a guideline when designing new structures considering the coupling of torsional and soft-first-storey effects. It is concluded that nonductile structure with overstrength ratio of 5.0 is less likely to fail during the MCE event. For structures with overstrength ratio smaller than 5.0, ductility capacity needs to be increased in order to withstand the MCE ground motions at soft-soil sites in Singapore. As the overstrength ratios of the two generic models are larger than 5.0, it is thus concluded that the 15-storey and

30-storey generic models are unlikely to fail during MCE events when torsional effects are taken into account.

CHAPTER 7

CONCLUSIONS AND RECOMMENDATIONS

7.1 CONCLUSIONS

Singapore, an island country located at the southern tip of Malay Peninsula, is exposed to long-distance earthquakes originated from Sumatra. In this thesis, research has been done on the seismic performance assessment of the response of typical buildings in Singapore to long-distance Sumatran earthquake ground motions.

Relationships between the natural vibration period and the height of buildings have been derived empirically based on AVT measurements conducted on 116 high-rise residential buildings. Regression analyses have been carried out on the measured natural vibration periods of the buildings considering the site properties. It is found that the natural vibration periods estimated using the proposed period-height relationship for buildings located at soft-soil site are about 40% longer than those estimated using the relationship for buildings located at firm-soil site. Measurements have also been conducted to examine the influence of buildings on the measured frequency of surrounding soil. The radius of building influence on the measured frequency of the surrounding soil has been found to reach up to one building height for firm-soil site and two building heights for soft-soil site. It is thus advised that free-field microtremor measurements are to be conducted at distance more than one building height and two building heights away from the nearest building for firm-soil site and soft-soil site, respectively.

A systematic methodology for estimating the level of perception to tremors of occupants living in high-rise public residential buildings subjected to weak ground motions has been presented. Instead of using empirical or historical data, the proposed methodology is based on statistical analysis of analytical results of seismic response of generic building models to recorded ground motions. For this purpose, two generic models of 15 stories and 30 stories have been constructed using *OpenSEEs*. The generic models are representative of reinforced concrete infilled frame with shear wall buildings, which are typically found in Singapore. Three tremor events reportedly felt in Singapore due to distant Sumatran earthquakes have been used as case studies. The estimated perception level to tremors during the three events using the proposed methodology agrees well with the reports from local newspapers and the authorities.

Efforts have been made to determine the seismic capacity of the generic building models using static pushover analysis. It has been found that beam-column joint shear failure may occur prior to column shear failure. The overstrength ratios of the 15-storey and 30-storey generic building models are found to be 5.47 and 6.90, respectively. The responses of the 15-storey and 30-storey generic building models to the maximum credible Sumatran earthquake ground motions at both rock and soft-soil sites are then subsequently studied. The maximum inter-storey drift ratio of the generic models due to the MCE ground motions has been found to be less than 0.1%. It is also found that beam-column joint shear failure is unlikely to occur in the generic building models due to maximum credible Sumatran earthquake ground motions at soft-soil site. However, torsional effects, which are likely to amplify the displacement responses, are not taken into account in these analyses.

In order to estimate the amplification in displacement responses when torsional effects are taken into account, simplified two-storey models with two-way eccentricities subjected to bidirectional ground motion excitations have been used. The stiffness and strength ratios, stiffness and strength eccentricities, as well as ductility capacity and overstrength ratio of the models have been varied to examine the effect of these parameters on the torsional responses. The results can be used to estimate the response amplification of the generic models due to torsional effects. Ductility demand-capacity curves have been subsequently constructed. The curves can be used to approximately assess the seismic performance of existing structures, and as a guideline when designing new structures considering the coupling of torsional and soft-first-storey effects. Using the curves, it is found that nonductile structure with overstrength ratio of 5.0 is less likely to fail during the MCE event. For structures with overstrength ratio smaller than 5.0, ductility capacity needs to be increased in order to withstand the MCE ground motions at soft-soil sites in Singapore. As the overstrength ratios of the two generic building models are larger than 5.0, it is thus concluded that the 15-storey and 30-storey generic building models are unlikely to fail during MCE events when torsional effects are taken into account.

7.2 RECOMMENDATIONS

The recommendations for future studies are as follows:

- (a) The period-height relationships proposed in Chapter 2 are derived based on reinforced concrete high-rise residential buildings with height ranges from 4 stories to 30 stories. Research can be done on determining the natural vibration period of buildings with height more than 30 stories, steel structures and commercial buildings in Singapore.

- (b) The torsional response problems are tackled using simplified two-storey model with two-way eccentricities. Research can be done using three-dimensional multi-storey model with soft-first-storey.

- (c) Coupling of torsional response and soft-first-storey may be studied using the simplified analytical procedures for typical building in Singapore.

CHAPTER 8

REFERENCES

Altoontash, A. (2004) "Simulation and Damage Models for Performance Assessment of Reinforced Concrete Beam-Column Joints", Ph.D. Thesis, California, USA, Stanford University.

Architectural Institute of Japan (2004) "AIJ-GEH-2004. Guidelines for evaluation of habitability to building vibration" Maruzen Publishing.

Balendra, Tan, T., K. H. and Kong, S. K. (1999) "Vulnerability of reinforced concrete frames in low seismic region, when designed according to BS 8110", Earthquake Engineering and Structural Dynamics, Vol. 28, No. 11, pp. 1361-1381.

Biggs J. M. (1964) "Introduction to structural dynamic".

Bozorgnia Y. and Tso W. K. (1986) "Inelastic earthquake response of asymmetric structures", Journal and Structural Engineering, Vol. 112, No. 2, pp. 383-400.

British Standard Institution (1997) "Structural use of concrete, part 1. code of practice for design and construction".

Brownjohn, J. M. W. (2003), "Ambient vibration studies for system identification of tall buildings", Earthquake Engineering and Structural Dynamics, Vol. 32, No. 1, pp. 71-95.

Castro, R. R., Mucciarelli, M., Pacor, F., Federici, P. and Zaninetti, A. (1998), “Determination of the characteristic frequency of two dams located in the region of Calabria, Italy”, Bulletin of the Seismological Society of America, Vol. 88, No. 2, pp. 503-511.

Chandler, A.M., Hutchinson, G.L. and Jiang, W. (1991) “Inelastic Torsional Response of buildings to the 1985 Mexican Earthquake: A Parametric Study”, Soil Dynamics and Earthquake Engineering, Vol 10, No. 8, pp. 429-439.

Chintanapakdee, C. and Chopra, A. K. (2004) “Seismic response of vertically Irregular frames: Response history and modal pushover analyses”, Journal of Structural Engineering, Vol. 130, No. 8, pp. 1177-1185

Clinton, J. F., Bradford, S. C., Heaton, T. H. and Favela, J. (2006), “The observed wander of the natural frequencies in a structure”, Bulletin of the Seismological Society of America, Vol. 96, No. 1, pp. 237-257.

Crowley, H. and Pinho, R. (2006) “Simplified equations for estimating the period of vibration of existing buildings”, First European Conference on Earthquake Engineering and Seismology, Geneva, Switzerland.

De la Llera J. C. and Chopra A. K. (1996) “Inelastic behaviour of asymmetric multistorey buildings”, Journal of Structural Engineering, Vol. 112, No. 6, pp. 567-606

De Stefano, M. and Pintucchi, B. (2008). “A review of research on seismic behaviour of irregular building structures since 2002”, Bulletin of Earthquake Engineering, Vol. 6, No. 2, pp. 285-308

Di Giulio, G., Azzara, R., Cultrera, M., G., Giammarinaro, M. S., Vallone, P. and Rovelli, A. (2005), “Effect of local geology on ground motion in the City of Palermo, Italy, as inferred from aftershocks of the 6 September 2002 M_w 5.9 earthquake”, Bulletin of the Seismological Society of America, Vol. 95, No. 6, pp. 2328-2341.

DSTA (2009) “Geology of Singapore, 2nd Edition”, Defence Science and Technology Agency (DSTA), Singapore.

Elenas, A. and Meskouris, K. (2001) “Correlation study between seismic acceleration parameters and damage indices of structures”, Engineering Structures Vol. 23, No. 6, pp. 698-704.

Federal Emergency Management Agency. (2000) “FEMA 356, Prestandard and Commentary for the Seismic Rehabilitation of Buildings”, Washington D.C.

Fragiadakis, M., Vamvatsikos, D. and Papadrakakis, M. (2006) “Evaluation of the influence of vertical irregularities on the seismic performance of a nine-storey steel frame”, Earthquake Engineering and Structural Dynamics, Vol. 35, No. 12, pp. 1489-1509

Gallipoli, M. R., Mucciarelli, M. and Vona, M. (2009), “Empirical estimate of fundamental frequencies and damping for Italian buildings”, Earthquake Engineering and Structural Dynamics , Vol. 38, No. 8, pp. 973-988.

Gallipoli, M. R., Mucciarelli, M., Castro, R. R., Monachesi, G. and Contri, P. (2004), “Structure, soil-structure response and effects of damage based on

observations of horizontal-to-vertical spectral ratios of microtremors”, Soil Dynamics and Earthquake Engineering, Vol. 24, No. 6, pp. 487-495.

Gallipoli, M. R., Mucciarelli, M., Šket-Motnikar, B., Zupančić, P., Gosar, A., Prevolnik, S., Herak, M., Stipčević, J., Herak, D., Milutinović, Z. and Olumčeva, T. (2010), “Empirical estimates of dynamic parameters on a large set of European buildings”, Bulletin of Earthquake Engineering, Vol. 8, No. 3, pp. 593-607.

Goh, K. S., Megawati, K., and Pan, T. C. (2012) “Seismic performance of typical tall buildings in Singapore”, Proceedings, The 15th World Conference on Earthquake Engineering.

Guler, K., Yuksel, E. and Kocak, A. (2008), “Estimation of the fundamental vibration period of existing RC buildings in Turkey utilizing ambient vibration records”, Journal of Earthquake Engineering, Vol. 12, SUPPL. 2, pp. 140-150.

Haselton, C. B., Goulet, C. A., Mitrani-Reiser, J., Beck, J. L., Deierlein, G. G., Porter, K. A., Stewart, J. P. and Taciroglu, E. (2009) “An assessment to benchmark the seismic performance of a code-conforming reinforced concrete moment-frame building”, Pacific Earthquake Engineering Research Centre, PEER 2007/12.

Hong, L. L. and Hwang, W. L. (2000) “Empirical formula for fundamental vibration periods of reinforced concrete buildings in Taiwan”, Earthquake Engineering and Structural Dynamics, Vol. 29, No. 3, pp. 327-337.

Housing Development Board. (2012) “HDB Annual Report 2011/2012”, HDB, Singapore

Hudson, D. E. (1997), “Dynamic tests of full-scale structures”, Journal of Engineering Mechanics Division, Vol. 103, No. 6, pp. 1141-1157.

Ibarra, L. F., Medina, R. A. and Krawinkler, H. (2005). “Hysteretic models that incorporate strength and stiffness deterioration”, Earthquake Engineering and Structural Dynamics, Vol. 34, No. 12, pp 1489-1511.

Idriss, I. M. and Sun, J. I. (1992) “User’s manual for SHAKE91” Center for Geotechnical Modeling, Department of Civil Engineering, University of California, Davis.

International Code Council. (2012). “International Building Code”.

Japanese Meteorological Agency (1996) “Shindo wo Shiru (Note on the JMA seismic intensity)”, Gyosei, pp. 46-224.

Kanda, J., Tamura, Y., Fujii K., Ohtsuki, T., Shioya, K. and Nakata, S. (1994) “Probabilistic evaluation of human perception threshold of horizontal vibration of buildings (0.125Hz to 6.0Hz)”, American Society of Civil Engineers, Atlanta, GA, USA.

Karabalis, D. L., Cokkinides, G. J. and Rizos, D. C. (1994), “Interactive computer code for generation of artificial earthquake records”, Computing in Civil Engineering (ASCE), pp. 1122-1155, Washington, DC, USA.

Kaushik, H. B., Rai, D. C. and Jain, S. K. (2007) “Stress-strain characteristics of clay brick masonry under uniaxial compression”, Journal of Materials in Civil Engineering, Vol. 19, No. 9, pp. 728-739.

Li, B., Wu, Y. and Pan, T. C. (2002), "Seismic behavior of nonseismically detailed interior beam-wide column joints - Part I: Experimental results and observed behavior", ACI Structural Journal, Vol. 99, No. 6, pp. 791-802.

Liel, A. B., Haselton, C. B. and Deierlein, G. G. (2011) "Seismic collapse safety of reinforced concrete buildings. II: Comparative assessment of nonductile and ductile moment frames". Journal of Structural Engineering, Vol. 137, No. 4, pp. 492-502.

Lucchini, A., Monti, G. and Kunnath, S. (2009) "Seismic Behaviour of Single-Story Assymmetric-Plan Buildings under Uniaxial Excitation", Earthquake Engineering and Structural Dynamics, Vol 38, pp. 1053-1070.

Mander, J. B., Priestley, M. J. N. and Park, R. (1988). "Theoretical Stress-Strain Model for Confined Concrete", Journal of Structural Engineering New York. Vol. 114, No.8, pp. 1804-1826.

Martinelli, P. and Filippo, F. C. (2009), "Simulation of the Shaking Table Test of a Seven-Story Shear Wall Building", Earthquake Engineering and Structural Dynamics, Vol. 38, No.5, pp. 587-607.

Megawati, K. and Pan T. C. (2010) "Ground-motion attenuation relationship for the Sumatran megathrust earthquakes", Earthquake Engineering and Structural Dynamics, Vol 39, No. 8, 827-845.

Megawati, K. and Pan, T. C. (2002) "Prediction of the maximum credible ground motion in Singapore due to a great Sumatran subduction earthquake: The worst-case scenario", Earthquake Engineering and Structural Dynamics, Vol. 31, No. 8, pp. 1501-1523.

Megawati, K. and Pan, T. C. (2009), “Regional seismic hazard posed by the Mentawai segment of the Sumatran megathrust”, Bulletin of the Seismological Society of America, Vol. 99, No. 2A, pp. 566-584.

Megawati, K., Pan, T. C. and Kazuki Koketsu (2003), “Response spectral attenuation relationships for Singapore and the Malay Peninsula due to Distant Sumatran-fault earthquakes”, Earthquake Engineering and Structural Dynamics, Vol. 32, pp. 2241-2265.

Michel, C., Guéguen, P., Lestuzzi, P. and Bard, P. Y. (2010) “Comparison between seismic vulnerability models and experimental dynamic properties of existing buildings in France”, Bulletin of Earthquake Engineering, Vol. 8, No. 6, pp. 1295-1307.

Mitra, N. and Lowes, L. N. (2007), “Evaluation, Calibration, and Verification of a Reinforced Concrete Beam-Column Joint Model”, Journal of Structural Engineering, Vol. 133, No. 1, pp. 105-120.

Mucciarelli, M., Bettinali, F., Zaninetti, A., Vanini, M., Mendez, A., and Galli, P. (1996), “Refining Nakamura's technique: processing techniques and innovative instrumentation”, Proceedings of XXV General Assembly of ESC, Reykjavik, Washington, D.C.

Musson, R. M. W. (2005) “On the perceptibility of earthquakes”, Journal of Seismology, Vol. 10, pp. 157-162.

Myslimaj B. and Tso W. K. (2003) "A design-oriented approach to strength distribution in single story asymmetric systems with elements having strength-dependent stiffness", Earthquake Spectra, Vol. 21, pp. 197-212

Nakamura, Y. (1989), "Method for dynamic characteristics estimation of subsurface using microtremor on the ground surface", Quarterly Report of RTRI (Railway Technical Research Institute) (Japan), Vol. 30, No. 1, pp. 25-33.

Navarro, M., Vidal, F., Enomoto, T., Alcalá, F. J., García-Jerez, A., Sánchez, F. J. and Abeki, N. (2007) "Analysis of the weightiness of site effects on reinforced concrete (RC) building seismic behaviour: The Adra town example (SE Spain)", Earthquake Engineering and Structural Dynamics, Vol. 36, No. 10, pp. 1363-1383.

Omote, S., Narahashi, H., Sekizawa, A., and Zama, S. (1990) "Seismic intensity distribution in high-rise buildings subjected to large earthquake motions as determined from responses to questionnaire surveys", Journal of Natural Disaster Science Vol. 12, No. 2, pp. 1-20.

OpenSEEs (2009). "Open System for Earthquake Engineering Simulations". Berkeley, CA.

Pan, T. C., Goh, K. S., and Megawati, K. (2013) "Empirical relationships between natural vibration period and height of buildings in Singapore", Earthquake Engineering and Structural Dynamics, Vol 43, No. 3, pp. 449-465.

Pan, T. C. and Lee, C. L. (2002) "Site response in Singapore to long-distance Sumatra earthquakes", Earthquake Spectra, Earthquake Engineering Research Institute, Vol. 18, No. 2, pp. 347 – 367.

Pan, T. C., Megawati, K. and Goh, K. S. (2011) “Response of high-rise buildings in Singapore due to a potential giant earthquake in the Sumatran megathrust”, Journal of Earthquake Engineering, Vol. 15, SUPPL. 1, pp. 90-106.

Pan, T. C., Megawati, K. and Goh, K. S. (2011) “Response of high-rise buildings in Singapore due to a potential giant earthquake in the sumatran megathrust”. Journal of Earthquake Engineering Vol. 15, SUPPL. 1, pp. 90-106.

Pan, T.-C., You, X. T., and Cheng, K. W. (2004) “Building response to long-distance major earthquakes”, Proceedings, The 13th World Conference on Earthquake Engineering, 1 – 6 August 2004, Vancouver, Canada, Paper No. 804.

Pantazopoulou, S. J. and Moehle, J. P. (1990) “Identification of effect of slabs on flexural behavior of beams”, Journal of Engineering Mechanics, Vol. 116, No. 1, pp. 91-106.

Pantazopoulou, S. J. and Moehle, J. P. (1990), “Identification of Effect of Slabs on Flexural Behavior of Beams”, Journal of Engineering Mechanics, Vol. 116, No. 1, pp. 91-106.

Peruš, I. and Fajfar, P. (2005) “On the Inelastic Torsional Response of Single-Storey Structures under Bi-Axial Excitation”, Earthquake Engineering and Structural Dynamics, Vol 34, pp 931-941.

Pitts, J. (1984), “A review of geology and engineering geology in Singapore”, Quarterly Journal of Engineering Geology, Vol. 17, No. 2, pp. 93-101.

Sadashiva, V. K., Macrae, G. A. and Deam, B. L. (2012) “Seismic response of structures with coupled vertical stiffness-strength irregularities”, Earthquake Engineering and Structural Dynamics, Vol. 41, No. 1, pp. 119-138

Saneinejad, A. and Hobbs, B. (1995) “Inelastic design of infilled frames” Journal of structural engineering New York, N.Y. Vol. 121, No. 4, pp. 634-649.

Schnabel, P. B., Lysmer, J. and Seed, H. B. (1972) “SHAKE: A computer program for earthquake response analysis for horizontally layered sites”, Earthquake Engineering Research Center, University of California, Berkeley.

Seed, H. B. and Idriss, I. M. (1970), “Soil moduli and damping factors for dynamic response analysis”, Earthquake Engineering Research Center, University of California, Berkeley.

Sezen, H. and Moehle, J. P. (2004), “Shear strength model for lightly reinforced concrete columns”, Journal of Structural Engineering, Vol. 130, No. 11, pp. 1692-1703.

Singapore Department of Statistics (2012) “Monthly Digest of Statistics Singapore 2012” Singapore

Singhal, A. and Kiremidjian A. S. (1996) “Method for probabilistic evaluation of seismic structural damage”. Journal of Structural Engineering Vol. 122, No. 12, pp. 1459-1467.

Trifunac, M. D., Ivanović, S. S., Todorovska, M. I., Novikova, E. I. and Gladkov, A. A. (1999) “Experimental evidence for flexibility of a building foundation supported

by concrete friction piles”, Soil Dynamics and Earthquake Engineering, Vol. 18, No. 3, pp. 169-187.

Tso W. K. and Myslimaj B. (2003) “A yield displacement distribution-based approach for strength assignment to lateral force-resisting elements having strength dependent stiffness”, Earthquake Engineering and Structural Dynamics, Vol. 32, pp. 2319-2351

Valmundsson, E. V. and Nau, J. M. (1997) “Seismic response of building frames with vertical structural irregularities”, Journal of Structural Engineering, Vol. 123, No. 1, pp. 30-40

Vucetic, M. and Dobry, R. (1991), “Effect of soil plasticity on cyclic response”, Journal of Geotechnical Engineering”, Vol. 117, No. 1, pp. 89-107.

Wald, D. J., Quitoriano, V., Heaton, T. H. and Kanamori, H. (1999a) “Relationships between peak ground acceleration, peak ground velocity, and modified mercalli intensity in California”. Earthquake Spectra Vol. 15, No. 3, pp. 557-564.

Wald, D. J., Quitoriano, V., Heaton, T. H., Kanamori, H., Scrivner, C. W. and Worden, C. B. (1999b) “TriNet "ShakeMaps": Rapid generation of peak ground motion and intensity maps for earthquakes in southern California”. Earthquake Spectra Vol. 15, No. 3, pp. 537-554.

APPENDIX A

LOCATION OF BUILDINGS FOR AMBIENT VIBRATION MEASUREMENTS

Table A-1 Details of measured buildings at Kallang Formation

No.	Address	Number of storey	Natural period, T (sec)
1	172 Bukit Batok West Avenue 8, (S) 650172	25	1.37
2	171 Bukit Batok West Avenue 8, (S) 650171	25	1.37
3	9 Gloucester Road (S) 210009	14	0.87
4	46 Dorset Road (S) 210049	13	0.80
5	10 Gloucester Road (S) 210010	14	0.85
6	41 Sims Drive (S) 380041	16	0.87
7	42 Sims Drive (S) 380042	12	0.60
8	22 Boon Keng Road (S) 330022	12	0.49
9	104 Towner Road (S) 327827	10	0.65
10	105 Towner Road (S) 321105	11	0.69
11	1 Saint George's Road (S) 320001	12	0.70
12	2 Saint George's Road (S) 320002	14	0.79
13	8 Saint George's Lane (S) 320008	12	0.78
14	5 Saint George's Lane (S) 320005	12	0.72
15	7 Saint George's Lane (S) 320007	15	1.02
16	15 Saint George's Road (S) 320015	12	0.68
17	21 Saint George's Road (S) 320021	25	1.32
18	72 Geylang Bahru (S) 330072	13	0.85
19	93 Geylang Bahru (S) 330093	13	0.85
20	73 Geylang Bahru (S) 330073	13	0.75
21	68 Geylang Bahru (S) 330068	18	0.89
22	61 Geylang Bahru (S) 330061	13	0.76
23	60 Geylang Bahru (S) 330060	21	1.02
24	59C Geylang Bahru (S) 332059	21	1.02

Table A-1 (Con't)

No.	Address	Number of storey	Natural period, T (sec)
25	54 Geylang Bahru (S) 330054	25	1.20
26	45 Bendermeer Road (S) 330045	12	0.55
27	46 Bendermeer Road (S) 330046	21	0.97
28	48 Bendermeer Road (S) 330048	19	0.89
29	1 Beach Road (S) 190001	16	0.78
30	17 Beach Road (S) 190017	20	1.08
31	12 North Bridge Road (S) 190012	25	1.32
32	19 Jalan Sultan (S) 190019	16	1.14
33	466 Crawford Lane (S) 190466	16	1.00
34	8 North Bridge Road (S) 190008	20	1.28
35	801 French Road (S) 200801	12	0.73
36	804 King George's Avenue (S) 200804	14	0.91
37	94 Geylang Bahru (S) 330094	14	0.79

Table A-2 Details of measured buildings at Bukit Timah Granite

No.	Address	Number of storey	Natural Period, T (sec)
1	547 Choa Chu Kang Street 52 (S) 680547	13	0.56
2	544 Choa Chu Kang Street 52 (S) 680544	12	0.51
3	558 Choa Chu Kang North 6, (S) 680558	12	0.51
4	601 Choa Chu Kang Street 62 (S) 680601	9	0.37
5	827 Woodlands Street 81 (S) 730 827	11	0.47
6	825 Woodlands Street 81 (S) 730825	10	0.51
7	830 Woodlands Street 83 (S) 730830	12	0.58
8	831 Woodlands Street 83 (S) 730831	10	0.50
9	834 Woodlands Street 83 (S) 730834	12	0.48
10	836 Woodlands Street 83 (S) 730836	11	0.50
11	850 Woodlands Street 82 (S) 730850	12	0.51
12	107 Ang Mo Kio Ave 4 (S) 560107	11	0.55
13	102 Ang Mo Kio Avenue 3 (S) 560102	12	0.58
14	115 Ang Mo Kio Avenue 4 (S) 560115	12	0.58
15	117 Ang Mo Kio Avenue 4 (S) 560117	12	0.61
16	170 Ang Mo Kio Avenue 4 (S) 560170	10	0.54
17	171 Ang Mo Kio Avenue 4 (S) 560171	16	0.73
18	174 Ang Mo Kio Avenue 4 (S) 560174	11	0.60

Table A-3 Details of measured buildings at Jurong Formation

No.	Address	Number of storey	Natural period, T (sec)
1	108 Bukit Batok West Avenue 6 (S) 650108	8	0.36
2	110 Bukit Batok West Avenue 6 (S) 650110	25	1.02
3	111 Bukit Batok West Avenue 6 (S) 650111	25	1.01
4	622 Bukit Batok Central (S)650622	30	1.37
5	621 Bukit Batok Central (S)650621	30	1.32
6	119 Bukit Batok West Avenue 6 (S) 650119	11	0.49
7	131 Bukit Batok West Avenue 6 (S) 650131	12	0.44
8	121 Bukit Batok Central (S) 650121	17	0.78
9	168 Bukit Batok West Avenue 8 (S) 650168	8	0.43
10	162 Bukit Batok Street 11 (S) 650162	10	0.51
11	161 Bukit Batok Street 11, (S) 650161	13	0.61
12	226 Jurong East Street 21 (S) 600226	25	1.08
13	227 Jurong East Street 21 (S) 600227	25	1.05
14	231 Jurong East Street 21 (S) 600231	12	0.57
15	221 Jurong East Street 21 (S) 600221	4	0.22
16	94 Henderson Road (S)150094	16	0.75
17	126 Bukit Merah View (S) 151126	25	1.08
18	125 Bukit Merah View (S) 151125	18	0.69
19	121 Bukit Merah View (S) 151121	9	0.36
20	120 Bukit Merah View (S)152120	16	0.66
21	11 York Hill (S) 162011	12	0.54
22	9 Jalan Kukoh (S) 160009	12	0.57

Table A-3 (Con't)

No.	Address	Number of storey	Natural period, T (sec)
23	2 Jalan Kukoh (S) 163002	12	0.55
24	3 Jalan Kukoh (S) 161003	16	0.76
25	1 Jalan Kukoh (S) 161001	17	0.85
26	51 Chin Swee Road (S) 160051	20	0.95
27	53 Chin Swee Road (S) 160053	26	1.23

Table A-4 Details of measured buildings at Old Alluvium

No.	Address	Number of storey	Natural Period, T (sec)
1	155 Bedok South Avenue 3 (S) 460155	4	0.24
2	156 Bedok South Avenue 3 (S) 460156	12	0.53
3	157 Bedok South Avenue 3 (S) 460157	13	0.65
4	158 Bedok South Avenue 3 (S) 460158	4	0.24
5	159 Bedok South Avenue 3 (S) 460159	13	0.63
6	160 Bedok South Avenue 3 (S) 460160	13	0.56
7	163 Bedok South Road (S) 460163	13	0.63
8	164 Bedok South Road (S) 460164	12	0.54
9	170 Bedok South Road (S) 460170	12	0.58
10	43 Bedok South Road (S) 460043	16	0.72
11	44 Bedok South Road (S) 460044	16	0.72
12	46 Bedok South Avenue 3 (S) 460046	15	0.65
13	50 Bedok South Avenue 3 (S) 460050	16	0.67
14	51 New Upper Changi Road (S) 461051	16	0.68
15	33 Bedok South Avenue 2 (S) 460033	16	0.66
16	34 Bedok South Avenue 2 (S) 460034	15	0.72
17	62 New Upper Changi Road (S) 461062	16	0.70
18	10B Bedok South Avenue 2 (S) 461010	20	0.73
19	10D Bedok South Avenue 2 (S) 463010	23	0.97
20	10E Bedok South Avenue 2 (S) 464010	21	0.87
21	10F Bedok South Avenue 2 (S) 465010	24	0.93
22	18 Bedok South Avenue 2 (S) 460018	12	0.55
23	407 Bedok North Avenue 3 (S) 460407	25	1.14
24	410 Bedok North Avenue 2 (S) 460410	11	0.56
25	411 Bedok North Avenue 2 (S) 460411	12	0.54
26	418 Bedok North Avenue 2 (S) 460418	9	0.44
27	419 Bedok North Street 1 (S) 460419	12	0.58
28	423 Bedok North Avenue 1 (S) 460423	12	0.54

Table A-4 (Con't)

No.	Address	Number of storey	Natural Period, T (sec)
29	111 Bedok North Road (S) 460111	13	0.58
30	115 Bedok North Road (S) 460115	13	0.62
31	118 Bedok North Street 2 (S) 460118	19	0.85
32	138 Bedok North Street 2 (S) 460138	12	0.55
33	127 Bedok North Street 2 (S) 460127	14	0.67

APPENDIX B:

VALIDATION OF USING A SIMPLIFIED TWO-STOREY MODEL TO REPRESENT A MULTI-STOREY MODEL

B.1 NUMERICAL MODELS

In this section, the use of a simplified two-storey model to represent a multi-storey model with soft-first-storey is validated. For this purpose, three multi-storey models are considered. They are: ten-storey model, twenty-storey model, and thirty-storey model, as shown in Table B-1. The models have only the translational degrees of freedom. The stiffness ratio of the N -storey models, $\alpha_{k,N}$, is defined as

$$\alpha_{k,N} = \frac{K_{2,N}}{K_{1,N}} \quad \text{Eq. B-1}$$

where $K_{1,N}$ and $K_{2,N}$ are the stiffness of the first-storey and the upper-storeys of the N -storey models, respectively, as shown in Table B-1. N is the number of storey. The lumped masses at each storey is defined as M_N , and they are assumed to be the same at each storey. The stiffness ratios considered in this study are 2.0, 5.0, 10.0, 20.0 and 50.0. The first-storey stiffness $K_{1,N}$ is assigned with an arbitrary value, while stiffness of upper storeys $K_{2,N}$ can be derived by displacing upper storeys by a constant unit displacement. The relationship between $K_{1,N}$ and $K_{2,N}$ is shown in Eq. B-1. The lumped masses at each storey, M_N , is then iterated so that the 1st natural vibration period of the multi-storey models are similar to the empirically derived results as presented in Chapter 2. The empirically derived 1st natural vibration

period of the ten-storey, twenty-storey and thirty-storey models are 0.48 sec, 0.87 sec, and 1.23 sec, respectively.

The simplified two-storey model has only the translational degree of freedom. The simplified two-storey models are equivalent to the corresponding multi-storey models in terms of: (a) the 1st natural vibration period and (b) the stiffness ratio. The first-storey and second-storey stiffness of the simplified two-storey model, K_1 and K_2 , is set to be the same as the first-storey and upper-storeys stiffness of the corresponding multi-storey model, $K_{1,N}$ and $K_{2,N}$, respectively. The lumped masses at each storey of the two-storey model are then iterated so that the 1st natural vibration period is the same as the corresponding multi-storey model. The overstrength ratio of both multi-storey and the equivalent two-storey model is defined as $\Omega=2.5$. The hysteretic model presented in section 6-4 is used. The deterioration coefficient is defined as $\gamma=75$.

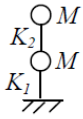
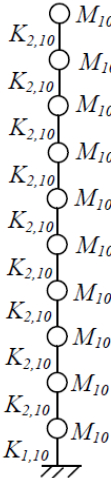
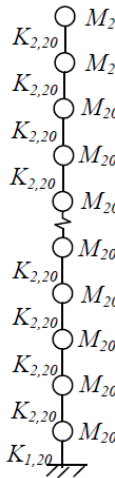
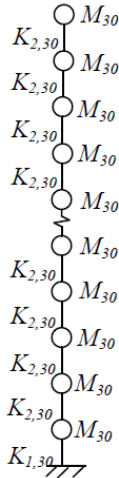
	Simplified two-storey model	Ten-storey model	Twenty-storey model	Thirty-storey model
				
1st natural vibration period (sec)		0.48	0.87	1.23
Degree of freedom	2	10	20	30

Table B-1 The degree of freedoms and the 1st natural vibration periods of multi-storey models

B.2 GROUND MOTION

One of the twenty ground motions in Singapore caused by the maximum credible earthquake (MCE) event in the Sumatran subduction zone, as described in section 5-4, is used. The time history and the response spectral displacement are shown in Figure B-1.

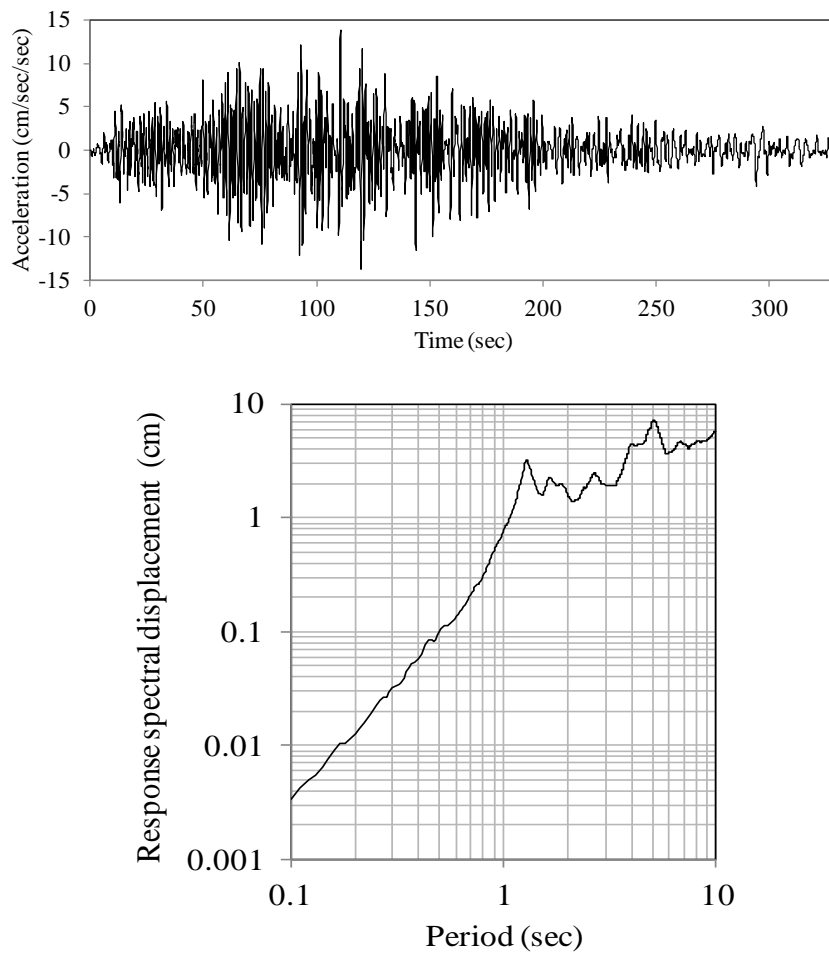


Figure B-1 Ground motion time history of the maximum credible Sumatran subduction earthquake and the corresponding response spectral displacement

A.2 RESULTS AND DISCUSSIONS

The analyses are conducted in *OpenSEEs* (2009). Standard Rayleigh damping is utilized, proportional to the initial stiffness and mass matrices, with 5% of critical damping. Figure B-2 shows the comparison between the responses at the top of multi-storey models and the equivalent two-storey models. Figure B-3 shows the percentage differences of maximum displacement at the top of multi-storey models and the equivalent two-storey models. The percentage differences range from

around 25% to around 5%. It can be seen that the percentage differences between the maximum displacement at the top of multi-storey models and the equivalent two-storey models decrease as the stiffness ratio increase. Figure B-4 shows the normalized mode shape of the 1st vibrational mode of the multi-storey models with different stiffness ratios. The upper storeys of the multi-storey models approaches a "rigid upper-storeys" as the stiffness ratio increases. Figure B-5 shows the 1st mode participation ratio of the multi-storey models and the simplified two-storey model with different stiffness ratios. The participation ratios fall into a narrow band of 0.85-0.99 and approaches 1.0 as the stiffness ratio increases. This could possibly explain the decreasing percentage differences between the maximum top displacement relative to the ground of the multi-storey models and that of the equivalent two-storey models as the stiffness ratio increases. From the analyses it can be concluded that the multi-storey model can be represented by the equivalent simplified two-storey model with acceptable differences.

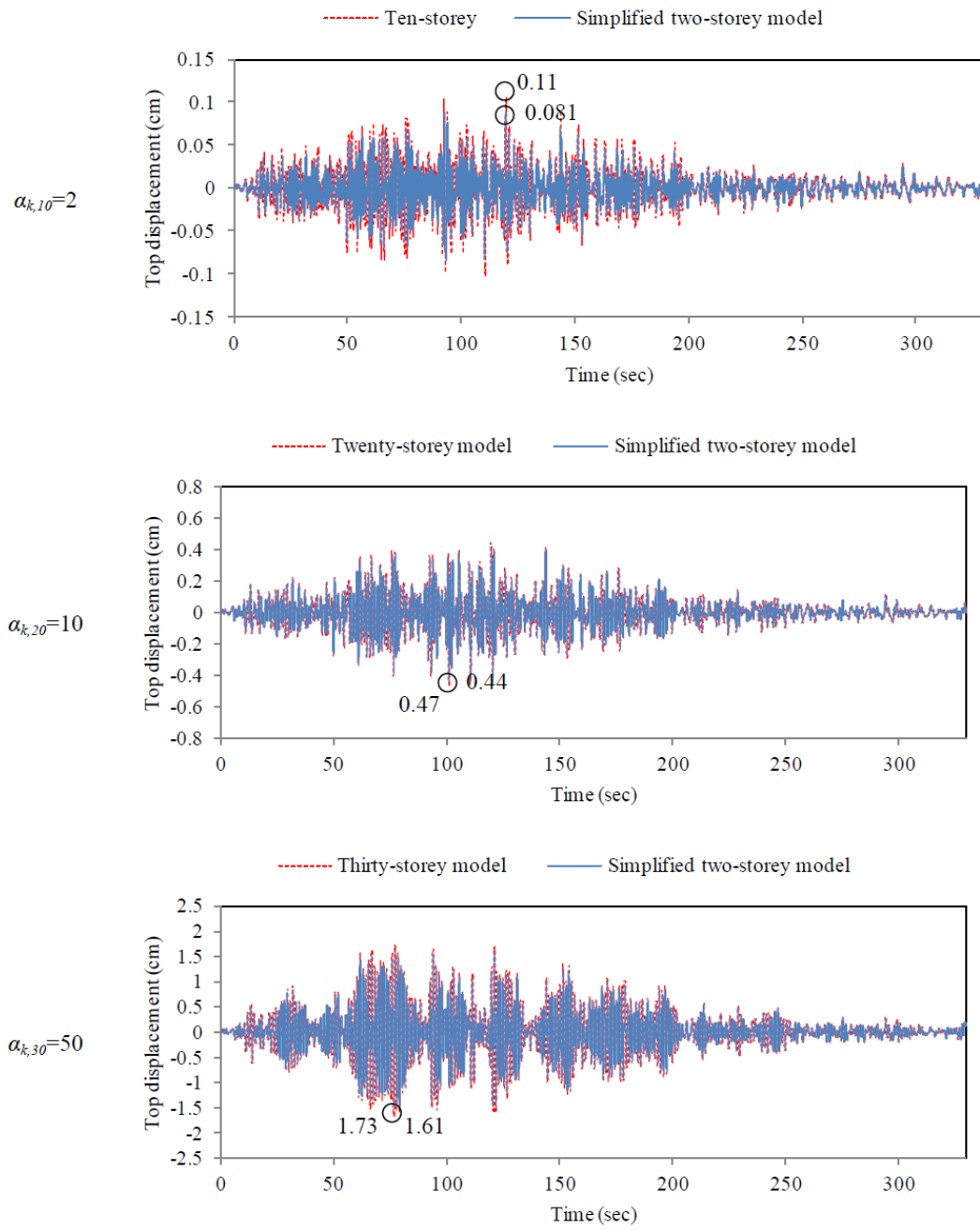


Figure B-2 Comparison between the top displacement responses of multi-storey models and the equivalent simplified two-storey models

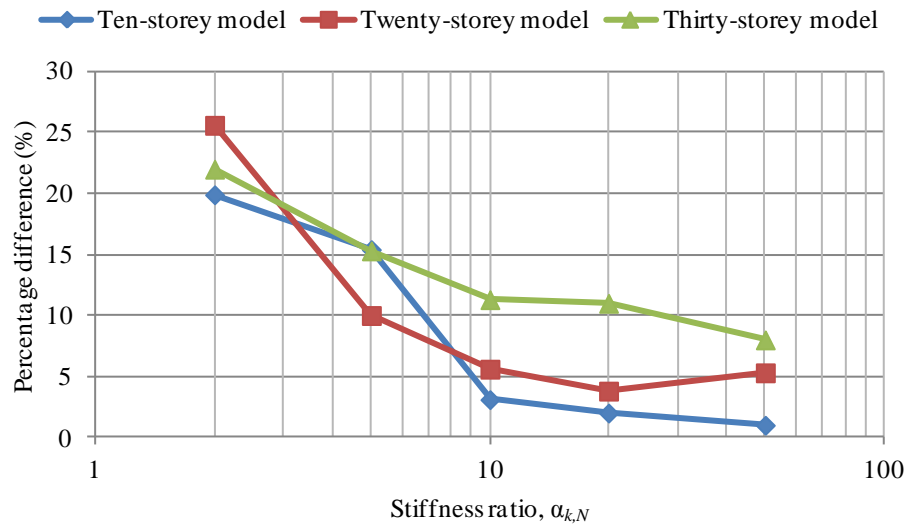


Figure B-3 Percentage differences between the maximum top displacement responses of multi-storey models and the equivalent two-storey models

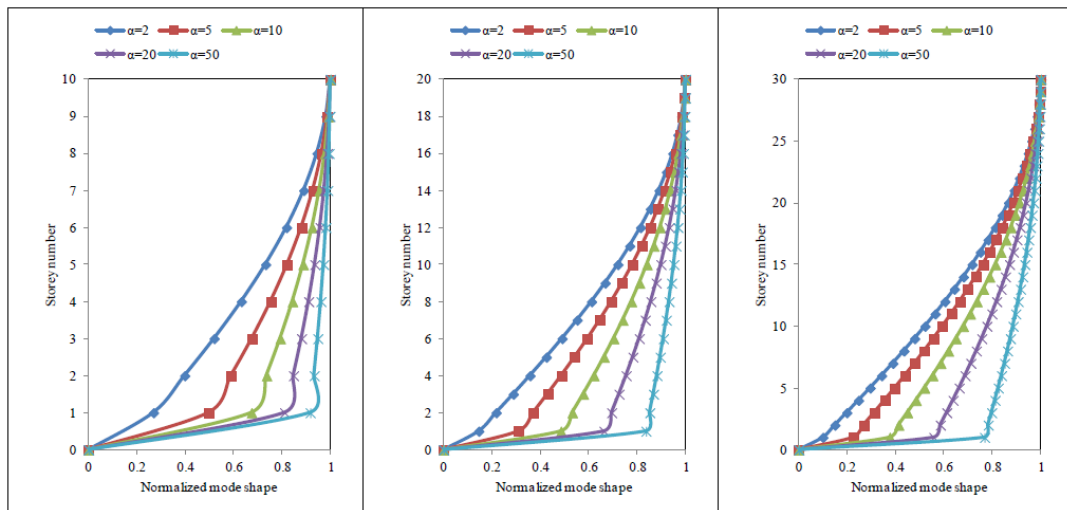


Figure B-4 Normalized 1st mode shape of: (a) ten-storey model, (b) twenty-storey model, (c) thirty-storey model with different stiffness ratio

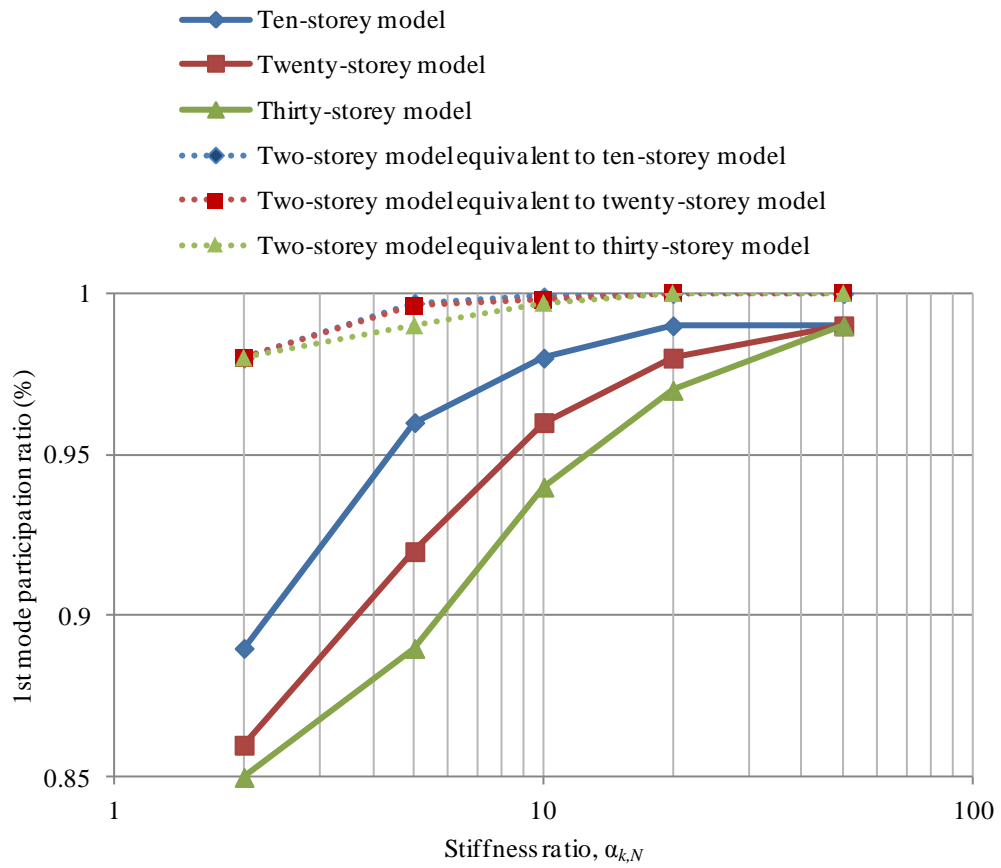


Figure B-5 1st mode participation ratio of the two-storey and multi-storey models with different stiffness ratio